U.S. DEPARTMENT OF COMMERCE
National Technical Information Service

PB-285 077

Application of Fourier Transform Spectroscopy to Air Pollution Problems

Ohio State Univ, Research Foundation, Columbus

Prepared for

Environmental Sciences Research Lab, Research Triangle Park, N C

Jun 78

United States
Environmental Protection
Agency

Environmental Sciences Research
Laboratory
Research Triangle Park NC 27711

EPA-600/3-78-057
June 1978

Research and Development

PB 285 077

EPA

Application of Fourier Transform Spectroscopy to Air Pollution Problems

Interim Report -1977

REPRODUCED BY
NATIONAL TECHNICAL
INFORMATION SERVICE
U. S. DEPARTMENT OF COMMERCE
SPRINGFIELD, VA. 22161

RESEARCH REPORTING SERIES

Research reports of the Office of Research and Development, U.S. Environmental Protection Agency, have been grouped into nine series. These nine broad categories were established to facilitate further development and application of environmental technology. Elimination of traditional grouping was consciously planned to foster technology transfer and a maximum interface in related fields. The nine series are:

1. Environmental Health Effects Research
2. Environmental Protection Technology
3. Ecological Research
4. Environmental Monitoring
5. Socioeconomic Environmental Studies
6. Scientific and Technical Assessment Reports (STAR)
7. Interagency Energy-Environment Research and Development
8. "Special" Reports
9. Miscellaneous Reports

This report has been assigned to the ECOLOGICAL RESEARCH series. This series describes research on the effects of pollution on humans, plant and animal species, and materials. Problems are assessed for their long- and short-term influences. Investigations include formation, transport, and pathway studies to determine the fate of pollutants and their effects. This work provides the technical basis for setting standards to minimize undesirable changes in living organisms in the aquatic, terrestrial, and atmospheric environments.

This document is available to the public through the National Technical Information Service, Springfield, Virginia 22161.

TECHNICAL REPORT DATA

(Please read Instructions on the reverse before completing)

1. REPORT NO.
EPA-600/3-78-057

2.

3. RECIPIENT'S ACCESSION NO.
PB285077

4. TITLE AND SUBTITLE
APPLICATION OF FOURIER TRANSFORM SPECTROSCOPY TO AIR POLLUTION PROBLEMS
Interim Report-1977

5. REPORT DATE
June 1978

6. PERFORMING ORGANIZATION CODE

7. AUTHOR(S)
Yoon S. Chang, J.H. Shaw, E. Niple, J.G. Calvert, W.H. Chan, S.Z. Levine, and W.M. Uselman

8. PERFORMING ORGANIZATION REPORT NO.

9. PERFORMING ORGANIZATION NAME AND ADDRESS
The Ohio State University Research Foundation
1314 Kinnear Road
Columbus, Ohio 43212

10. PROGRAM ELEMENT NO.
1AA603 AI-03 (FY-77)

11. CONTRACT/GRANT NO.
R803868-2

12. SPONSORING AGENCY NAME AND ADDRESS
Environmental Sciences Research Laboratory-RTP,NC
Office of Research and Development
U.S. Environmental Protection Agency
Research Triangle Park, North Carolina 27711

13. TYPE OF REPORT AND PERIOD COVERED
Interim

14. SPONSORING AGENCY CODE
EPA/600/09

15. SUPPLEMENTARY NOTES
See companion reports EPA-600/3-77-026, EPA-600/3-77-025

16. ABSTRACT

An atlas of observed and calculated air spectra from 700 to 2300 cm^{-1} has been prepared. Methods of analyzing air spectra to identify spectral features and to determine simultaneously the abundances of atmospheric gases such as CO, N_2O, CH_4, O_3, H_2O, and CO_2 have been explored. These methods include ratioing observed and calculated spectra and correlation analysis of absorption bands to obtain abundances by linear regression and non linear least squares methods. Absorbing features of atmospheric gases such as O_3, H_2O, and N_2O have been removed from solar spectra to isolate underlying features of F-12 near 1160 cm^{-1}.

New data were obtained related to the rate constant for the reaction, HO + CO H + CO_2, as a function of pressure. This rate constant is pressure sensitive: k = 439 ± 24 $ppm^{-1} min^{-1}$ at 700 Torr air; k = 203 ± 29 $ppm^{-1} min^{-1}$ in air at 100 Torr. The FTIRS system was employed in other studies to determine the rate constants for the reactions: $HO_2 + NO_2$ HO_2NO_2 (Ref.22) and $HO_2 + NO_2$ HONO + O_2 (Ref. 21); in 700 Torr of air at 25 ± 2°C, the data suggest k_{22} 7.2×10^1 and k_{21} 5.3×10^1 $ppm^{-1} min^{-1}$. Simulations of the reactions in a typical NO_x-RH-RCHO-polluted atmosphere exposed to sunlight show that the theoretical rate of HO_2NO_2 generation is similar in magnitude to those expected (and observed in real atmospheres) for peroxyacylnitrates.

17. KEY WORDS AND DOCUMENT ANALYSIS

a. DESCRIPTORS	b. IDENTIFIERS/OPEN ENDED TERMS	c. COSATI Field/Group
* Air pollution * Infrared spectroscopy * Optical equipment Solar spectrum * Reaction kinetics * Photochemical reactions	Fourier transform spectroscopy	13B 14B 20F 03B 07D 07E

18. DISTRIBUTION STATEMENT RELEASE TO PUBLIC	**19. SECURITY CLASS** *(This Report)* UNCLASSIFIED	**21. NO. OF PAGES** 121
	20. SECURITY CLASS *(This page)* UNCLASSIFIED	**22. PRICE** PCA06/MF A01

EPA Form 2220-1 (9-73)

EPA-600/3-78-057
June 1978

APPLICATION OF FOURIER TRANSFORM SPECTROSCOPY TO AIR POLLUTION PROBLEMS

Interim Report - 1977

by

Yoon S. Chang
J. H. Shaw
Edward Niple
J. G. Calvert
W. H. Chan
S. Z. Levine
W. M. Uselman
The Ohio State University
Research Foundation
Columbus, Ohio 43212

Grant Number R803868-2

Project Officer
John Spence
Atmospheric Chemistry and Physics Division
Environmental Sciences Research Laboratory
Research Triangle Park, North Carolina 27711

ENVIRONMENTAL SCIENCES RESEARCH LABORATORY
OFFICE OF RESEARCH AND DEVELOPMENT
U.S. ENVIRONMENTAL PROTECTION AGENCY
RESEARCH TRIANGLE PARK, NORTH CAROLINA 27711

DISCLAIMER

This report has been reviewed by the Environmental Sciences Research Laboratory, U.S. Environmental Protection Agency, and approved for publication. Approval does not signify that the contents necessarily reflect the views and policies of the U.S. Environmental Protection Agency, nor does mention of trade names or commercial products constitute endorsement or recommendation for use.

ABSTRACT

Progress in the application of Fourier Transform Spectroscopy to air pollution problems is described. An atlas of observed and calculated air spectra from 700 to 2300 cm^{-1} has been prepared. Methods of analyzing air spectra to identify spectral features and to determine simultaneously the abundances of atmospheric gases such as CO, N_2O, CH_4, O_3, H_2O, and CO_2 have been explored. These methods include ratioing observed and calculated spectra and correlation analysis of absorption bands to obtain abundances by linear regression and non linear least squares methods. Absorbing features of atmospheric gases such as O_3, H_2O, and N_2O have been removed from solar spectra to isolate underlying features of F-12 near 1160 cm^{-1}.

During the past year kinetic studies of several systems of general interest to atmospheric chemists have been completed using the FTIRS-photochemical reactor system. New data were obtained related to the rate constant for the reaction, $HO + CO \rightarrow H + CO_2$, as a function of pressure. This rate constant is pressure sensitive: $k = 439 \pm 24$ $ppm^{-1}min^{-1}$ at 700 Torr air; $k = 203 \pm 29$ $ppm^{-1}min^{-1}$ in air at 100 Torr. Atmospheric scientists should note that the adjustment of the HO-radical rate constants with other reactants in the lower atmosphere must be made where these estimates have been based on the low pressure value of this constant.

The FTIRS system was employed in other studies to determine the rate constants for the reactions: $HO_2 + NO_2 \rightarrow HO_2NO_2$ (Ref. 22) and $HO_2 + NO_2 \rightarrow HONO + O_2$ (Ref. 21); in 700 Torr of air at 25 ± 2°C, the data suggest $k_{22} \cong 7.2 \times 10^1$ and $k_{21} \cong 5.3 \times 10^1$ $ppm^{-1}min^{-1}$. Simulations of the reactions in a typical NO_x-RH-RCHO-polluted atmosphere exposed to sunlight show that the theoretical rate of HO_2NO_2 generation is similar in magnitude to those expected (and observed in real atmospheres) for peroxyacylnitrates.

This report was submitted in fulfillment of Grant Number R803868-2 by The Ohio State University under the sponsorship of the U.S. Environmental Protection Agency. This report covers a period from 7/15/76 to 7/14/77.

CONTENTS

Abstract iii
Figures vi
Tables xii

1. Introduction 1
2. Conclusion 2
3. Recommendations 3
4. Analysis of Long Path Air Spectra 6

    Introduction 6
    Methods of spectral analysis 15
    Comparison of observed and calculated spectra of individual gases 42
    Acquisition of a high resolution interferometer 42
    Stratospheric simulation chamber 49

5. Study of Some Key Reactions of Probable Importance In Photochemical Smog Formation 54

    Introduction 54
    The pressure dependence of the rate constant for the reaction: $HO + CO \rightarrow H + CO_2$ 55
    The kinetics and mechanism of the HO_2-NO_2 reaction the significance of peroxynitric acid formation in photochemical smog 62
    Experimental details of FTIRS and photolysis cell 80
    Experimental detail of photochemical and spectral measurements 82
    Infrared spectra of compounds 87
    Future plans 97

References 98
Appendices 104

A. Summary of objectives form 1975 proposal 104
B. Papers presented at meetings 106
C. Papers published or accepted for publication 107

Preceding page blank

FIGURES

Number		Page
1	The transmittance (T) of an absorbing path is defined as P/P_0 where P_0 is the incident and P is the emerging radiant power	7
2	(a) Frequency dependence of the absorption coefficient of an absorption line with a Lorentz shape; (b) Dependence of the transmittance due to a Lorentz line on the $k(\nu)\rho\ell$ product	9
3	The dependence of the transmittance of an air path containing various number densities of an absorbing gas with an absorption coefficient k on path length	11
4	(a) Laboratory spectrum of HCl between 2700 and 2900 cm^{-1} of 0.02 Torr HCl and 50 Torr N_2 in 171 m path; (b) Corresponding region of the solar spectrum (large zenith angle); (c) Spectrum of HCl between 2740 and 2780 cm^{-1}; (d) Corresponding region of the solar spectrum	12
5	(a) Spectrum of 8.5 m path of air with some CO_2 and H_2O removed; (b) Spectrum of 993 m path of ground level air, T = 290 K, P = 750 Torr; (c) Solar spectrum recorded at Columbus, Ohio, solar zenith angle 86°	13
6	(a) Spectrum of 7.0 m ground level air, T = 294 K, P = 750 Torr; (b) Spectrum of 993 m ground level air, T = 294 K, P = 750 Torr; (c) Solar spectrum, solar zenith angle = 82°	14
7	(a) Background spectrum of evacuated absorption cell between 650 and 1350 cm^{-1}; (b) Spectrum of absorption cell containing a sample of NO_2 and N_2O_4; (c) Ratio of spectrum b/spectrum a	16
8	(a) Laboratory spectrum of $CHCCF_2$ between 760 and 900 cm^{-1}; (b) Laboratory spectrum of $CHCl_2F$ between 760 and 900 cm^{-1}; (c) Laboratory spectrum of CCl_4 between 760 and 900 cm^{-1}; (d) Laboratory spectrum of CCl_3F between 760 and 900 cm^{-1}; (e) Ground level solar spectrum between 760 and 900 cm^{-1}	19
9	(a) Spectrum of 51 Torr CO_2 in 171 m path at 295 K between 800 and 820 cm^{-1}; (b) Calculated spectrum of CO_2 for the same conditions	20

FIGURES (Continued)

Number Page

10 (a) Calculated spectrum of CO between 2170 and 2250 cm^{-1}; (b) Calculated spectrum of CO_2 between 2170 and 2250 cm^{-1}; (c) Calculated spectrum of N_2O between 2170 and 2250 cm^{-1}; (d) Observed spectrum of 171 m of air at 294 K and 700 Torr 23

11 (a) The ratio of the spectra d and a in Fig. 10; (b) The ratio of the spectra in Fig. 11a and Fig. 10b; (c) The ratio of the spectra in Fig. 11b and Fig. 10c; (d) Observed spectrum of 171 m of air at 294 K and 700 Torr 24

12 (a) Ratio of the spectra in c and b; (b) Calculated spectrum of CO_2 between 2230 and 2250 cm^{-1}; (c) Observed spectrum of CO_2 broadened to atmospheric pressure with air 25

13 (a) Calculated spectrum between 1155 and 1165 cm^{-1} of O_3 in an atmospheric slant path; (b) Calculated spectrum between 1155 and 1165 cm^{-1} of H_2O in an atmospheric slant path; (c) Calculated spectrum between 1155 and 1165 cm^{-1} of N_2O in an atmospheric slant path; (d) Observed solar spectrum (solar zenith angle 45°) 27

14 (a) Laboratory spectrum of F-12 between 1155 and 1165 cm^{-1}; (b) Solar spectrum with O_3, N_2O, and H_2O lines ratioed out; (c) Calculated solar spectrum; (d) Observed solar spectrum 28

15 Portion of a spectrum of 171 m path of air at 294 K and 700 Torr. The intervals chosen for the linear regression method of obtaining abundances are indicated together with the position of the H_2O line and the $P_0(\nu)$ position. 33

16 (a) Ratio of observed $P(\nu)$ and values obtained from non linear least squares method; (b) Air spectrum between 2190 and 2210 cm^{-1} 38

17 (a) Ratio of spectra in Fig. 17b and 17c; (b) Observed spectrum of 1.52×10^{-3} Torr of N_2O and 100 Torr N_2 in 171 m path, at 294 K; (c) Calculated spectrum of N_2O for the same conditions as used to obtain Fig. 17b 39

18 (a) Ratio of the spectra shown in b and c; (b) Calculated solar spectrum corresponding to the conditions under which Fig. 18c was obtained; (c) Observed low sun spectra between 1158.0 and 1163.0 cm^{-1}, spectral resolution ~ 0.25 cm^{-1}, solar zenith angle 81° 41

FIGURES (Continued)

Number Page

19 (a) 300 Torr CO_2 in 171 m path at room temperature; (b) Calculated spectrum for same conditions; (c) 51 Torr CO_2 in 171 m path at room temperature; (d) Calculated spectrum for same conditions 43

20 (a) 300 Torr CO_2 in 171 m path at room temperature; (b) Calculated spectrum for same conditions; (c) 51 Torr CO_2 in 171 m path at room temperature; (d) Calculated spectrum for same conditions 44

21 (a) 0.15 Torr N_2O and 700 Torr N_2 in 171 m path; (b) Calculated spectrum for same; (c) 0.015 Torr N_2O and 700 Torr N_2 in 171 m path; (d) Calculated spectrum for same 45

22 (a) 0.15 Torr N_2O and 700 Torr N_2 in 171 m path; (b) Calculated spectrum for same; (c) 0.015 Torr N_2O and 700 Torr N_2 in 171 m path; (d) Calculated spectrum for same 46

23 (a) 0.38 Torr CH_4 and 700 Torr N_2 in 171 m path; (b) Calculated spectrum for same; (c) 0.076 Torr CH_4 and 700 Torr N_2 in 171 m path; (d) Calculated spectrum for same 47

24 (a) 4.18×10^{-3} Torr CO and 700 Torr N_2 in 171 m path; (b) Calculated spectrum for same; (c) 1.14×10^{-3} Torr CO and 100 Torr N_2 in 171 m path; (d) Calculated spectrum for same 48

25 Details of mirror adjusting system 50

26 Details of mirror adjusting system 51

27 The experimental photolysis system employed in this work 57

28 Plot of the ratio $\overline{[CO_2]_t/[\Delta C_4H_{10}]_t}$ versus $[CO]_0/[$iso-$C_4H_{10}]_0$ from the photolysis of HONO, CO, iso-C_4H_{10}, NO_x mixtures in synthetic air; open circles refer to experiments at 700 Torr total pressure; squares are from experiments at 100 Torr total pressure 61

FIGURES (Continued)

Number Page

29 Spectra of uv-irradiated HONO, NO_x, CO, air and Cl_2, NO_2, H_2, air mixtures; (a) spectrum of cell contents after 5.9 min irradiation of the initial mixture; total $[HONO]_0 = 2.70$, $[NO]_0 = 2.77$, $[NO_2]_0 = 1.5$, $[CO]_0 = 0.0$ ppm in synthetic air, 700 Torr; (b) residual spectrum resulting from that of (a) following computer subtraction of remaining cis, trans-HONO, $HONO_2$, and H_2O; note absence of HO_2NO_2 67

(c) spectrum of cell contents following 5.9 min irradiation of the initial mixture: total $[HONO]_0 = 4.29$, $[NO]_0 = 2.8$, $[NO_2]_0 = 1.1$, $[CO]_0 = 3.8 \times 10^4$ ppm in synthetic air, 700 Torr; (d) residual spectrum resulting from that of (c) following computer subtraction of remaining cis, trans-HONO, CH_4, and H_2O 68

(e) spectrum of cell contents following 6.0 min irradiation of the initial mixture: $[Cl_2]_0 = 30$, $[NO_2]_0 = 22$, $[H_2]_0 = 8026$ ppm in synthetic air at 700 Torr; (f) residual spectrum resulting from that of (e) following computer subtraction of the remaining $HONO_2$ and $ClNO_2$ products; compare the characteristic absorption peaks of HO_2NO_2 at 802.7 and 1303.9 cm^{-1} in (d) and (f) 69

30 Comparison of observed total [HONO]- and $[CO_2]$-time data with those predicted by the simulation model for irradiated HONO, NO_x, CO mixtures in air; (a) initial concentrations: total $[HONO]_0 = 2.70$, $[NO]_0 = 2.77$, $[NO_2]_0 = 1.5$ ppm in synthetic air, 700 Torr; (b) initial concentrations: total $[HONO]_0 = 4.35$, $[NO]_0 = 20.4$, $[NO_2]_0 = 17.4$, $[CO]_0 = 2.23 \times 10^3$ ppm in synthetic air, 700 Torr. 71

31 Comparison of observed total [HONO]-, $[CO_2]$-, and $[HO_2NO_2]$-time data with those predicted by the simulation model involving reactions (21) through (49), Table VII, initial concentrations, total $[HONO]_0 = 4.29$, $[NO]_0 = 2.8$, $[NO_2]_0 = 1.1$, $[CO]_0 = 3.8 \times 10^4$ ppm, in synthetic air, 700 Torr; values of k_{21}/k_{22} chosen in simulations: ∞ (—O—); 5.0 (------); 0.74 (———); 0.00 (— — —); $k_{23}/(k_{21} + k_{22}) = 10$ in all runs shown 73

FIGURES (Continued)

Number Page

32 The first order loss of HO_2NO_2 in three different dark runs; the squares are from data taken from a run with HONO-NO-NO_2-CO mixture; the remaining data points are from two different Cl_2-H_2-NO-NO_2 mixtures. The slope of this plot gives a first order loss constant of 9.1×10^{-2} min^{-1} 74

33 (a) 3.2 ppm HONO; (b) initial conditions of Cl_2 = 7.5, H_2 = 8026, NO = 3.25 and NO_2 = 2.74 ppm. In (b) the spectrum 1 represents the filled cell at start before the lights are turned on, 2 is the spectrum after almost 1 min of irradiation time, 3 is the same mixture as spectrum 2 but with CH_4 subtracted out, 4 is the same mixture as spectrum 2 but with CH_4 and 6% of spectrum (a) subtracted out 76

34 Photolysis of Cl_2, H_2, NO_x, mixture in synthetic air; initial concentrations (ppm): (Cl_2) = 7.5; (H_2) = 8026; (NO) = 3.25; (NO_2) = 2.74; air added to a total pressure of 700 Torr; (a) experimental data; (b) computer simulation 78

35 Photolysis of Cl_2, H_2, NO_x, mixture in synthetic air; initial concentrations (ppm): (Cl_2) = 15; (H_2) = 8026; (NO) = 1.28; (NO_2) = 11.1; total pressure of 700 Torr; (a) experimental data; (b) computer simulation 79

36 Infrared spectrum of ClNO (nitrosyl chloride), top spectrum = 0.10 ppm, bottom spectrum = 1.36 ppm 88

37 Infrared spectrum of $ClNO_2$ (nitryl chloride), top spectrum = 0.88 ppm, bottom spectrum = 3.38 ppm 89

38 a) 7.5 ppm $HONO_2$
b) ≈ 1.5 ppm $ClONO_2$ and 7.5 ppm $HONO_2$ formed during photolysis (0.7 min) of Cl_2 (90 ppm), NO_2 (13 ppm), O_3 (18 ppm) in a synthetic air mixture (P_T = 700 Torr) 90

39 HOCl formed during photolysis of Cl_2 (90 ppm), O_3 (20 ppm), hydrocarbon (5 ppm) mixtures in synthetic air (P_T = 700 Torr)
a) from iso-butane (2 min photolysis) with 4.3 ppm $(CH_3)_2CO$ removed

FIGURES (Continued)

Number		Page
39(cont.)	b) from propane (1 min photolysis) with 3.2 ppm $(CH_3)_2CO$ removed c) from ethane (2 min photolysis)	91
40	Infrared spectrum of HCl, top spectrum = 1.83 ppm, bottom spectrum = 68.3 ppm	92
41	Infrared spectrum of $HONO_2$, top spectrum = 0.39 ppm, bottom spectrum = 3.43 ppm	93
42	Infrared spectrum of O_3, top spectrum = 0.26 ppm, bottom spectrum = 12.0 ppm	94
43	Infrared spectrum of N_2O_5, top spectrum = 0.4 ppm, bottom spectrum = 2.2 ppm	95
44	HO_2NO_2 (1.1 ppm) c) spectrum of cell contents following 5.9 min irradiation of the initial mixture: total $[HONO]_0$ = 4.3 ppm, $[NO]_0$ = 2.8, $[NO_2]_0$ = 1.1, $[CO]_0$ = 3.8 x 10^4 ppm in synthetic air d) residual spectrum resulting from c) following computer subtraction of cis, trans-HONO, CH_4, and H_2O	96

TABLES

Number		Page
I	Abundances of CO, N_2O, and CO_2 Obtained by Ratioing Observed and Calculated Spectra of a 171 m Air Path	22
II	Absorption Coefficients of CO, N_2O, and H_2O Calculated from the AFCRL Listing and for a Spectral Resolution of 0.075 cm^{-1} Between 2000 and 2005 cm^{-1}	32
III	Dependence of Abundance Values of N_2O, CO, and H_2O Determined by Unweighted Linear Regression Analysis of Air Spectra on Spectral Regions Analyzed. $P_0(\nu)$ is 1.00 in All Cases	34
IV	Dependence of Abundance Values of N_2O, CO, and H_2O Determined by Unweighted Linear Regression Analysis of Air Spectra on Assumed Value of $P_0(\nu)$. Spectral Region Analyzed 2190 to 2210 cm^{-1}	34
V	Dependence of the Abundance of N_2O, CO, and H_2O Determined by Non Linear Least Squares Analysis of Air Spectra on the Spectral Region Analyzed	37
VI	Summary of Rate Data from the Photolysis of HONO in Mixtures with CO, iso-C_4H_{10}, NO_x, in Synthetic Air	60
VII	Summary of the Reaction Mechanism and Rate Constants Employed in the Simulation of HONO, NO_x, CO, Air Mixture Photolyses	65
VIII	Additional Reactions and Rate Constants Required in the Simulation of the Dilute Cl_2, NO_2, NO, H_2 Mixtures in Air	77
IX	Extinction Coefficients (base e, 1 cm^{-1} resolution, 700 Torr pressure, 25°C, 170 meter path, box-car apodization)	83

1. INTRODUCTION

This report summarizes progress made during the second year of EPA Grant No. R803868. This grant began in July 1975 and was a successor to EPA Grant No. R803075 which extended from April 1974 to July 1975. The work completed under the initial grant is described in the EPA Ecological Research Series Report EPA-600/3-76-084 and the work accomplished during the first year of the grant R803868 is described in a report to EPA issued in 1976. A summary of the research objectives in the proposal for this latter grant is given in Appendix I.

During the first year of the present grant methods of analyzing air spectra were developed. These included generating programs for calculating synthetic spectra from the line parameters of gases. By comparing calculated and observed spectra, features of F-12 were identified in solar spectra. In the current year an atlas of observed and calculated air spectra covering the region from 700 to 2300 cm^{-1} has been issued and quantitative estimates of the abundance of F-12 in the troposphere have been made. A variety of methods of analyzing both ground level air spectra and solar spectra has been developed. It has been shown that the abundances of gases such as N_2O, CO, and CO_2 can be simultaneously determined from a spectrum with precisions of the order of 1%. It is also possible to remove features of N_2O, O_3, and H_2O from solar spectra to isolate spectral features of gases such as F-12.

A multiple traversal cell to simulate the stratospheric environment has been constructed and it is currently being used to obtain spectra of ozone.

The FTIRS system and the photochemical reactors built in the first years of this study are well suited for the measurement of the rates of chemical change in systems designed to simulate the conditions present in NO_x-RH-polluted urban atmospheres and in the NO_x and Freon contaminated stratosphere. During the past year kinetic studies of several systems of general interest have been made. These relate largely to the reactions of the HO and HO_2 radicals, the two dominant chain carrying species which promote many of the important changes which occur in the atmosphere. The results obtained in these chemical studies provide very significant new information of special significance to both the chemistry of the troposphere and the stratosphere.

As a result of this work a number of papers have been presented at meetings, published, or accepted for publication. These are described in Appendices II and III, respectively.

2. CONCLUSIONS

Synthetic spectra calculated from line parameters can be used to interpret spectra of long air paths. By using these line parameters the abundances of gases such as H_2O, CO_2, N_2O, CH_4, and CO can be simultaneously determined with precisions of 1% by correlation analyses employing linear regression and non-linear least squares techniques to the analysis of ground level air spectra. Similarly, the total amounts of these gases and of other gases such as F-12 in a vertical column through the atmosphere can be simultaneously obtained by applying these methods to the analysis of solar spectra. These methods can be adapted to the analysis of laboratory spectra provided suitable computing facilities are available. These procedures increase the accuracy with which the abundances of gases can be obtained compared with many other methods. By using these line parameters or by exchanging information on the measured spectral absorption coefficients of entire bands of gases, it is possible to standardize measurements made in different laboratories and to make them independent of the particular instrumentation used.

New data have been obtained in this work which prove that the reaction, $HO + CO \rightarrow H + CO_2$, is pressure sensitive; the results show that the rate constant for this reaction is a factor of two larger (at one atmosphere in air) than that derived by many workers from results at relatively low pressures of added inert gases. The result is of great value in the estimation of the correct lifetime of the CO molecule in the atmosphere. In addition, the present results bear directly on the estimate of the reaction rate constant for the HO-radical with many other atmospheric contaminants. Thus the rate constant for the seemingly important atmospheric reaction of SO_2 oxidation, $HO + SO_2(+M) \rightarrow HOSO_2(+M)$, is twice the value suggested earlier from comparative rate measurements based upon the low CO - HO rate constant.

The reactions of HO_2 radicals with NO_2 have been studied using two different ultraviolet irradiated systems: dilute HONO, NO_x, CO mixtures in air; and, dilute Cl_2, H_2, NO_x mixtures in air. One important product of this mixture, peroxynitric acid, arises from the reaction, $HO_2 + NO_2 \rightarrow HO_2NO_2$. The first direct estimates of the rate constant for this reaction have been determined in this study. The application of these estimates in computer simulation of the reactions in an NO_x, RH-RCHO-polluted atmosphere suggest that peroxynitric acid may be a significant component of photochemical smog. In view of its recognized highly oxidizing character, HO_2NO_2 may contribute to the eye irritation and other manifestations of photochemical smog.

New infrared spectral data have been determined for several compounds of interest to the atmospheric scientists: NO_2Cl, NOCl, $ClONO_2$, HOCl, HO_2NO_2, N_2O_5, HCl, $HONO_2$, and O_3.

3. RECOMMENDATIONS

The development of accurate methods of quantitatively analyzing spectra should be continued with emphasis on refining the procedures to increase the speed and ease of application to actual spectra. Particular emphasis should be placed on the application of these methods to interpreting solar spectra, but their use in obtaining information from other types of spectra should be explored.

The accuracy of the line parameters used to calculate spectra should be verified by comparison with laboratory spectra of individual gases, especially for those lines which appear in air spectra and interfere with the identifications of features of pollutant gases.

A program of applying these analytical methods to the analysis of air spectra should be undertaken. This will require the continuation of the collection of air spectra with the highest available spectral resolution through the use of the Nicolet interferometer which is scheduled for delivery in May 1977.

It is also recommended that a cooperative effort be initiated among interested workers to establish a library of accurate spectral absorption coefficient data or line parameter information so that standardized methods of interpreting spectral data can be established based on the analytical techniques described above. This program should also establish the ranges of physical conditions of the gas samples for which the absorption coefficient data are reliable.

The FTIRS system and the photochemical reaction chamber have been shown to be well designed to study reaction mechanisms and to determine rate constants which are of special interest to the understanding of photochemical smog formation and its control, and reactions in the polluted stratosphere. There are several key systems which we plan to study during this last year of the current project. These include: (1) the reactions of the HO_2, CH_3O_2, and t-$C_4H_9O_2$ radicals with NO ($RO_2 + NO \rightarrow RO + NO_2$) and with NO_2 ($RO_2 + NO_2 \rightarrow RO_2NO_2$); (2) the role of the aldehydes (CH_2O, and CH_3CHO) in photochemical smog formation; (3) some potentially important removal mechanisms for SO_2 in the atmosphere; and (4) the effects of Cl_3CF addition on O_3 generation under stratospheric conditions. These are outlined in the following sections.

THE REACTIONS OF THE ALKYLPEROXY RADICALS WITH NITRIC OXIDE AND NITROGEN DIOXIDE.

Present computer models of photochemical smog invoke the reactions, $RO_2 + NO \rightarrow RO + NO_2$, as the most important reactions necessary to rationalize the rapid conversion of NO to NO_2 which occurs in irradiated RH, NO_x, air systems. However, there are no accurate estimates of the rate constants of these reactions with varied size of the alkyl group R. In this work we will follow the NO to NO_2 conversion in irradiated $(CH_3)_2N_2$, NO, air mixtures and $(t\text{-}C_4H_9)_2N_2$, NO, air mixtures. From our knowledge of the absolute values of the rate constants of the reactions, $2CH_3O_2 \rightarrow$ Products, and $2t\text{-}BuO_2 \rightarrow$ Products, and the product rates, estimates of the rate constants for the seemingly important reactions, $CH_3O_2 + NO \rightarrow CH_3O + NO_2$, and $t\text{-}BuO_2 + NO \rightarrow t\text{-}BuO + NO_2$ will be derived. The effect of structure of the alkyl group on the rate of the NO oxidation which we will learn from these experiments, will be very valuable in assigning realistic rate constants to the many similar reactive RO_2 species encountered in smog simulation mechanisms.

The studies of the past year which dealt with the unusual HO_2NO_2 compound and the rate constant for its formation will be continued and extended to include studies of the structurally similar compounds, $CH_3O_2NO_2$ and $t\text{-}C_4H_9O_2NO_2$. Our preliminary estimates of the rate constant for the reaction, $HO_2 + NO_2 \rightarrow HO_2NO_2$ carried out at 700 Torr (air) will be refined in further experiments, and the pressure dependence of this rate constant will be established in similar experiments at 100 and 10 Torr of added air. The evaluation of the possible role of the peroxynitric acid as a sink for NO_2 in stratospheric reactions requires such kinetic information.

Preliminary experiments performed in our laboratory using $(CH_3)_2N_2$ (5ppm), NO_2 (5 ppm) in synthetic air mixtures gave an indication of the formation of some transient compound with absorption in the 790-800 cm^{-1} range and with a halflife in the dark of less than 3 min. This is the characteristic absorption region for one of the bands associated with the peroxynitrate grouping, and the data suggest that $CH_3O_2NO_2$ may have been formed here.

A similar experiment was performed employing a $t\text{-}Bu_2N_2$, NO mixture in synthetic air, and transient bands at 1300, 790, and 860 cm^{-1} were observed. The band at 790 cm^{-1}, characteristic of the peroxynitrate group, had a dark halflife of about 14 min in this case. It appears likely from these preliminary data that alkylperoxynitrate compounds, analogues to the recently identified HO_2NO_2, do participate in these smog simulation systems. Rate constants for their formation and decay paths will be derived in this study so that the possible significance of these compounds in the real atmosphere can be determined.

THE ROLE OF ALDEHYDES IN PHOTOCHEMICAL SMOG FORMATION.

The aldehydes, demonstrated products of combustion reactions and smog reactions involving hydrocarbon-O_3 and hydrocarbon-OH reaction, have the potential of generating free radicals to stimulate smog formation. However, present data do not allow an unambiguous assignment of the primary rates of radical generation from CH_2O and CH_3CHO irradiated in the lower atmosphere. In this study dilute mixtures of CH_2O in air; CH_2O, NO in air, CH_3CHO in air; and CH_3CHO, NO, in air, will be photolyzed. From the rates of aldehyde loss and products formed in these experiments, coupled with the known wavelength distribution of the UV-light and its absolute intensity, we can estimate the quantum efficiency of the primary steps in the aldehyde photolyses. The similarity of the wavelength distribution and the intensity of the UV-light in the photochemical chamber employed in our work to that of the solar distribution will allow a reasonable extrapolation of our results to the real atmosphere. This information is of particular value in the evaluation of ozone generation in the long range transport of urban air masses.

In addition, attempts will be made in CH_2O, NO_x, HONO, air photolyses to generate the elusive peroxyformylnitrate which has not been observed to date.

A STUDY OF SOME POTENTIALLY IMPORTANT ATMOSPHERIC SO_2 REMOVAL MECHANISMS.

The relatively simple chemical systems which we plan to employ in these studies should provide a new and more direct measure of the rates of several seemingly important reactions leading to the homogeneous oxidation of SO_2 in the RH-NO_x-polluted atmospheres. By proper choice of initial levels of HONO, SO_2, and CO in air we should be able to derive rather directly the rate constants for the reactions,
$HO + SO_2\ (+M) \rightarrow HOSO_2\ (+M)$ and $HO_2 + SO_2 \rightarrow HO + SO_3$.

THE NATURAL REMOVAL MECHANISMS OF FREONS AND THEIR INFLUENCE ON O_3 LEVELS IN THE STRATOSPHERE.

The new photochemical reactor which has been constructed will be tested in a series of experiments designed to simulate the stratospheric conditions of pressure and temperature. The generation of ozone by short wavelength irradiation (1750-2200 Å) in relatively pure air will be followed using infrared analysis; the effect of added $CFCl_3$ on this process will be determined in subsequent experiments. Through these experiments we will be able to evaluate the importance of unwanted wall reactions in the chamber. The data will be used to improve the cell construction to better simulate the stratospheric reactions and further study the reactions of the primary CCl_2F and Cl fragments for the simulated stratospheric conditions.

4. ANALYSIS OF LONG PATH AIR SPECTRA

INTRODUCTION

The objectives of this phase of the work include:

1. The identification of the absorption features of air pollutants in long path air spectra;
2. The quantitative determination of the abundances of atmospheric gases by analyses of air spectra.

During the past three years spectra of long path lengths of ground level air and also of solar spectra have been obtained with the interferometer available to us. Since these spectra are recorded digitally the principal methods explored to analyze these spectra have been based on the computer manipulation of the data and the search for rapid methods of achieving the above objectives. Some of these methods are described in this section after the basic theory of atmospheric transmittance and its dependence on the absorbing characteristics of air molecules has been discussed.

If radiant energy of power $P_o(\nu)$ at some frequency ν is incident on an absorbing path, as shown in Fig. 1, and the emerging power is $P(\nu)$, the transmittance $T(\nu)$ of the path is defined as

$$T(\nu) = P(\nu)/P_o(\nu) . \tag{1}$$

For the conditions with which the data described in this report were collected, the transmittance is related to the absorbing properties of the path by

$$T(\nu) = P(\nu)/P_o(\nu) = \exp[-k(\nu)u] , \tag{2}$$

when $k(\nu)$ is the monochromatic absorption coefficient of the medium and u is a measure of the amounts of the absorbing constituents in the path. For a homogeneous path containing m absorbing gases each with a characteristic absorbing coefficient $k_i(\nu)$ and a number density ρ_i a more general form of Eq. (2) is required

$$T(\nu) = \exp\left[- \sum_{i=1}^{m} k_i(\nu)\rho_i \ell\right] , \tag{3}$$

where ℓ is the optical path length.

If the path is not homogeneous, Eq. (3) becomes

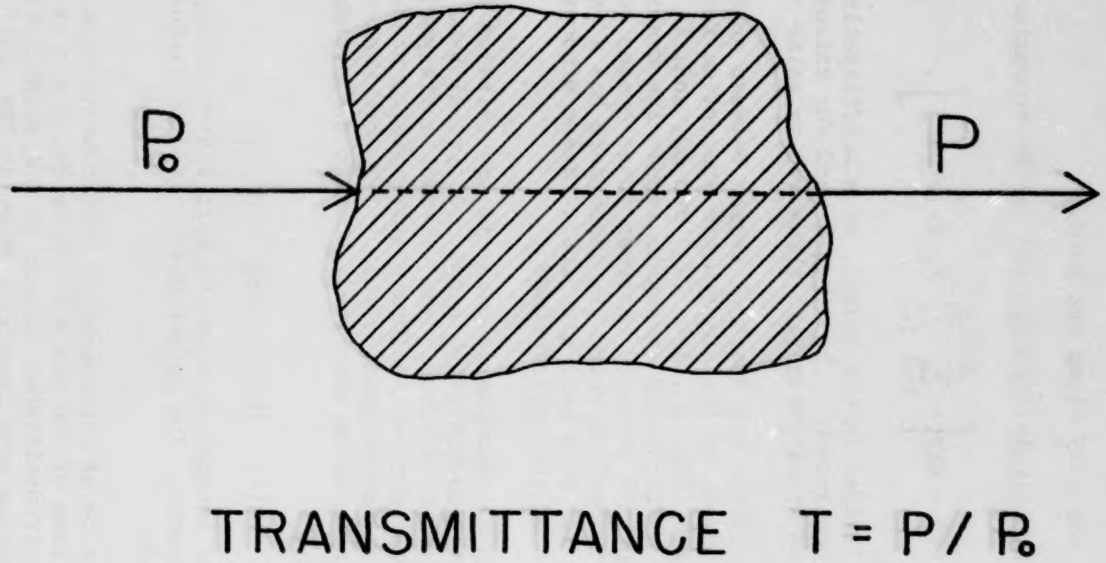

P_o
P
TRANSMITTANCE $T = P/P_o$

Fig. 1 - The transmittance (T) of an absorbing path is defined as P/P_o when P_o is the incident and P is the emerging radiant power

$$T(\nu) = \exp\left[-\int_0^{\ell} \sum_{i=1}^{m} k_i(\nu)\rho_i d\ell\right] . \qquad (4)$$

where $k_i(\nu)$ and ρ_i may vary along the path.

For purposes of calculation, Eq. (4) can be approximated by

$$T(\nu) = \exp\left[-\sum_{k=1}^{N} \sum_{i=1}^{m} k_{ik}(\nu)\rho_{ik}\Delta\ell_k\right] , \qquad (5)$$

where the path is divided into N layers, each sufficiently thin that it may be considered homogeneous. Eq. (5) is used for calculating the transmittance of the atmospheric path traversed by solar radiation.

We have investigated the spectral region between approximately 400 and 4000 cm^{-1}. Most of the atmospheric absorption features in this region are due to H_2O, CO_2, O_3, N_2O, CH_4, and CO, and, in some spectral regions, these are sufficiently strong to reduce the transmittance of long path lengths of air to zero. Between these opaque regions there are atmospheric "windows" in which the atmosphere has a relatively high transmittance even for very long air paths. These windows also contain absorption features of atmospheric gases.

The absorption by atmospheric gases in the infrared is primarily associated with rotation-vibration bands. A typical band consists of many individual absorption lines, each of which corresponds to a transition of the absorbing molecule from a lower energy state E" to an upper state E'. At pressures greater than a few torr the absorption coefficients of the lines can be described, to a good approximation, by the Lorentz line shape

$$k(\nu) = S\alpha/\pi[(\nu-\nu_0)^2 + \alpha^2] , \qquad (6)$$

where S is the line intensity, α is the half width, and ν_0 is the position of the line center. The dependence of $k(\nu)$ on frequency is illustrated in Fig. 2(a).

The transmittance of a homogeneous path containing a gas with a single absorption line of the shape given by Eq. 6 can be calculated from Eq. (3). The transmittance depends on the product $k(\nu)\rho\ell$ and decreases with increasing path length as drawn in Fig. 2(b). If the number density or mixing ratio of a gas is to be determined from such transmittance measurements it is readily shown that, for a given signal to noise ratio in the observed spectrum, the most accurate measurements can be made for transmittance values $T(\nu) \approx 1/e \approx 0.37$. Thus, to determine the abundance of a gas with a fixed absorption coefficient and a variable mixing ratio it is desirable to adjust the absorbing path length so that the observed transmittance lies in the range 0.1 to 0.9. The

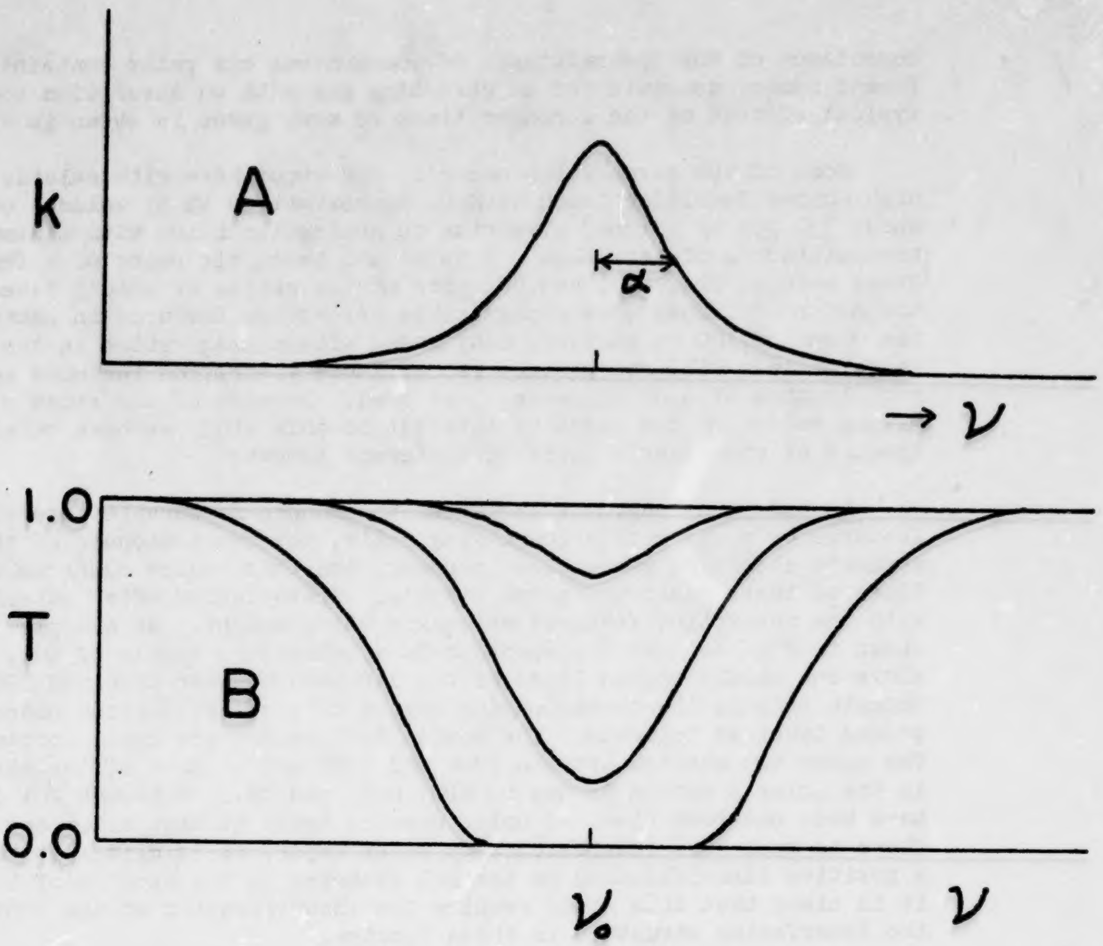

$$T = P / P_0 = e^{-k \rho l}$$

Fig. 2a - Frequency dependence of the absorption coefficient of an absorption line with a Lorentz shape

2b - Dependence of the transmittance due to a Lorentz line on the $k(\nu)\rho\ell$ product dependence of the transmittance of homogeneous air paths containing different number densities of an absorbing gas with an absorption coefficient typical of that of the stronger lines of many gases is shown in Fig. 3.

Some of the gases which occur in the atmosphere with relatively high number densities (such as H_2O, approximately 1% by volume, or CO_2 about 330 ppm by volume) give rise to absorption lines with minimum transmittances of less than 0.5 in ground level air paths of a few meters. Gases such as CH_4, N_2O, and CO, with mixing ratios at ground level of the order of 1 ppm, give recognizable absorption features in paths of the order of 100 m; however, many gases with mixing ratios in the ppb range or less will not produce recognizable absorption features unless path lengths of many kilometers are used. Because of the range of the mixing ratios of the gases of interest to this study we have obtained spectra of atmospheric paths of different lengths.

As the path length is increased to produce measurable absorption features by a gas with a low mixing ratio, the total amounts of the more abundant absorbing gases also increase, and this causes numerous weak lines of these gases to become visible. These latter often interfere with the absorption features which are being sought. An example is shown in Fig. 4. The top spectrum is a laboratory sample of HCl. It shows the widely spaced lines of the 1-0 band between 2700 and 2900 cm^{-1}. Beneath this is the corresponding region of a solar spectrum observed at ground level at Columbus. The bottom two spectra are small portions of the upper two spectra between 2740 and 2780 cm^{-1}. Most of the structure in the solar spectrum is due to HDO, H_2O, and CH_4. Although HCl features have been observed (1-4) in solar spectra taken at high altitudes where there is much less interference by water vapor, it is difficult to make a positive identification of the HCl features in the spectra of Fig. 4. It is clear that this would require the identification of the sources of the interfering structure in these spectra.

Other examples of long path atmospheric spectra are shown in Fig. 5 and 6. Figure 5 shows spectra of approximately 8 m, and 1000 m of ground level air and a solar spectrum over the region from 700 to 1500 cm^{-1}. Figure 6 shows a similar set of spectra of the region from 1800 to 2300 cm^{-1}. As the path length increases numerous weaker lines become visible throughout the entire region. The extent of the "windows" is curtailed in solar spectra by strong bands of CO_2 and H_2O. The intensities of these bands is decreased by making observations at high altitudes and studies of the solar spectrum by high flying aircraft, balloons, etc., and other detection methods (5-19) have enabled a number of gases such as F-11, F-12, HNO_3, and HCl to be identified as atmospheric constituents. Little is known about the abundances of some of these gases in the troposphere; hence, the analyses of solar spectra observed at ground level can serve as a unique resource for such investigations.

Many of the lines of H_2O, CO_2, O_3, N_2O, CH_4, and CO in Figs. 4, 5, and 6 can be identified by comparing their positions and intensities with the corresponding spectra of individual gases obtained in the

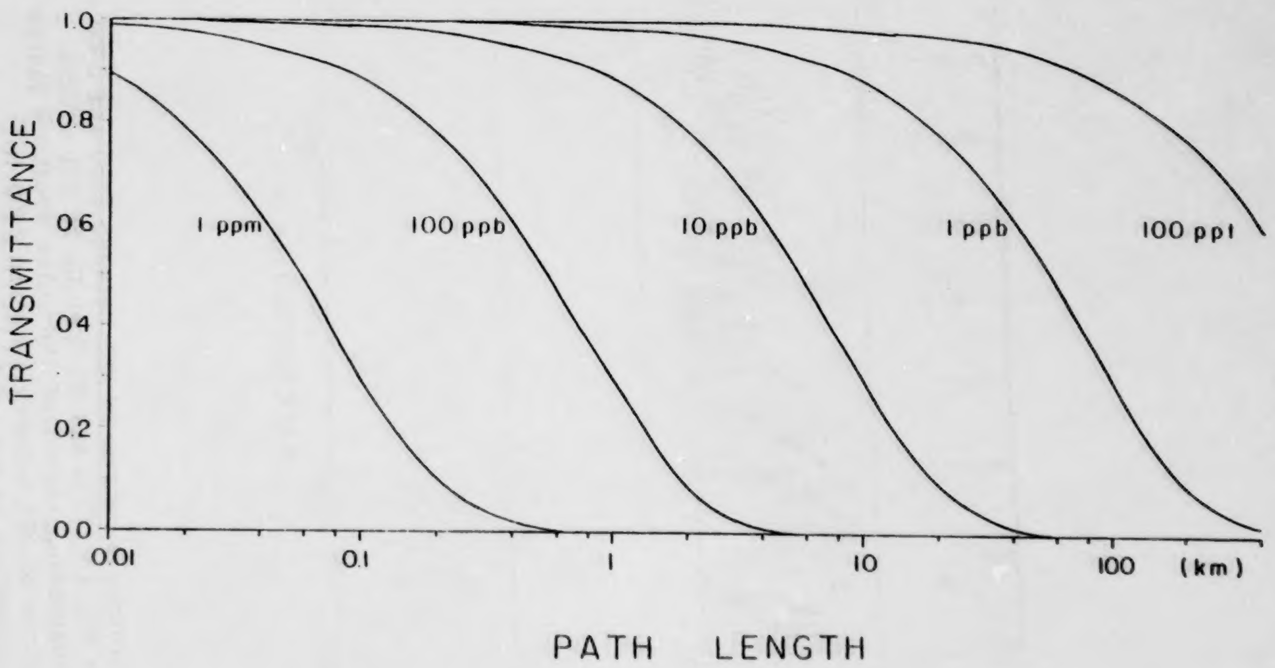

Fig. 3 - The dependence of the transmittance of an air path containing various number densities of an absorbing gas with an absorption coefficient k on path length

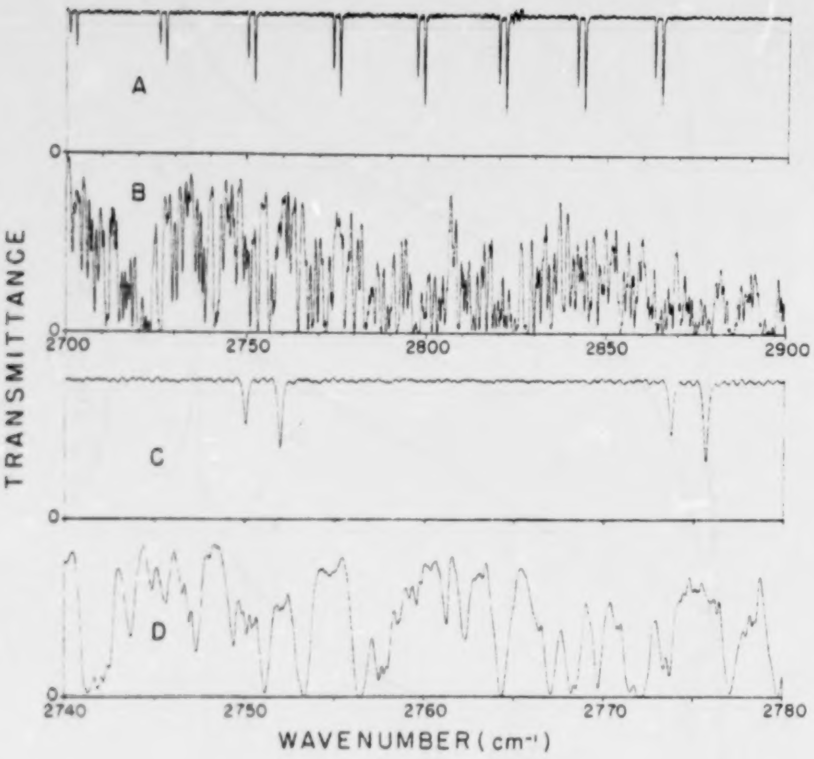

Fig. 4a - Laboratory spectrum of HCl between 2700 and 2900 cm^{-1} 0.02 Torr HCl in 171 m and 50 Torr N_2 in 171 m path
4b - Corresponding region of the solar spectrum (large zenith angle)
4c - Spectrum of HCl between 2740 and 2780 cm^{-1}
4d - Corresponding region of the solar spectrum

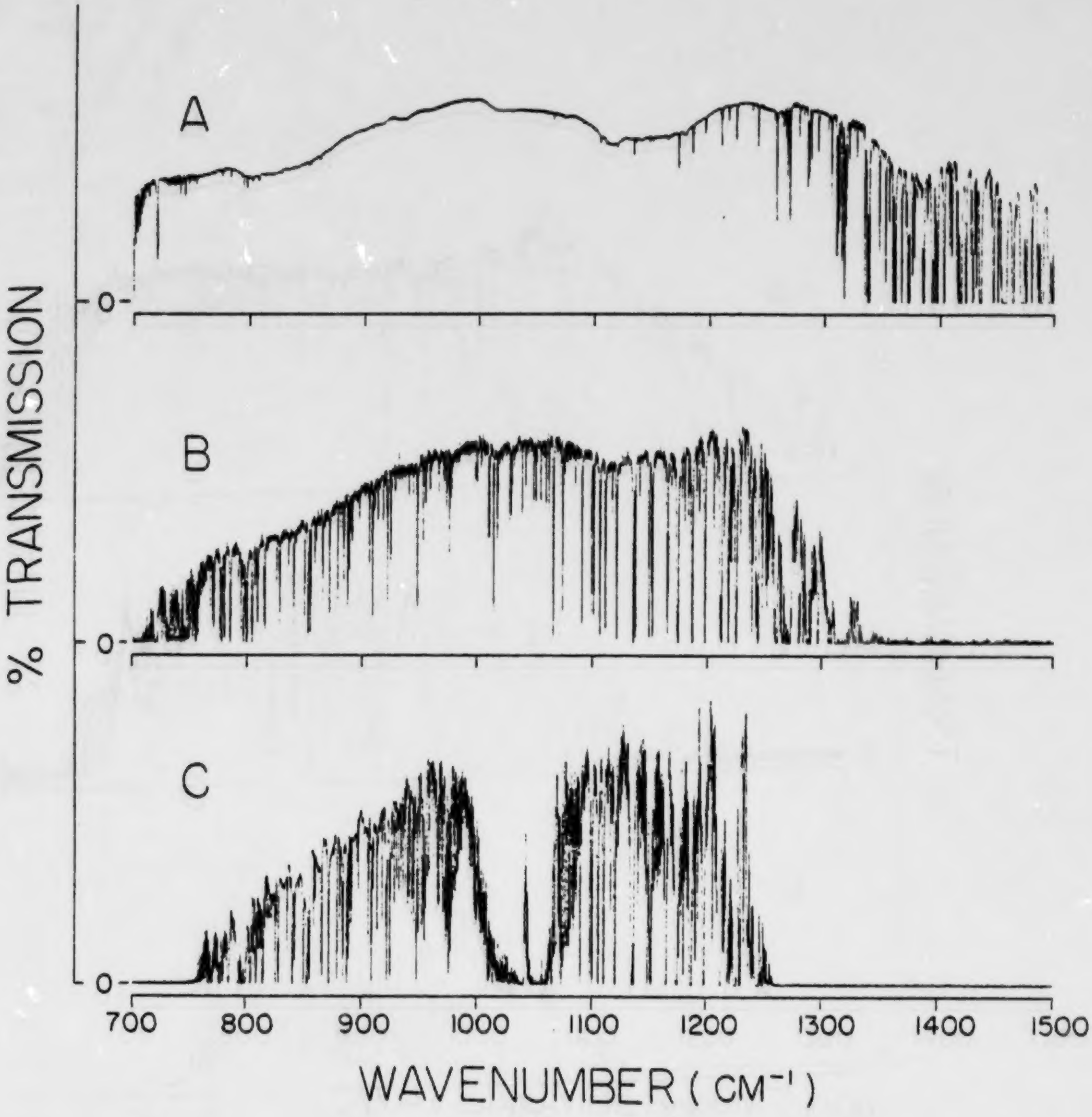

Fig. 5a - Spectrum of 8.5 m path of air with some CO_2 and H_2O removed
5b - Spectrum of 993 m path of ground level air, T = 290 K, P = 750 Torr
5c - Solar spectrum recorded at Columbus, Ohio, solar zenith angle 86°

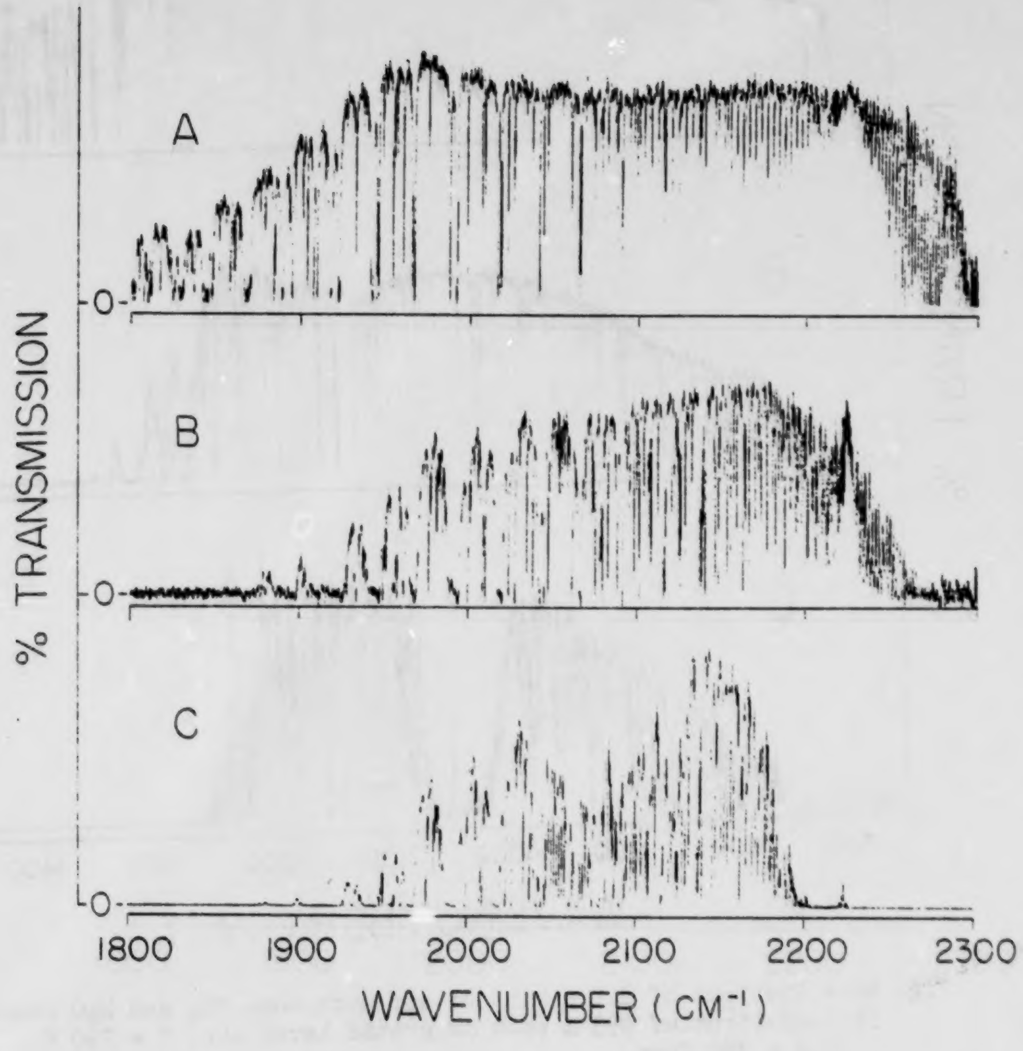

Fig. 6a - Spectrum of 7.0 m ground level air, T = 294 K, P = 750 Torr
6b - Spectrum of 993 in ground level air, T = 294 K, P = 750 Torr
6c - Solar spectrum, solar zenith angle = 82°

laboratory. However, because of the low vapor pressure of H_2O at room temperature, it is not possible, even with the long path lengths available in the multiple traversal cells in our laboratory, to obtain spectra of a sufficient amount of this gas to match the amount occurring in the atmospheric paths traversed by solar radiation. Thus not all the water lines in solar spectra can be readily identified. This is of concern because water vapor lines occur throughout the spectral region of interest. However, as all who have attempted to do so have found, it is time-consuming to identify individual features line by line even for frequency comparisons only. Even when the lines have been identified, obtaining quantitative estimates of the mixing ratios of the gases from the spectra is difficult and subject to inaccuracies if only individual lines are analyzed.

During the past year we have investigated other techniques of analyzing spectra with the aim of reducing the time taken for the analysis and to improve the accuracy of the measurements. The progress in this area is described below.

METHODS OF SPECTRAL ANALYSIS

Spectral ratioing

Spectral rationing is a commonly used technique for investigating spectra. An example is illustrated in Fig. 7. The top spectrum is that of an evacuated cell and the few meters of air in the transfer optics path between 650 and 1350 cm^{-1}. Bands of CO_2 near 700 cm^{-1} and H_2O beyond 1200 cm^{-1} are superposed on the background, which is determined primarily by the variations in spectral sensitivity of the Cu:Ge detector. The middle spectrum shows absorption bands of NO_2 after this gas had been introduced into the cell. Both of these spectra were recorded digitally at equally spaced frequency intervals, and they can be ratioed at each frequency as shown in the bottom curve. In this ratioed spectrum the detector spectral sensitivity variations have been removed as well as most of the features due to CO_2 and H_2O, thus allowing a direct measurement of the NO_2 transmittance to be obtained. If the amount of NO_2 in this sample were not known, it could be estimated by ratioing this transmittance spectrum with other transmittance spectra of samples containing known amounts of NO_2 at the same temperature and pressure as the unknown sample.

The transmittance of long air paths in multiple traversal cells can also be obtained by ratioing spectra with the cell evacuated and containing the air sample. The absorption features of the individual gases can then be removed by ratioing the air transmittance spectra with transmittance spectra of each of the gases present. This allows both the abundance of these gases to be estimated and also underlying features of other gases can be made more easily visible in the ratioed spectra.

We have applied this technique to the study of ground level air spectra obtained with a spectral resolution of 0.1 cm^{-1} at Columbus,

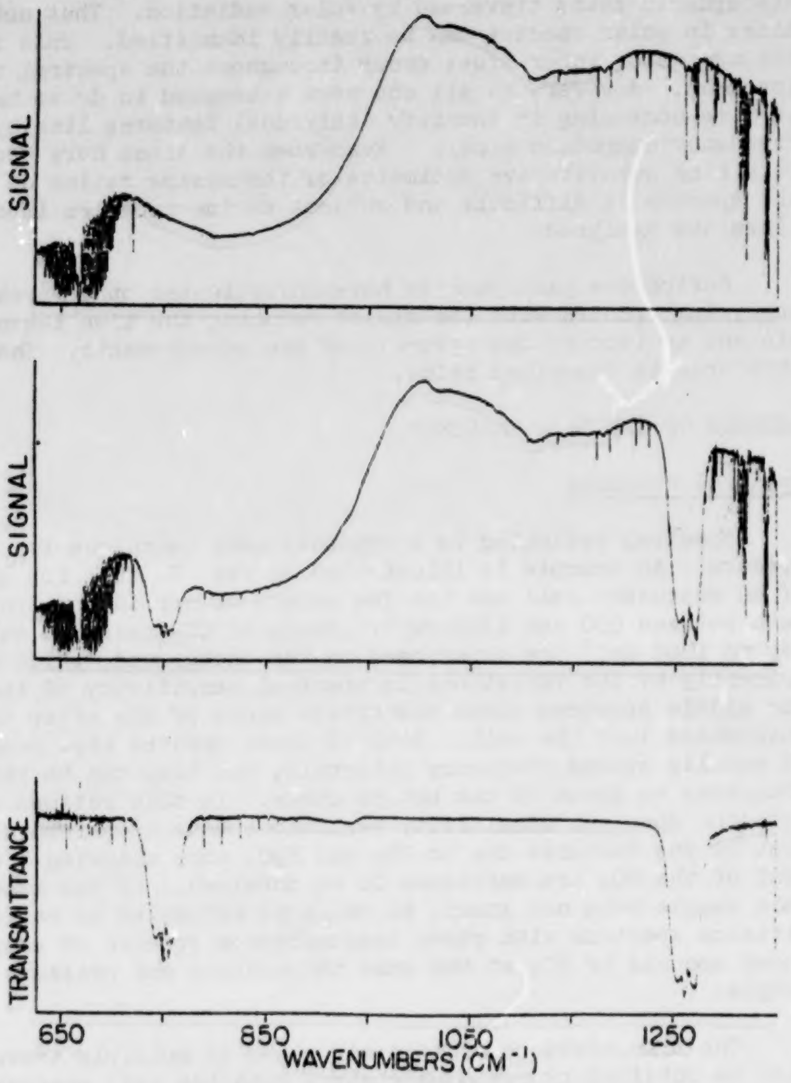

Fig. 7a - Background spectrum of evacuated absorption cell between 650 and 1350 cm^{-1}

7b - Spectrum of absorption cell containing a sample of NO_2 and N_2O_4

7c - Ratio of spectrum b/spectrum a

Ohio. The precision of the abundance values obtained by these techniques is not high, the uncertainty typically being of the order of 10%. This inaccuracy is caused in part by the noise level in the spectra and the uncertainty in the amount of gas in the standard sample. It has been found that most of the expected air pollutants occur at such low levels in the Columbus atmosphere that their absorption features cannot readily be detected with the path lengths (~ 1 km) and spectral resolution available, and that, as indicated in Fig. 3, the longer path lengths obtained in solar spectra are required. Unfortunately solar spectra cannot readily be ratioed with spectra of individual gases because:

1. It is not possible to obtain a background spectrum for solar spectra.
2. The temperature and pressure vary along the atmospheric path traversed by the solar energy and these effects cannot readily be simulated in the laboratory.
3. The large amounts of H_2O in the solar path cannot be obtained in laboratory spectra.

Comparison of observed spectra and synthetic spectra

In view of the difficulties noted above, we have considered the information obtained by comparing air spectra, and in particular, solar spectra with calculated spectra. Synthetic spectra can be calculated provided the parameters of all the absorbing lines of atmospheric gases in the spectral region of interest are known and the pressure, temperature, path length, and the mixing ratios of the absorbing gases are specified. This information can then be used with Eq. (5) and (6) to calculate the transmittance of the path.

Recently the Air Force Cambridge Research Laboratory (AFCRL) - now the Air Force Geophysics Laboratory (AFGL) - has prepared a listing of the parameters of atmospheric lines (20) which we have used to calculate synthetic atmospheric spectra corresponding to observed spectra. This work, described in an Interim Technical Report (21), shows observed and calculated spectra over the region from 700 to 2300 cm^{-1} for approximately 10, 100, and 1000 m paths of ground level air and for high and low sun spectra observed at Columbus, Ohio. A letter to the editor of Applied Optics describing this atlas has been accepted for publication and is included as Appendix III of this report. Comparisons of the observed and calculated spectra in this atlas show that, in general, the line positions and relative intensities in the calculated spectra are in good agreement with those in the observed spectra, over the entire region. These spectra are intended to serve as references for the continuing detailed analysis of such spectra.

A detailed line-by-line comparison of these observed and calculated spectra has been made over the past year. Instances of incorrect line positions and relative intensities, and, in some cases, missing lines, are found in the calculated spectra. Most of these differences can be seen by comparing the spectra in the interim report (21) and are not described here. Caution must be exercised in the use of calculated spectra until the accuracies of the line parameters have been verified.

One of the conclusions reached from these comparisons is that absorption features due to gases whose line parameters are not given in the line listing do not give recognizable features in the ground level air spectra and these features are also difficult to identify even in solar spectra because of one or more of the following reasons:

1. They may not consist of discrete lines but rather form a continuous absorption band which is difficult to recognize due to the presence of the absorption lines of the permanent gases.
2. They are too weak to be observed, even if they consist of discrete lines.
3. They lie in spectral regions occupied by features of other gases which interfere with the identification.

Some of these problems are indicated in Fig. 4.

The calculated spectra have, however, allowed absorption features of F-12 to be identified in solar spectra and estimates of its tropospheric abundance to be obtained. A preliminary account of this work was presented in an earlier report (22). A more detailed description of these results will be published in Applied Spectroscopy later this year and a preprint of this paper is given in Appendix III.

The weakness of the F-12 features in these spectra is typical of that expected for many other trace atmospheric gases. Laboratory spectra of relatively large amounts of $CHClF_2$, $CHCl_2F$, CCl_4, and CCl_3F are shown in Fig. 8 together with a corresponding portion of a ground level solar spectrum between 760 and 900 cm^{-1}. Most of the structure in the solar spectrum is due to H_2O and CO_2 and this obscures the weak features of the halocarbons if they are present. This spectral region is of interest because the observed low sun solar spectra (21) show a series of regular spaced weak lines between approximately 800 and 820 cm^{-1} which do not appear in the calculated spectra. By comparing laboratory spectra of CO_2 with the corresponding calculated spectra, as shown in Fig. 9, the weak lines in the solar spectrum have been identified with CO_2, although we have not been able to assign the vibration rotation band to where they belong. Similar comparisons of laboratory spectra and calculated spectra for other gases are described elsewhere in this report.

Progress in ratioing observed and synthetic air spectra

Analysis of ground level air spectra--

The identification of F-12 features in solar spectra has illustrated the usefulness of the synthetic spectra. In their present form these

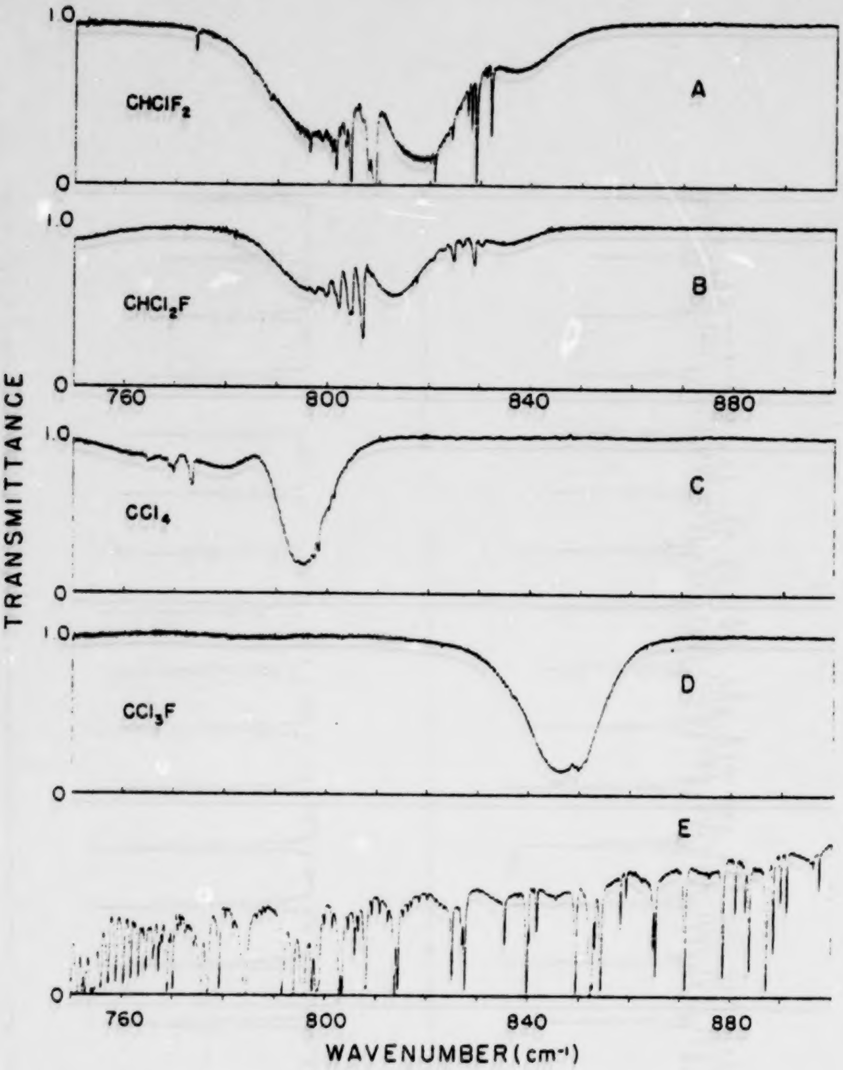

Fig. 8a - Laboratory spectrum of CHCCF$_2$ between 760 and 900 cm^{-1}
8b - Laboratory spectrum of CHCl$_2$F between 760 and 900 cm^{-1}
8c - Laboratory spectrum of CCl$_4$ between 760 and 900 cm^{-1}
8d - Laboratory spectrum of CCl$_3$F between 760 and 900 cm^{-1}
8e - Ground level solar spectrum between 760 and 900 cm^{-1}

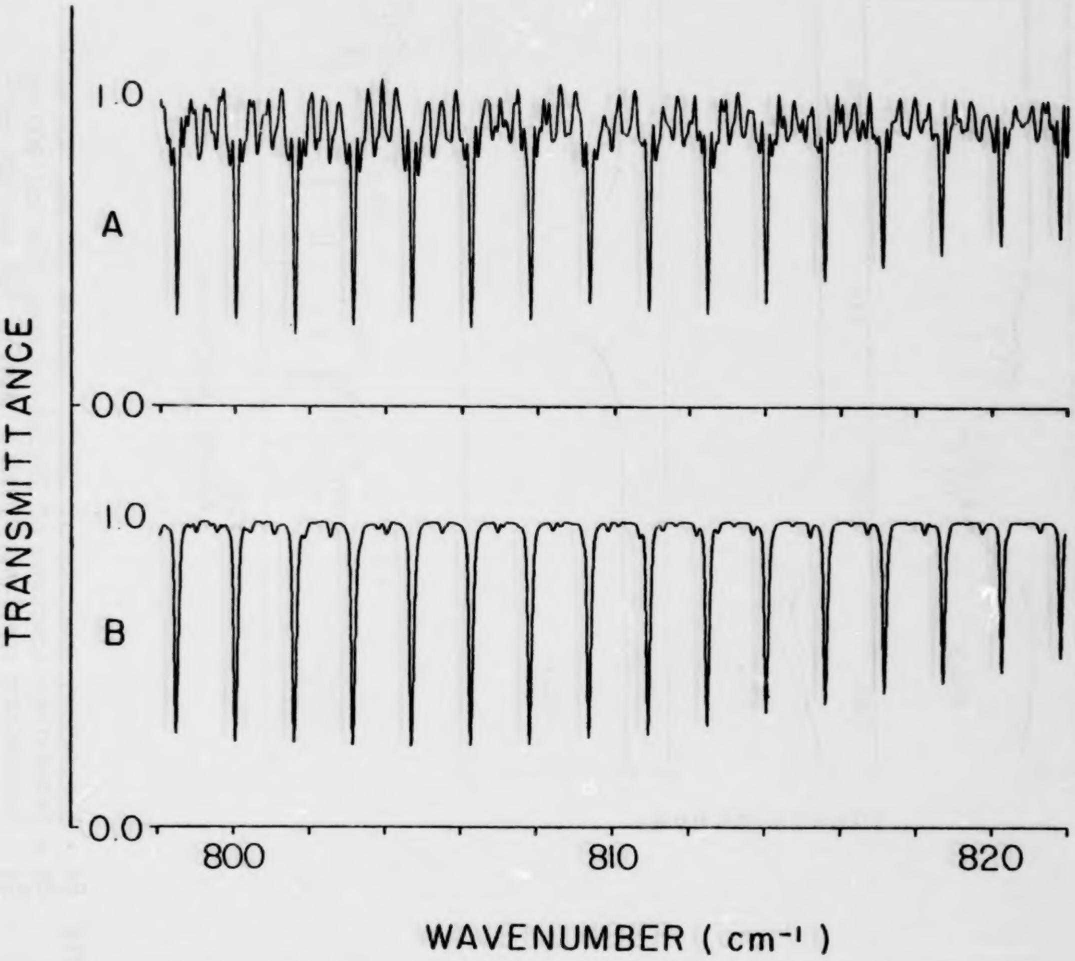

Fig. 9a - Spectrum of 51 Torr CO_2 in 171 m path at 295 K between 800 and 820 cm^{-1}
9b - Calculated spectrum of Co_2 for the same conditions

calculated spectra are not suitable for the quantitative determination of the abundances of pollutants or other permanent gases primarily because a relatively large change in the abundance ($\approx 20\%$) of a gas causes a much smaller change ($\approx 5\%$) in the peak absorptance of a typical line. These changes are difficult to detect by visual comparisons of the spectra. A higher accuracy may be achieved by ratioing observed and calculated spectra. As discussed earlier, this technique, provided the line parameters used are accurate, will allow estimates of the permanent gas abundances to be made and, at the same time allow these features to be "removed" from the spectra to reveal the underlying structure due to other gases.

Several difficulties were encountered in attempting to ratio observed and computed spectra. These included the limited capability of the present spectrometer system which does not allow the required computations to be performed readily. The university IBM 370 computer has therefore been used to perform the ratioing. This required devising methods of allowing the IBM computer to read the magnetic tapes containing spectral information generated by the spectrometer. We wish to acknowledge the assistance of Dr. Peter Griffiths of Ohio University in developing this latter procedure. It was found that the IBM computer was unable to read the end of file markers put on the tape by the spectrometer. For several months this necessitated transferring only a single spectrum to each tape read by the IBM computer and caused delays in the data processing. During a visit by a spectrometer engineer it was found that this defect was due to the spectrometer system and several spectral files can now be read from each tape.

The program used for calculating the spectra in the air atlas was then modified to allow transmittances to be calculated at the same frequency intervals as on the observed spectra. These spectra are obtained from interferograms. If the beginning and ending frequencies in its observed spectra are ν_1 and ν_2 respectively, and these are N points in the spectra, then spectral information is obtained at discrete spectral intervals $\Delta\nu$ when

$$\Delta\nu = (\nu_2 - \nu_1)/(N - 1) \ . \tag{7}$$

A test of the feasibility of ratioing observed and calculated spectra was made by analyzing a spectrum of CO. A description of this work is given in Appendix III which is a preprint of an article to be published in Applied Optics later this year. This study showed that estimates of the abundance of a gas in the sample can be obtained from such ratios. For the particular spectrum analyzed it was necessary to match the positions of the observed and calculated line positions to better than 0.002 cm^{-1} and to match the spectral resolutions of the spectra to better than 5% in order to obtain the best ratio (indicated by the best approximation to a straight line). Under these conditions abundances were obtained, for the case of the CO spectrum analyzed, to better than 10%. Although reasonably accurate abundances are obtained by this procedure the trial and error process of matching the spectra was time consuming both to the computer and to the operator.

This technique was then applied to the analysis of the spectrum of a 171 m path of ground level air at 294 k and 700 Torr between 2170 and 2250 cm^{-1} shown in Fig. 10(d). The absorption lines are due to CO, N_2O, CO_2, and H_2O. Curves a, b, and c of Fig. 10 show calculated spectra of CO, CO_2, and N_2O respectively corresponding to the amounts of these gases in the air spectrum. The results of ratioing these spectra are shown in Fig. 11. The top curve in Fig. 11 shows the result of ratioing out the CO lines, the next curve shows the air spectrum with both CO and CO_2 removed and curve c shows the air spectrum with CO, CO_2, and N_2O removed. By trial and error matching of these spectra the abundances shown in Table I were obtained. The estimated precisions of these abundances were obtained by calculating spectra of varying amounts of these gases until significant deviations from a straight line were noted in the ratioed spectra. It should be noted that if the values of the line parameters in the AFCRL listing are incorrect systematic errors in the abundances will be made. No uncertainty is given for the CO_2 abundance because of the difficulties in ratioing the spectra.

Table I. Abundances of CO, N_2O, and CO_2 Obtained by Ratioing Observed and Calculated Spectra of a 171 m Air Path

Gas	Abundance (ppm)
CO	0.78 ± 0.03
CO_2	320
N_2O	0.29 ± 0.02

Examination of Fig. 11(c) reveals two weak absorption features at 2186.9 cm^{-1} and 2205.2 cm^{-1}. These are weak water vapor lines which have not been ratioed out although these line parameters are included in the AFCRL line listing.

The poor ratioing of the CO_2 lines indicates errors in the values of the parameters of these lines. This effect is shown in more detail in Fig. 12. A small portion of a CO_2 spectrum from 2230 to 2250 cm^{-1} from Fig. 10 is shown in curve c, curve b shows the corresponding calculated spectrum of CO_2, and the ratio is seen in curve a. Both line shifts and relative line intensity differences can be recognized in the ratioed spectrum. These differences do not appear as large for either the CO or N_2O parameters.

It would also have been possible to obtain estimates of the abundances of the individual gases by ratioing the spectra in Fig. 10 against

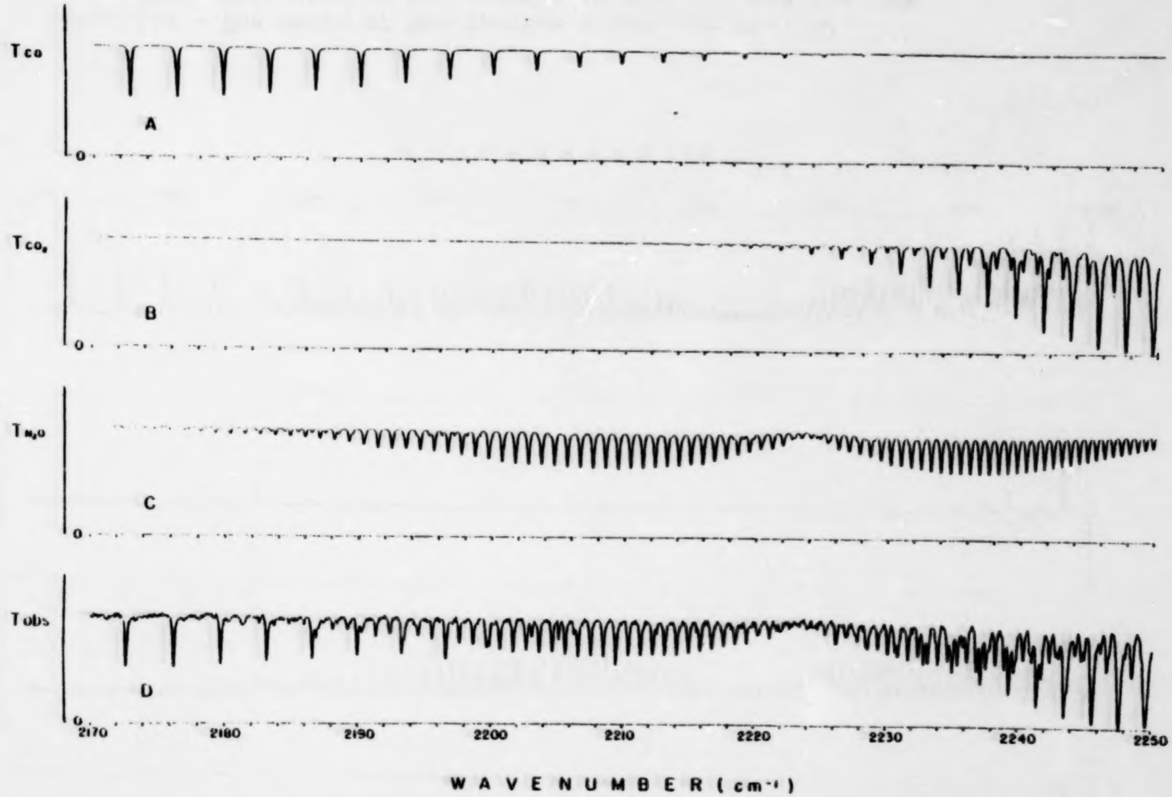

Fig. 10a - Calculated spectrum of CO between 2170 and 2250 cm^{-1}
10b - Calculated spectrum of CO_2 between 2170 and 2250 cm^{-1}
10c - Calculated spectrum of N_2O between 2170 and 2250 cm^{-1}
10d - Observed spectrum of 171 m of air at 294 K and 700 Torr

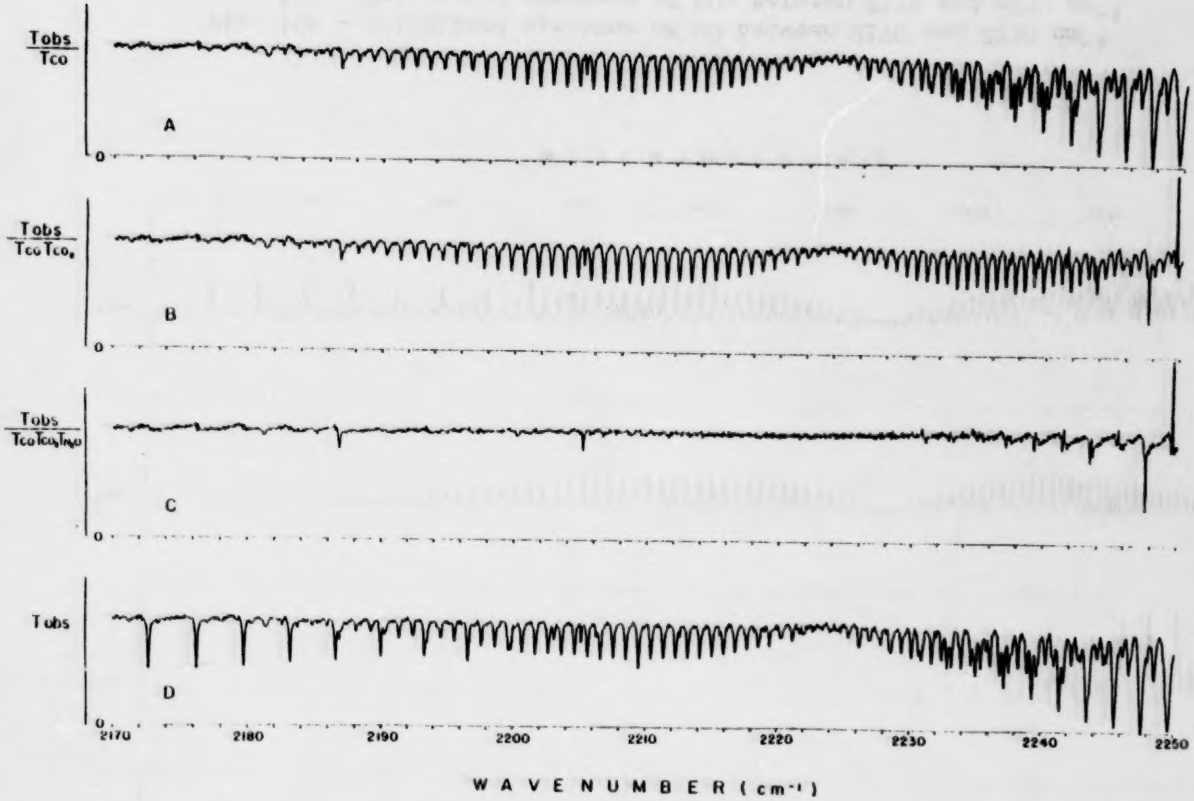

Fig. 11a - The ratio of the spectra d and a in Fig. 10
11b - The ratio of the spectra in Fig. 11a and Fig. 10b
11c - The ratio of the spectra in Fig. 11b and Fig. 10c
11d - Observed spectrum of 171 m of air at 294 K and 700 Torr

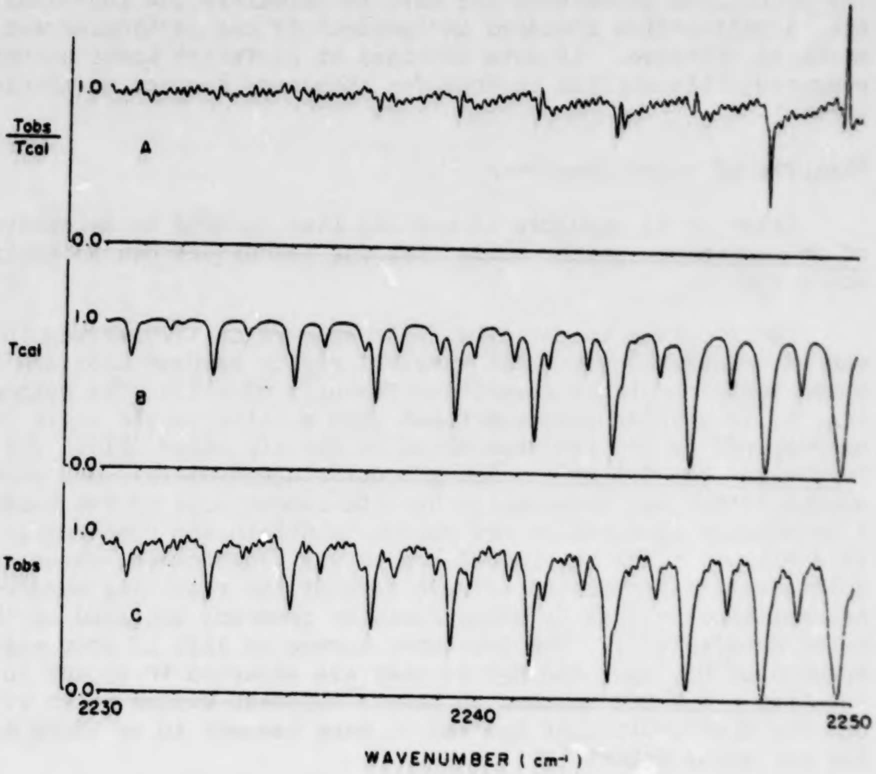

Fig. 12a - Ratio of the spectra in c and b
12b - Calculated spectrum of CO_2 between 2230 and 2250 cm^{-1}
12c - Observed spectrum of CO_2 broadened to atmospheric pressure with air

observed spectra of the individual gases. These abundance values would depend on the accuracy with which the amounts of the gases in the standard spectra are known. The reproducibility of transmittance measurements in most infrared measurements is rarely better than a few percent. If the AFCRL line parameters are used to calculate the individual gas spectra, a calibration standard independent of the particular set of experiments is obtained. If data obtained at different institutions are to be compared, this ability to transfer standards becomes particularly important.

Analysis of solar spectra--

Since it is possible to use the line listing to calculate spectra of inhomogeneous paths, these ratioing techniques can be applied to solar spectra.

Our progress in ratioing solar spectra is illustrated in Figs. 13 and 14. These show a small spectral region between 1155 and 1165 cm^{-1} which contains strong absorption features of F-12. The bottom curve in Fig. 13 is a solar spectrum taken with a solar zenith angle of 45° and corresponds to the spectrum shown in the air atlas (21). The nominal resolution was 0.1 cm^{-1}. The air atlas spectrum (21) was shown with essentially box car apodization but, to remove some of the worst features, a triangular apodization was chosen to obtain the spectrum in Fig. 13(d). In addition, after the interferogram was transformed, three additional points were interpolated between each of the resulting observed spectral transmittance values by using computer programs supplied by the spectrometer manufacturer. The top three curves in Fig. 13 show calculated spectra of O_3, N_2O, and H_2O as they are expected to appear in the solar spectrum. N_2O was assumed to have a constant mixing ratio with height, but the distribution of H_2O and O_3 were assumed to be those described in the air atlas report (21).

The results of removing O_3, N_2O, and H_2O features from the solar spectrum are shown in Fig. 14. Figure 14(a) is a laboratory spectrum of a trace amount of F-12. Figure 14(b) shows the ratioed solar spectrum after removal of O_3, N_2O, and H_2O features. The calculated and observed solar spectra are shown in Fig. 14(c) and 14(d), respectively. The weak feature in the ratioed spectrum near 1161 cm^{-1} agrees in position and contour with the strongest feature in the laboratory spectrum of F-12 although the other features are too weak to be seen in the ratioed spectrum. From the amounts of gases required to obtain the calculated spectra in Fig. 13 the total amounts of O_3, N_2O, and H_2O in a vertical path through the atmosphere can be determined. The amount of N_2O was determined to correspond to a mixing ratio of 0.23 ppm. This is a much lower number than expected. It has not yet been determined if this is due to inaccuracies in the program used or the line parameter listing.

The residual fluctuations in Fig. 14(b) are due partly to the inherent noise in the observed spectrum. Part is also caused by inaccuracies in the line parameters - the shift of the H_2O line at 1164 cm^{-1} is

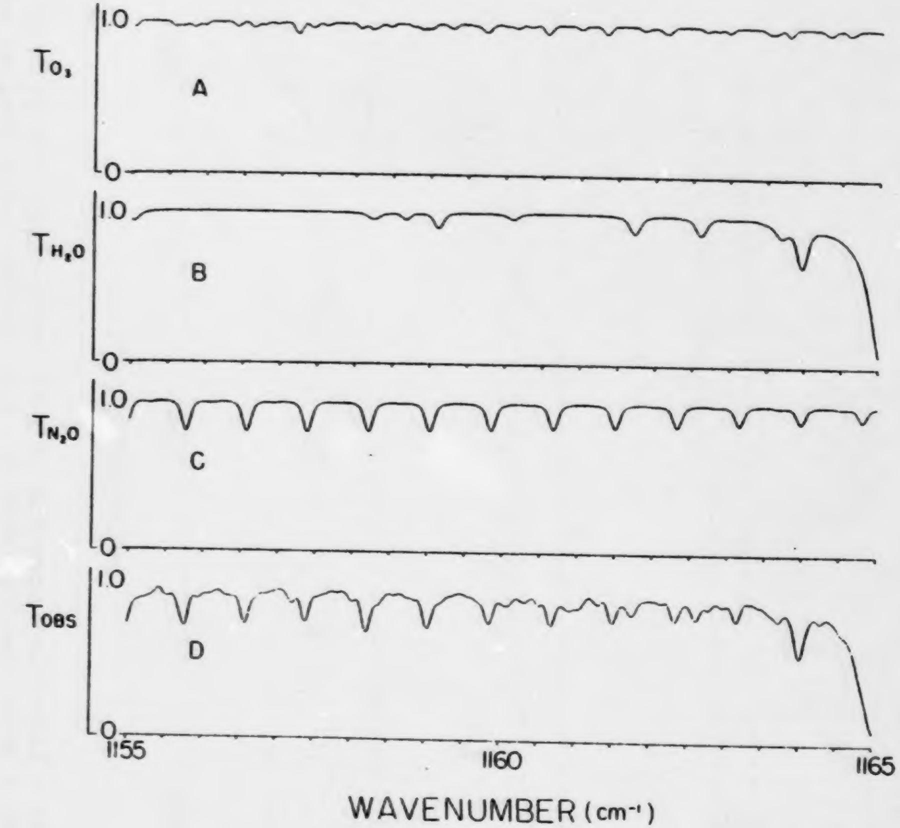

Fig. 13a - Calculated spectrum between 1155 and 1165 cm^{-1} of O_3 in an atmospheric slant path
13b - Calculated spectrum between 1155 and 1165 cm^{-1} of H_2O in an atmospheric slant path
13c - Calculated spectrum between 1155 and 1165 cm^{-1} of N_2O in an atmospheric slant path
13d - Observed solar spectrum (solar zenith angle 45°)

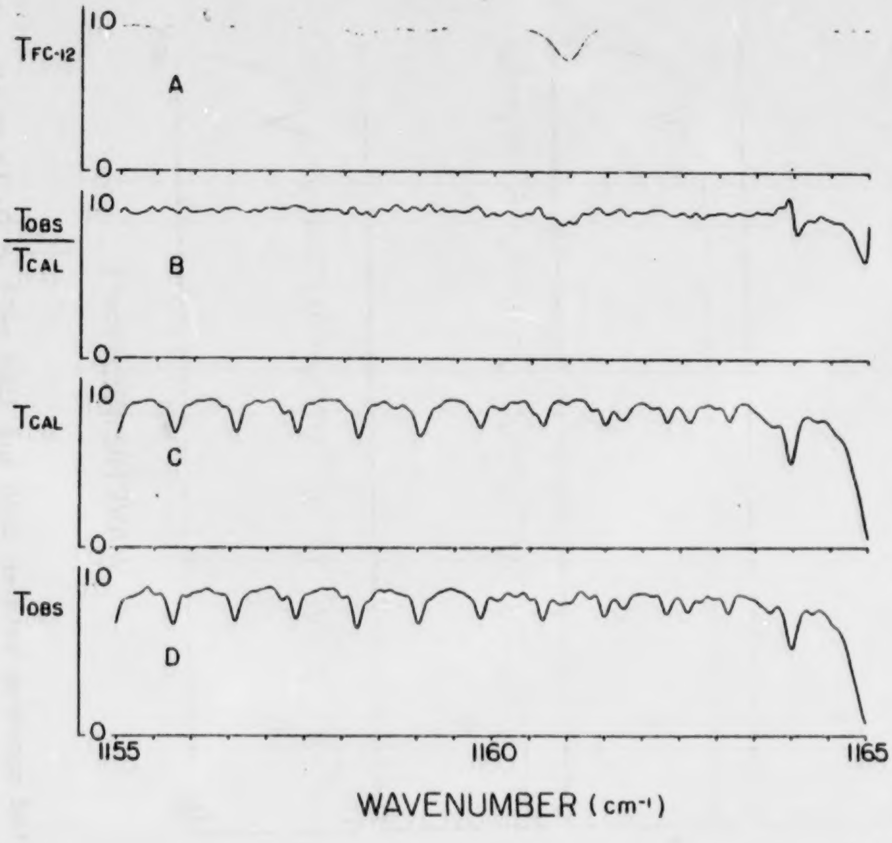

Fig. 14a - Laboratory spectrum of F-12 between 1155 and 1165 cm^{-1}
14b - Solar spectrum with O_3, N_2O, and H_2O lines ratioed out
14c - Calculated solar spectrum
14d - Observed solar spectrum

particularly obvious - and also to approximations in the model used to represent the atmospheric path, to uncertainties in the actual pressure and temperature variations with height in the atmosphere on the day the spectrum was obtained, to possible deviations in the actual O_3 and H_2O distributions from those assumed in the model, and to incorrect line shapes - a Voigt line profile would be more appropriate than the Lorentz line shape in representing the shapes of the O_3 lines. We are currently investigating some of these effects to determine their influence on our measurements.

The abundance of F-12 was estimated by measuring the equivalent width of the absorption feature near 1161 in the ratioed spectra of Fig. 14(b) and by using the laboratory calibration curve shown in Appendix V. A value of 80 parts per trillion was obtained if a uniform mixing ratio in the troposphere is assumed. This value is in reasonable agreement with the value of 110 ppt obtained in Appendix III. The present results must be regarded as tentative until more data have been analyzed.

Abundances by using linear regression techniques

The precision we have obtained for the abundances of gases found by ratioing observed and calculated spectra of both homogeneous or inhomogeneous paths is of the order of 10%. This uncertainty is due partly to the noise level in the original spectra and also to the method of estimation which relies on an observer making judgments of the goodness of the ratio point by point through the spectrum. If all the spectral information concerning the absorptance by a gas could be summarized in one measurement, an improved accuracy could be obtained. As pointed out by Harries and Chamberlain (23) this approach has been used by a number of workers in designing instruments to detect the presence of a gas by correlation methods. Examples of such instruments include the Barringer Research Corporation correlation spectrometer (24), the selective chopper and pressure modulated spectrometers described by Houghton et al. (25, 26), Smith et al. (27), and Goody (28).

The concept of spectral correlation to determine abundances of atmospheric gases from the direct analysis of spectra has also been discussed by Derr et al. (29). Other approaches to this problem are discussed below.

The monochromatic absorbance $A(\nu)$ at frequency ν of a single gas in a homogeneous sample is obtained from Eq. (2)

$$A(\nu) = \ell n - P(\nu)/P_0(\nu) = k(\nu)u \;, \tag{8}$$

when u is the amount of absorber in the sample and $k(\nu)$ is the sum of the absorption coefficients of all the lines at frequency ν. Provided $P_0(\nu)$ is known, an estimate of the abundance of the gas can be obtained at each frequency at which the gas absorbs

$$u_i = A(\nu_i)/k(\nu_i) \;. \tag{9}$$

If the abundance is determined at N positions in the spectrum the average value of the abundance $\bar{u}$

$$\bar{u} = (1/N) \sum_{i=1}^{N} A(\nu_i)/k(\nu_i) \; . \qquad (10)$$

If all the measurements are of equal weight then the precision in determining $\bar{u}$ will be increased over that of a single measurement by a factor of $\sqrt{N}$. Many bands of gases extend over intervals of 50 cm^{-1} or more, and if spectra of 0.1 cm^{-1} resolution are obtained, as with our interferometer, there will be ~ 800 observations over such bands causing an increase in the precision by a significant factor. If the measurements are not of equal weight the precision can be increased by suitably weighting the individual observations.

The above method is not directly applicable to the analysis of most air spectra because of the overlapping of lines and bands which occurs throughout the spectrum. In this case Eq. (8) must be modified,

$$A(\nu) = \ell n\,(-P(\nu_i)/P_0(\nu_i) = \sum_{j=1}^{m} k_j(\nu_i)u_j \qquad (11)$$

when m is the number of gases which absorb in the spectral region investigated. Again, provided the absorbance can be measured at a sufficient number, N, of frequencies and provided the absorption coefficients of each gas are known, the abundances of the individual gases can be obtained by solving the N equations of the form of Eq. (11) by standard mathematical procedures of linear regression (30).

The absorption coefficients of the individual gases can be obtained from spectra obtained with the same instrument (it is implicitly assumed that all the measurements will be made at the same spectral resolution) or from calculated spectra. In order to obtain the calculated absorption coefficients it is necessary to find the spectral transmittance $T'(\nu)$ of a known amount of the gas u_F for the same spectral resolution as the spectrum to be analyzed:

$$T'(\nu) = \int \left[\exp{-k(\nu)\, u_F} \right] \sigma(\nu,\nu')\, d\nu' \Big/ \int \sigma(\nu,\nu')\, d\nu' \qquad (12)$$

where $k(\nu)$ is the monochromatic absorption coefficient and $\sigma(\nu,\nu')$ describes the shape of the instrument spectral response function and the integration is carried out over the region when $\sigma(\nu,\nu') > 0$. In our work we have used both triangular and Gaussin shapes for this function.

It is then assumed that Beer's Law holds for the observed transmittance and that an apparent absorption coefficient can be obtained from

$$T'(\nu) = \exp(-k'(\nu)\, u_F) \qquad (13)$$

when $k'(\nu)$ is dependent on spectral resolution. The same assumption is also made when the absorption coefficient is derived from direct measurements of spectra.

We have tested this assumption on computer generated spectra. For the few cases so far investigated this appears to be a reasonable approximation provided the range of abundances for which a given value of $k'(\nu)$ is assumed is not large. We plan to make more extensive investigations of this assumption for various gases and spectral resolutions as time permits. This assumption is also made for cases when the absorption coefficients are obtained from experimental spectra and again it appears to be valid over small abundance ratios and is universally used in quantitative spectroscopy to obtain concentrations of absorbers in samples.

This method of analysis has been used to obtain the abundances of CO, N_2O, and H_2O in the air path giving rise to the spectrum shown in Fig. 10(d). Absorption coefficients for the individual gases were calculated from Eqs. (12) and (13) and the AFCRL line parameters listing and by choosing values for u_F and the spectral resolution equal to those obtained from the direct ratioing method. A small section of these tabulated values is shown in Table II.

In this table, which also contains information discussed in a later section, the final column shows the wavenumber for which the information shown in the other columns was calculated. The penultimate three columns show values relating to the degraded absorption coefficients of N_2O, CO, and H_2O. The values actually shown are the $k_i(\nu)\ \rho_i \ell$ products defined by Eq. (3) where $\ell = 171$ m and the ρ_i values were obtained from Table I. An arbitrary value of 2.72×10^{-3} was assumed for the H_2O mixing ratio (this spectrum was taken during the winter months).

The abundances were then determined by analysing the sections of the spectrum shown in Fig. 15 and assuming that the incident power $P_0(\nu)$ corresponded to the straight line shown in Fig. 15. The results are shown in Table III, which gives the ratio of the abundances determined by the linear regression method to those given in Table I. There is a considerable improvement in the precision compared with that obtained by direct ratioing of the spectra and the results are consistent with the previous values. No information concerning H_2O was obtained from the region from 2190 to 2200 cm^{-1} since there is no significant absorption in this region. The differences between the values of the abundances determined from the different spectral regions may be due to the incorrect placement of $P_0(\nu)$, or to small errors in the line parameters which would not be detectable by spectral ratioing of our spectra.

The effect of varying the position of $P_0(\nu)$ on the abundances is shown in Table IV. The abundances were determined by analysing the entire spectral region from 2190 to 2210 cm^{-1} and by changing $P_0(\nu)$ by ± 1% from its previous position. Although the precision of measurement was essentially unchanged, the fractional change in the position of $P_0(\nu)$ is

Table II. Absorption Coefficients of CO, N_2O, and H_2O Calculated from the AFCRL Listing and for a Spectral Resolution of 0.075 cm^{-1} Between 2000 and 2505 cm^{-1}

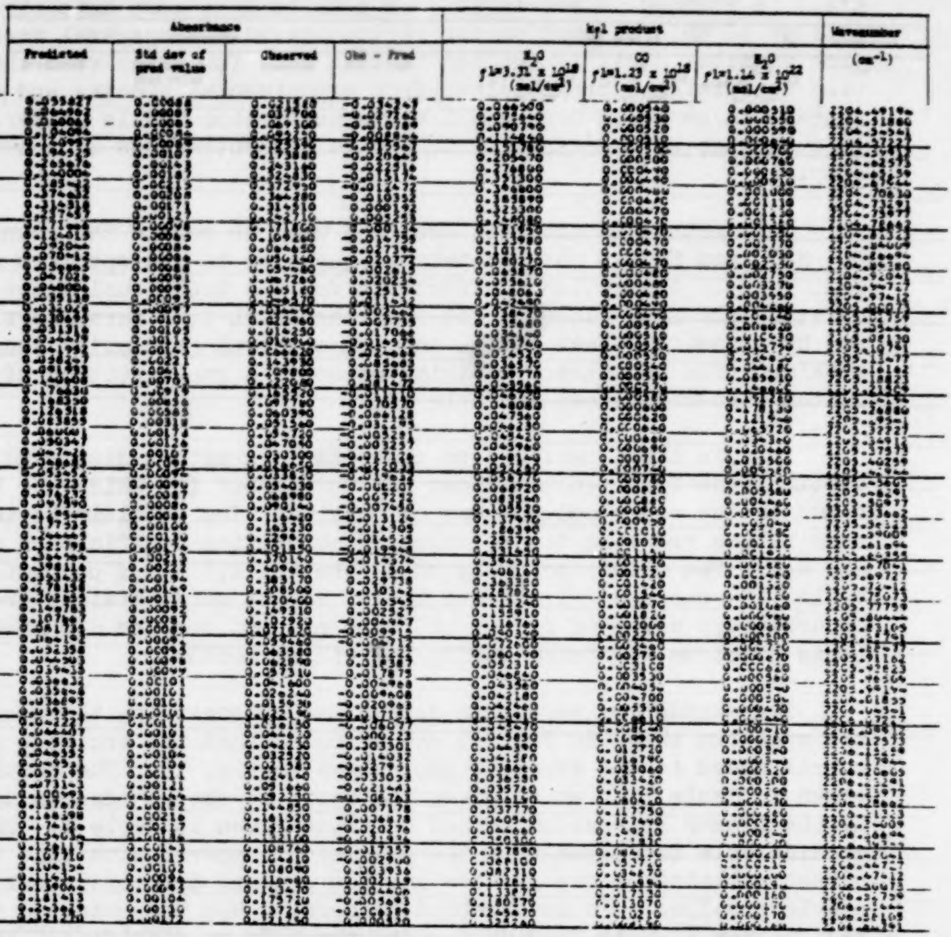

Absorbance				Kρl product			Wavenumber
Predicted	Std dev of pred value	Observed	Obs − Pred	H_2O $\rho l = 3.31 \times 10^{18}$ (mol/cm^2)	CO $\rho l = 1.23 \times 10^{18}$ (mol/cm^2)	H_2O $\rho l = 1.14 \times 10^{22}$ (mol/cm^2)	(cm^{-1})

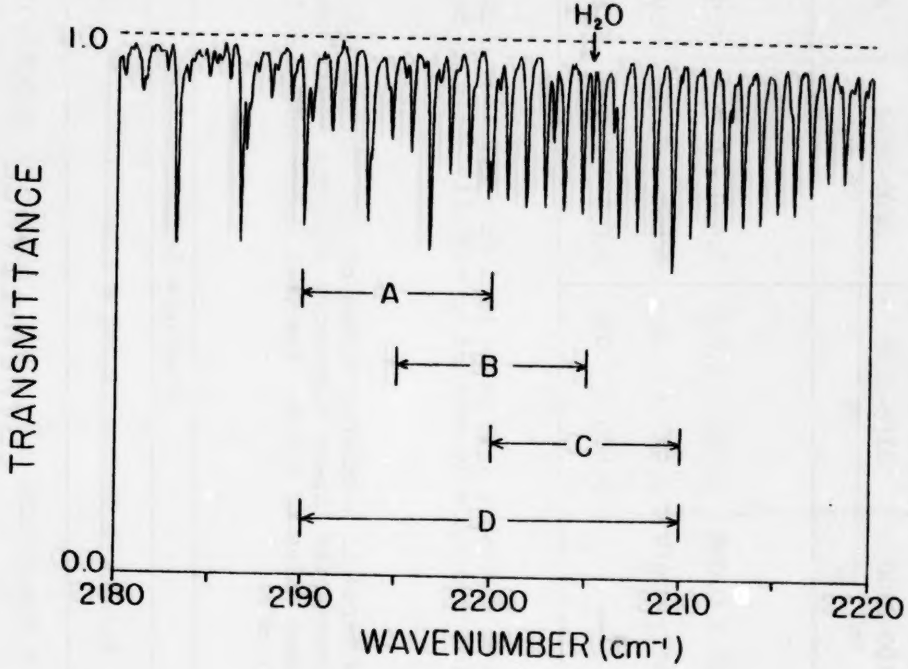

Fig. 15 - Portion of a spectrum of 171 m path of air at 294 K and 700 Torr. The intervals chosen for the linear regression method of obtaining abundances are indicated together with the position of the H_2O line and the $P_0(\nu)$ position.

Table III. Dependence of Abundance Values of N_2O, CO, and H_2O Determined by Unweighted Linear Regression Analysis of Air Spectra on Spectral Regions Analyzed. $P_o(\nu)$ is 1.00 in All Cases

	Abundance Ratio*			
Spectral Region / Gas	2190-2200 cm^{-1}	2195-2205 cm^{-1}	2200-2210 cm^{-1}	2190-2210 cm^{-1}
N_2O	0.918 ± 0.009	0.933 ± 0.008	0.958 ± 0.007	0.947 ± 0.005
CO	0.941 ± 0.014	0.928 ± 0.023	0.867 ± 0.038	0.917 ± 0.014
H_2O	—	0.680 ± 0.056	0.655 ± 0.059	0.660 ± 0.051

*This value is the abundance determined by linear regression divided by the corresponding abundance determined by visually ratioing the spectra (see Table I).

Table IV. Dependence of Abundance Values of N_2O, CO, and H_2O Determined by Unweighted Linear Regression Analysis of Air Spectra on Assumed Value of $P_o(\nu)$. Spectral Region Analyzed 2190 to 2210 cm^{-1}

	Abundance Ratio*		
Gas	$P_o(\nu) = 0.99$	$P_o(\nu) = 1.00$	$P_o(\nu) = 1.01$
N_2O	0.897 ± 0.006	0.947 ± 0.005	0.997 ± 0.005
CO	0.883 ± 0.017	0.917 ± 0.014	0.950 ± 0.013
H_2O	0.595 ± 0.061	0.660 ± 0.051	0.724 ± 0.048

*This value is the abundance determined by linear regression divided by the best value obtained by visual ratioing of the spectra (see Table I).

reflected as a much larger fractional change in the abundances. It is clear that it is necessary to determine the position of $P_O(\nu)$ accurately to avoid systematic errors and that the calculated precision does not reflect the absolute accuracy.

Other errors may occur if there are additional unrecognized absorption features present. A suitable strategy to avoid these difficulties in the case when the abundance of a known atmospheric constituent is to be determined is to ratio observed and calculated spectra and look for additional features before analyzing with the linear regression method.

Non Linear least squares methods of obtaining abundances

The linear regression method of determining abundances gives results which have a higher precision than can be obtained by direct ratioing of spectra but requires the position of $P_O(\nu)$ to be guessed and the absorption coefficient of all the gases contributing to the absorption in the spectral region being investigated to be known. It is not always possible to estimate the position of $P_O(\nu)$ accurately, and since we also wish to locate unidentified absorption features an analytical method of searching for them is of value.

Recently Chang and Shaw (31) have described a non linear least squares method of retrieving line intensities and half widths from spectra degraded by a finite instrumental resolving power. A modification of this method can be used to determine both the abundances of gases and the best position of the $P_O(\nu)$ curve from analysis of observed spectra.

From Eqs. (11) and (13)

$$\ell n\, P'(\nu_i) = \ell n\, P_O(\nu_i) - \sum_{j=1}^{m} k_j'(\nu_i)\, u_i \ , \qquad (14)$$

where $P'(\nu_i)$ is a measure of the power in the observed spectrum at ν_i and $k_j'(\nu_i)$ is the apparent absorption coefficient of the jth absorbing gas. If the shape of $P_O(\nu)$ is assumed to be of the form

$$P_O(\nu_i) = a + b(\nu_i-\nu_O) + c(\nu_i-\nu_O)^2 \ , \qquad (15)$$

when a, b, and c are constants and ν_O is some known frequency then

$$\ell n\, P'(\nu_i) = \ell n\left[a + b(\nu_i-\nu_O) + c(\nu_i-\nu_O)^2 \right] - \sum_{j=1}^{m} k_j'(\nu_i)\, u_i \ . \qquad (16)$$

If observations of $P'(\nu_i)$ are made at N frequencies in a given spectral region a series of N equations of the form of Eq. (16) is obtained which can be solved by the application of the non linear least squares method to retrieve the best values for a, b, c, and the abundances u_i. This program also gives the best fit calculated values $P_C'(\nu_i)$ and the differences $P'(\nu_i) - P_C'(\nu_i)$. If anomalous values of these differences occur, these can be interpreted as indicating the presence of unassigned absorption features.

We have used this method to analyze the three spectral regions shown in Fig. 15 of the 171 m air path spectrum. The results of the analysis are shown in Table V.

Other output from the analysis is shown in Table II. The first few columns in this table give the observed value of $\ln P'(\nu_i)$ as defined by Eq. (16), the calculated value $\ln P_C'(\nu_i)$ and its standard deviation and the difference between the observed and calculated values.

Inspection of the data in Table V and comparison with the values in Tables I, III, and IV shows that the precision of abundance determinations is similar to that obtained by the method of linear regression, but that the spread of the abundance values in Table V is considerably less than in Table III. This is attributed to the better determination of $P_O(\nu)$ by the non linear least squares method. The value obtained for $P_O(\nu)$ by considering the entire region from 2190 to 2210 cm^{-1} is close to one of the values assumed in Table IV ($P_O(\nu) = 1.01$) and the abundances determined for this value in Table IV agree well with the corresponding values and precisions in Table V indicating the uniqueness of the solutions.

Figure 16 shows the difference between the observed and calculated values (obtained from the set of constants shown in the last column of Table V) of $P(\nu)$ over the region from 2190 to 2210 cm^{-1}, the corresponding observed spectrum is shown in Fig. 16(b).

The abundances of CO and H_2O shown in Table V retrieved by analyzing different spectral regions agree within the accuracy of the measurements. The agreement between the different values obtained for N_2O are not so consistent, and this suggests the possibility of line parameter errors for this gas. The increasing N_2O abundances obtained as the frequency is increased indicates the relative intensities of tabulated line parameters decrease to higher frequencies. This has been verified by ratioing observed and calculated spectra of N_2O as shown in Fig. 17. It is seen that there are apparent line intensity anomalies near 2210 cm^{-1} and that, as indicated by the values in Table V, the calculated spectrum is weaker than the observed spectrum.

Comparison of spectra by using the interactive mode of computer operation

Several methods of obtaining abundances of gases by analyses of spectra have been discussed. We have stressed the comparison of observed and calculated spectra since this appears to be the only feasible method of analysing spectra of inhomogeneous paths such as solar spectra. However, the accuracy with which these abundances can be retrieved and the ability to locate unidentified spectral features in all of these methods

Table V. Dependence of the Abundance of N_2O, CO, and H_2O Determined by Non Linear Least Squares Analysis of Air Spectra on the Spectral Region Analyzed

Spectral Region Abundance Ratios	2190-2200 cm^{-1}	2195-2205 cm^{-1}	2200-2210 cm^{-1}	2190-2210 cm^{-1}
N_2O	0.956 ± 0.012	0.982 ± 0.011	1.012 ± 0.008	0.997 ± 0.007
CO	0.943 ± 0.013	0.957 ± 0.022	0.950 ± 0.035	0.940 ± 0.014
H_2O	—	0.790 ± 0.057	0.777 ± 0.054	0.736 ± 0.049
$P_0(\nu)$ Constants				
a	1.0005 ± 0.0020	1.0062 ± 0.0017	1.0044 ± 0.0037	1.0110 ± 0.0011
b	- 0.0036 ± 0.0009	- 0.00021 ± 0.00035	+ 0.0049 ± 0.0016	0.00034 ± 0.00011
c	- 0.00042 ± 0.00009	+ 0.00042 ± 0.00013	- 0.00048 ± 0.00014	- 0.000055 ± 0.000020

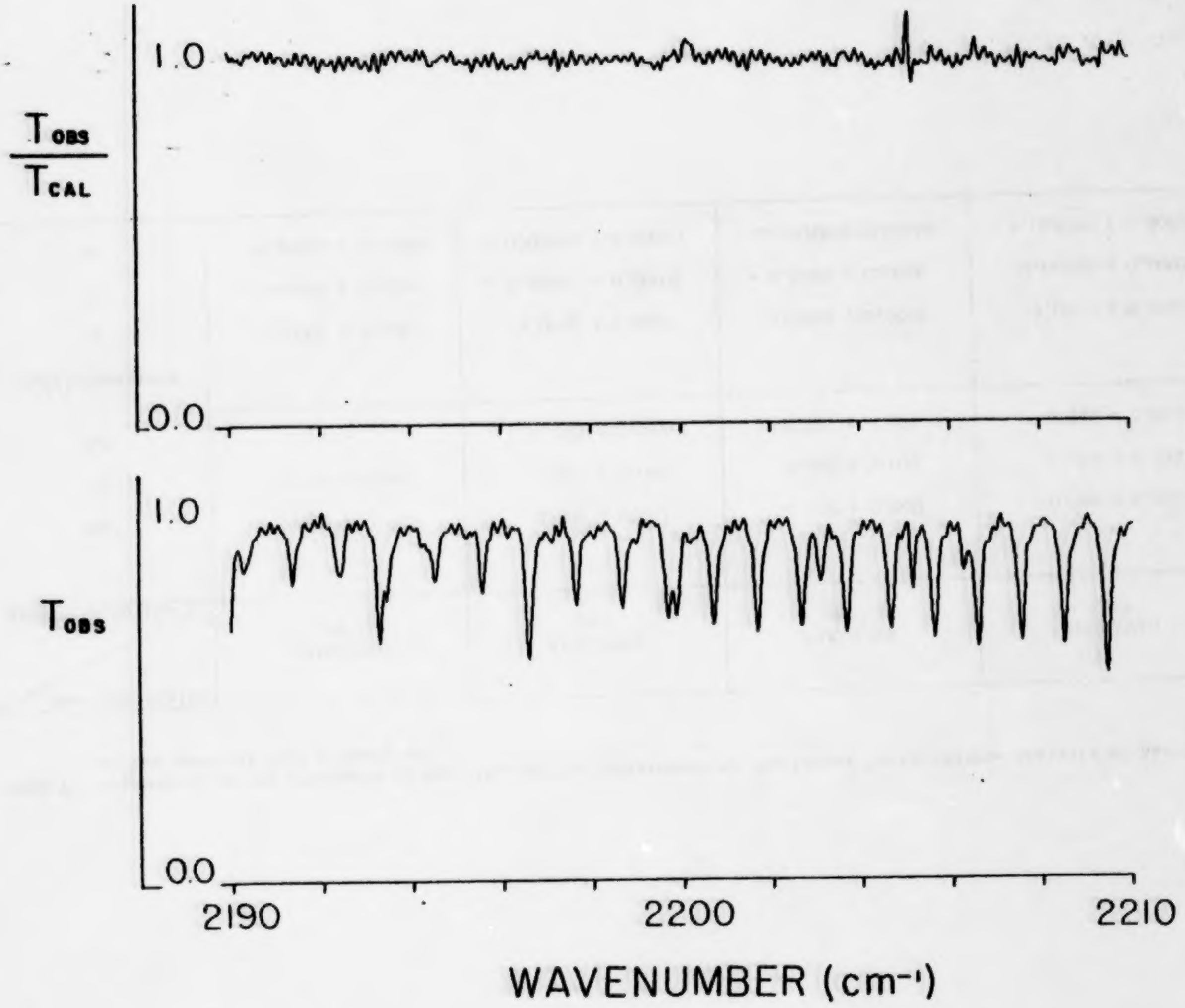

Fig. 16a - Ratio of observed $P(\nu)$ and values obtained from non linear least squares method

16b - Air spectrum between 2190 and 2210 cm^{-1}

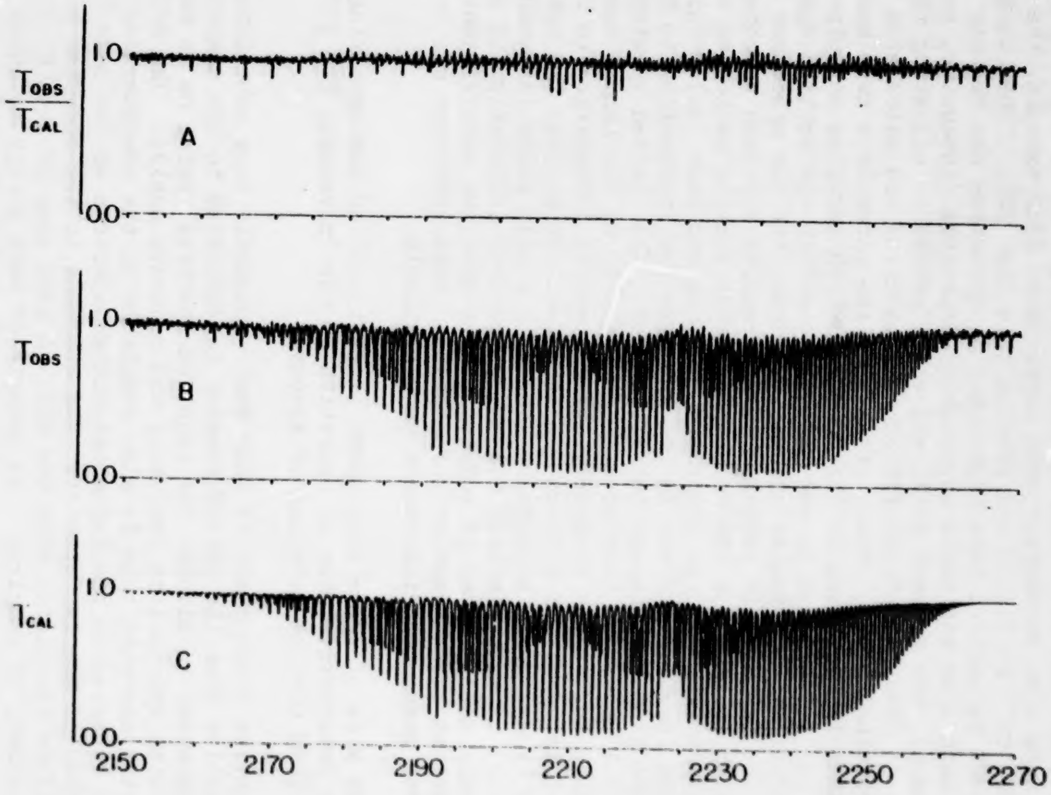

Fig. 17a - Ratio of spectra in Fig. 17b and 17c
17b - Observed spectrum of 1.52 x 10^{-3} Torr of N_2O and 100 Torr N_2 in 171 m path, at 294 K
17c - Calculated spectrum of N_2O for the same conditions as used to obtain Fig. 17b

depends on the accuracy with which the spectra can be calculated. It has been shown that the AFCRL line parameter listing is not completely accurate in its present form. Although improved versions of this listing are being prepared (32) it is desirable to incorporate changes based on our observations when necessary. Although in some instances only a few spectral lines in a spectral region have incorrect parameters (for example, the H_2O line near 1164 cm^{-1} in Fig. 14) in other spectral regions many line parameters need improvement (for example, the CO_2 lines near 800 cm^{-1} in Fig. 9 and 2240 cm^{-1} in Fig. 12). Other examples of incorrect parameters have been noted by Nordstrom and Skinner (33). Since each line has three adjustable parameters (intensity, position, and width), the present trial and error method of adjusting these parameters to obtain the best fit between observed and calculated spectra is excruciatingly slow. Thus, after the line parameters have been changed, a program is submitted to the computer which provides an output deck of cards to be submitted to the plotter to obtain the revised spectrum. Additional line parameter changes are made, and the procedure iterated until the best set is chosen. An alternative approach to obtaining the parameter is to apply the non linear least squares method to several lines in a spectral region as described by Chang and Shaw (31). This method has been investigated but is not suitable for application to the data obtained from the present interferometer. The limited spectral resolution (0.1 cm^{-1}) and limited storage capacity of the memory associated with this instrument typically allow spectral information to be obtained only at intervals of 0.05 cm^{-1} or greater. Thus, over the interval occupied by a typical absorption line with a half width (at atmospheric pressure) of approximately 0.1 cm^{-1}, spectral information is collected at a very small number of points. These data are insufficient to retrieve the desired line parameter information. This technique may be useful if a higher resolution instrument were available.

In view of these instrument limitations, we are exploring the use of the interactive mode of operation of the University IBM 370 computer to perform on-line ratioing of spectra.

In the first phase of this work a magnetic tape containing spectral information from the interferometer is submitted to the computer which is programmed to display the required spectral region on an oscilloscope (CRO) with appropriate frequency and ordinate scales. The AFCRL line parameter magnetic tape is also available to the computer and the computer can be asked to display a calculated spectrum on the same CRO and also the ratio of the two spectra. The commands to the computer are made from a teletype associated with the CRO. A hard copy of the CRO display can be obtained, if required. An example of such a copy is shown in Fig. 18. The top curve in this figure is the ratio of the two lower spectra. The middle curve is a calculated solar spectrum between 1158.0 and 1163.0 cm^{-1} for a spectral resolution of 0.25 cm^{-1} and the bottom spectrum is the observed solar spectrum. The ratio is not as flat as in some other spectra. The causes of this departure from flatness have not yet been established.

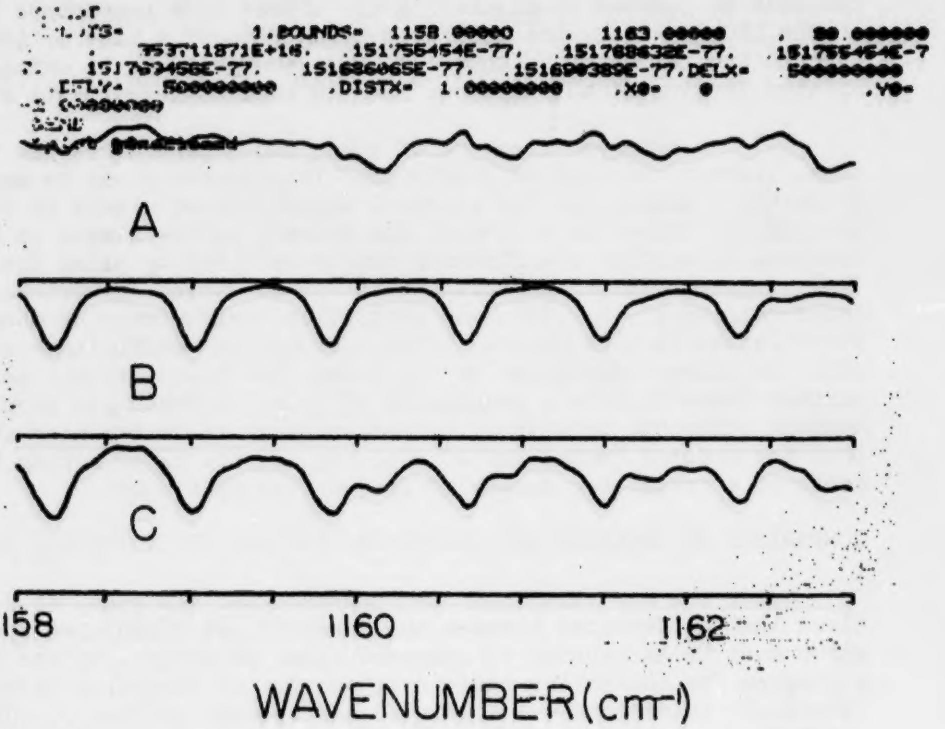

```
  .TS=          1.BOUNDS=  1158.00000     .  1163.00000     .  80.000000
    .  353711871E+16.  .1517554454E-77.  .1517688632E-77.  .1517554454E-7
7.   1517534456E-77.  .1516860065E-77.  .1516903389E-77.DELX=  .50000000
 .DELY=  .50000000     .DISTX=  1.00000000     .X0=  0              .Y0=
```

Fig. 18a - Ratio of the spectra shown in b and c
18b - Calculated solar spectrum corresponding to the conditions under which Fig. 18c was obtained
18c - Observed low sun spectra between 1158.0 and 1163.0 cm^{-1}, spectral resolution ~ 0.25 cm^{-1}, solar zenith angle 81°

Several applications of this system are under consideration.

(1) In spectral regions when the AFCRL line parameters are accurate, a rapid examination of observed air spectra for unidentified features can be made by ratioing observed and calculated spectra.

(2) Spectral regions when the AFCRL parameters are inaccurate can be identified and the particular gas whose lines are in error can be isolated. Laboratory spectra of this gas obtained under known conditions are compared with calculated spectra by the same method. The AFCRL tape can then be updated by displaying the stored line parameters for this gas on the CRO, changing the displayed parameters of a line or lines, and recalculating the spectrum until the desired agreement is obtained. This updated version of the tape can then be used to investigate air spectra.

(3) An observed spectrum of a gas whose parameters are not in the AFCRL listing can also be displayed. This spectrum can be manipulated to obtain a display of the spectral absorbance of a band or bands of the gas and, provided the amount of gas present in the sample is known, the spectral absorption coefficients can be obtained by using Eqs. (8) or (13). These absorption coefficients can be stored in various forms for later retrieval. A library of absorption coefficients of many gases can be collected in this manner. These absorption coefficients can be used with the linear regression or non linear least squares fit methods described above to obtain abundances of gases in other gas samples. These methods offer the promise of higher accuracy in determining abundances than the present techniques of ratioing spectra or of making hand measurements at a restricted number of frequencies in a band.

COMPARISON OF OBSERVED AND CALCULATED SPECTRA OF INDIVIDUAL GASES

After the air atlas had been prepared and analyzed, it was recognized that differences between the observed and calculated spectra exist which must be attributed to incorrect line parameters in the listing. A program for collecting individual spectra of the gases under controlled laboratory conditions was initiated and spectra of CO_2, O_3, CH_4, N_2O, CO, and H_2O were collected. Spectra of these gases for the same conditions were calculated and compared with the observed spectra. Some of these spectra are shown in Fig. 17 and Figs. 19 to 24.

Some differences between these spectra are readily apparent, but other differences which detract from the ability to ratio out features in air spectra are not easy to detect on these figures. One of the programs to be pursued in the coming year will be the resolution of these differences by using the appropriate analytical tools described above.

ACQUISITION OF A HIGH RESOLUTION INTERFEROMETER

The analyses of air spectra have indicated that the present interferometer with its limited spectral resolution ($0.1\ cm^{-1}$) and computer capabilities is inadequate to explore fully all the information contained

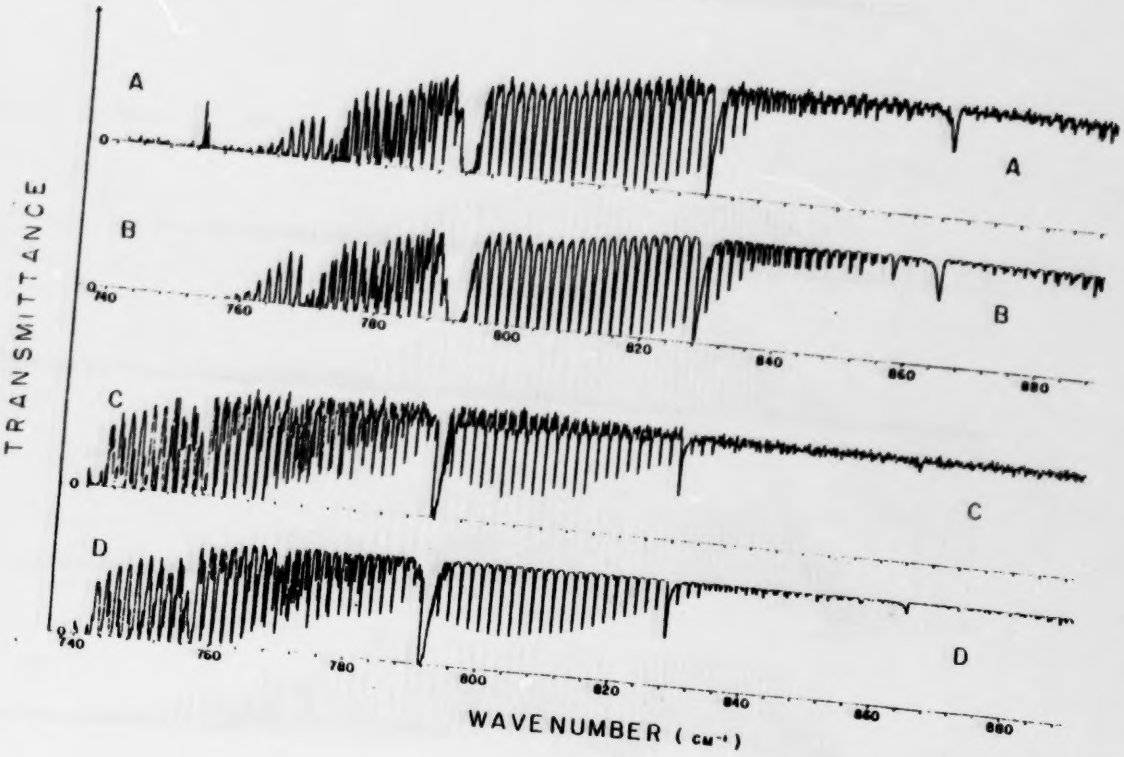

Fig. 19a - 300 Torr CO_2 in 171 m path at room temperature
19b - Calculated spectrum for same conditions
19c - 51 Torr CO_2 in 171 m path at room temperature
19d - Calculated spectrum for same conditions

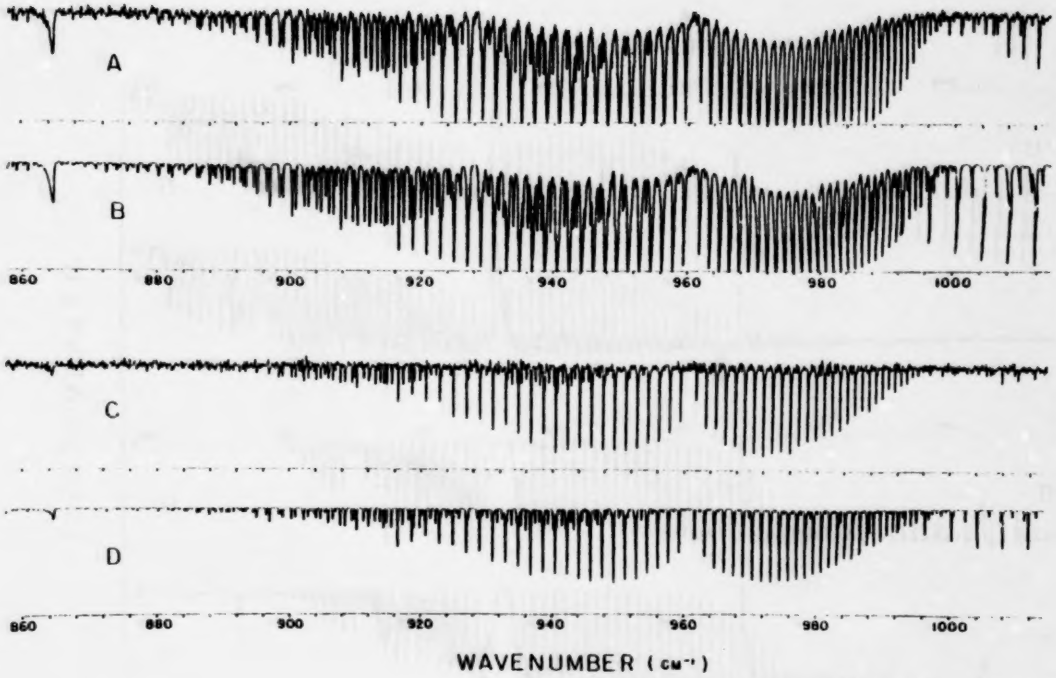

Fig. 20a - 300 Torr CO_2 in 171 m path at room temperature
20b - Calculated spectrum for same conditions
20c - 51 Torr CO_2 in 171 m path at room temperature
20d - Calculated spectrum for same conditions

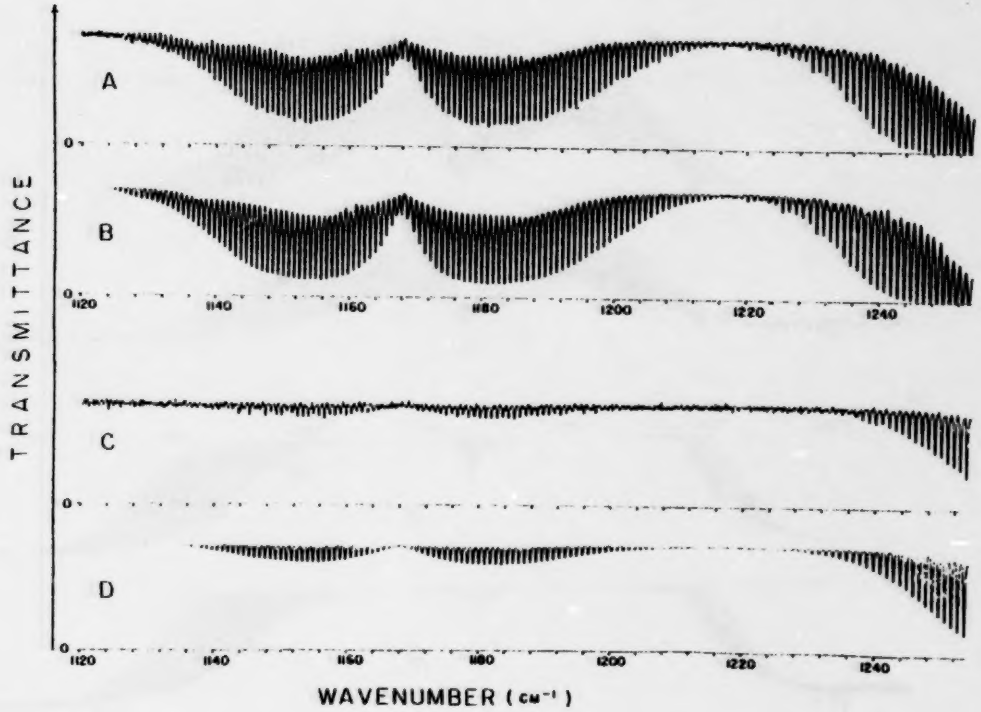

Fig. 21a - 0.15 Torr N_2O and 700 Torr N_2 in 171 m path
21b - Calculated spectrum for same
21c - 0.015 Torr N_2O and 700 Torr N_2 in 171 m path
21d - Calculated spectrum for same

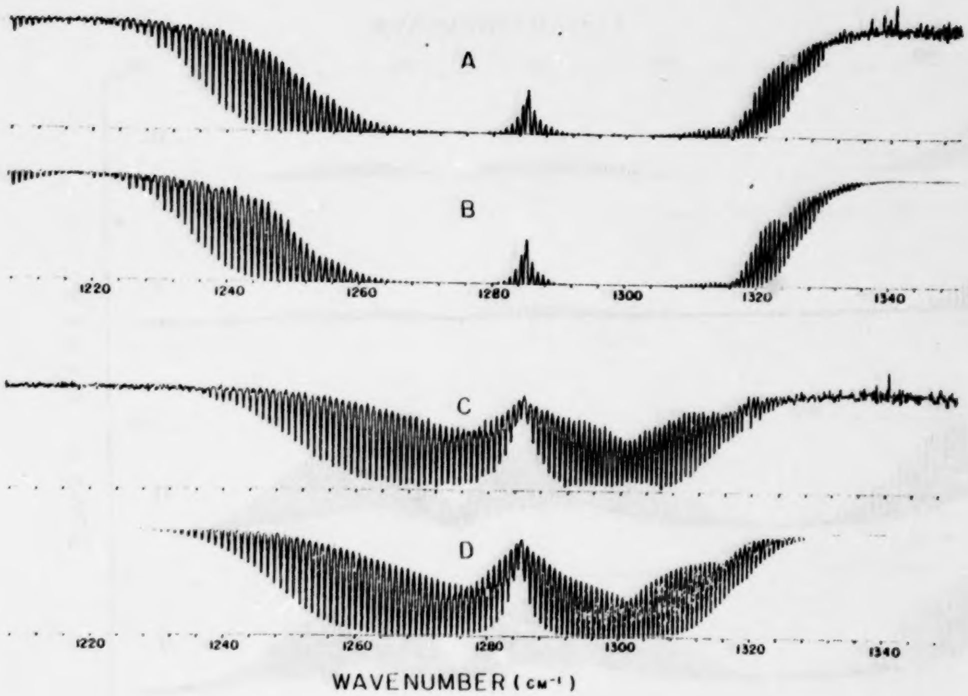

Fig. 22a - 0.15 Torr N_2O and 700 Torr N_2 in 171 m path
22b - Calculated spectrum for same
22c - 0.015 Torr N_2O and 700 Torr N_2 in 171 m path
22d - Calculated spectrum for same

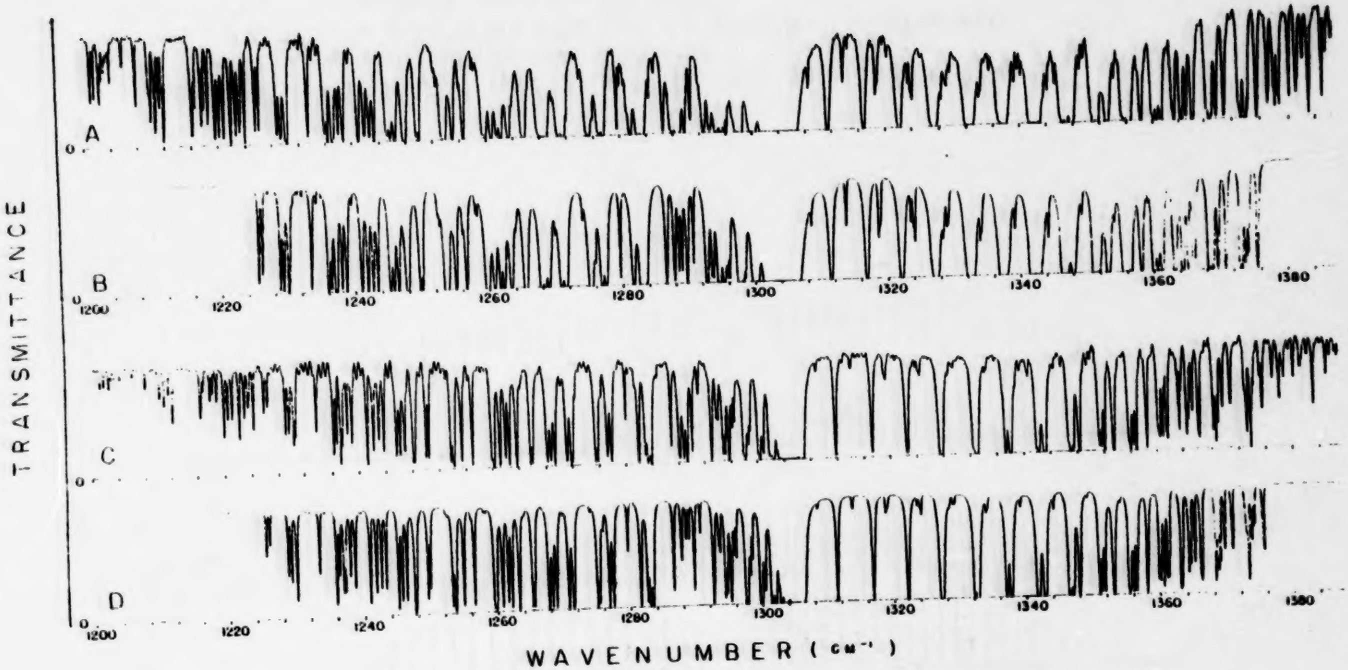

Fig. 23a - 0.38 Torr CH_4 and 700 Torr N_2 in 171 m path
23b - Calculated spectrum for same
23c - 0.076 Torr CH_4 and 700 Torr N_2 in 171 m path
23d - Calculated spectrum for same

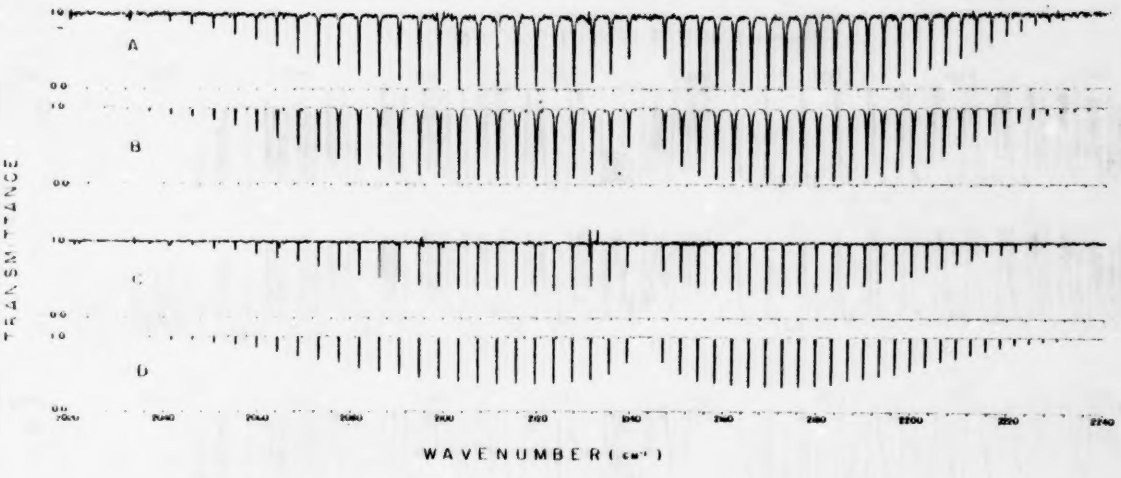

Fig. 24a - 4.18 x 10^{-3} Torr CO and 700 Torr N_2 in 171 m path
24b - Calculated spectrum for same
24c - 1.14 x 10^{-3} Torr CO and 100 Torr N_2 in 171 m path
24d - Calculated spectrum for same

in solar spectra observed at ground level or in long paths of ground level air. A higher resolution instrument is desirable for these studies, for other photochemical studies and for other investigations of atmospheric transmittance.

As a result of a cooperative effort by Professor J. G. Calvert (Chemistry), Professor R. K. Long (Electrical Engineering), and Professor J. H. Shaw (Physics) it has been possible for the University to acquire a Nicolet Instrument Corporation 7199 FT-IR System. This system includes a Michelson interferometer with a germanium on KBr beamsplitter, variable mirror rates of from 0.05 cm/sec to 4 cm/sec, a total optical retardation length of 16 cm and a nominal aperture of 5 cm diameter. This system will also include a NIC-1180 data system with a 40 k x 20-bit solidstate memory, a 15-bit analog to digital converter, and a 6-inch CRT interactive display with alphanumerals. A NIC-294B dual drive disk memory system with one fixed and one removable disk cartridge will provide a storage capacity of 4.8-million 20-bit words. This system will also include an interactive operating software package allowing data accumulation of up to 512 k data points and disk FFT routines for up to one million words. A mercury cadmium telluride detector will also be part of this system.

This instrument is expected to be delivered in the spring of 1977 and to be operational soon after delivery. This instrument will be used as required by several groups for their research work.

STRATOSPHERIC SIMULATION CHAMBER

The environments anticipated for the Stratochamber will be very harsh. For this reason we decided to develop a bellows-type feedthrough for optical adjustments during an experimental run. Such feedthroughs have a static face seal as opposed to the more unstable rotary seal of most feedthroughs. Unfortunately, most bellows designs only transmit a short linear motion. By carefully selecting the proper size bellows we were able to obtain about 1.25 cm of travel, which would be sufficient for nearly all anticipated adjustments. Only the mechanism that controls the number of traversals of the cell by the infrared radiation would require more. For this control we designed a magnification scheme allowing us to use the same bellows for all controls. The design of Blickensderfer et al. (34), in which rigid rods transmit the bellows motion to the mirrors was not well suited to our arrangement. We have all our optics mounted on a sturdy stainless steel table which is kinematically supported inside the cell. Consequently we wanted to avoid rigid connections between the cell wall and the optics. A common bicycle brake cable connecting the bellows to the mirror mounts accomplished this. The further problem of attaining sufficient stability in the system required a rather complex mechanism to do the actual moving of the mirrors. Once all the basic designs were developed, we had to construct everything out of corrosion resistant materials. Figures 25 and 26 show the details of our feedthrough-mirror control mechanisms. In both figures the handle (6) is connected to a threaded shaft which turns in a threaded hole in the

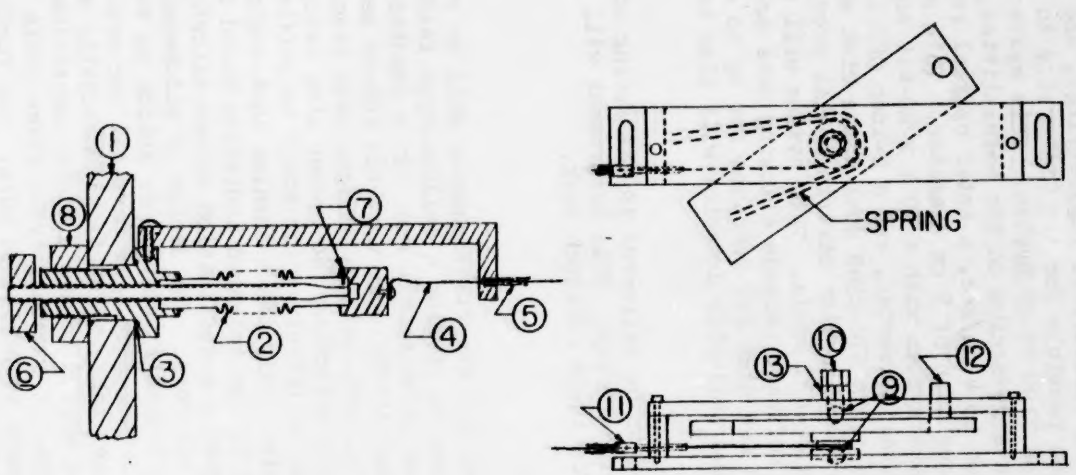
1
2
3
4
5
6
7
8
9
10
11
12
13
SPRING

Fig. 25 - Details of mirror adjusting system

1. Cell wall
2. Stainless steel bellows
3. Seal
4. Center cable
5. Outer cable
6. Handle
7. Retaining plug
8. Nut
9. 3/16" diameter sapphire balls
10. Bearing adjustment bolt
11. Screw adjustment nut
12. Rod
13. Locking nut

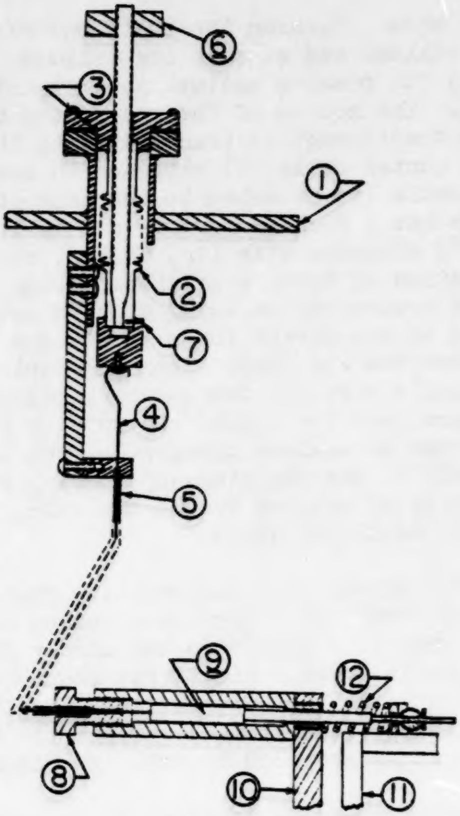

Fig. 26 - Details of mirror adjusting system

1. Cell wall
2. Stainless steel bellows
3. Seal
4. Center cable
5. Outer cable
6. Handle
7. Retaining plug
8. Screw adjustment nut
9. Plunger
10. Mirror mount base
11. Mirror holder
12. Spring

feedthrough base. Turning the shaft one way pushes its end against the end of the bellows and extends the bellows. Turning the shaft the other way retracts it, pushing against the retaining pin (7) and compressing the bellows. The motion of the end of the bellows with respect to the base of the feedthrough is transmitted to the mirror control by the motion of the center cable (4) attached to the bellows end with respect to the hollow cable (5) attached to the base of the feedthrough. The feedthrough base has a U-shaped groove cut in it designed to seal with any .238 m (3/8") diameter wire (In, Teflon, etc.). The traversal control is an adaptation of McCaa's original design. The traversal mirror of the White mirror system can be swung about a vertical axis by a 1-meter long arm attached to the mirror frame. This arm has a slot cut in its end that fits over the rod (12). When the cable (4) moves, it turns the rod (12) in a circle with the two sapphire balls (9) as bearings. This swings the arm back and forth. By putting the maximum swing of the rod at the position of maximum traversals, the sensitivity of the control adjusts itself to the changing sensitivity in the mirror orientation. Since the cable is wrapped around the axle, we gain the needed motion magnification mentioned above.

The other mirror controls are like that shown in Fig. 26. The plunger (9) slides freely in a precision reamed hole. A ball on the end of the plunger sits in a groove on the mirror frame, moving the mirror when the control cable moves. All mirror controls have a screw adjustment (8 in Fig. 26; 11 in Fig. 25) for initial alignment. Any realignment is then done with the feedthroughs. Since the bellows can only pull one direction, springs are used to pull the other direction.

The Stratochamber is designed to be portable. For ease in moving, the bulky 6-in. thick styrofoam insulation is made in six pieces that pound together with tongue-in groove joints.

The steel bath has been hot dip galvanized by the Brown Steel Galvanize Co. to rust-proof it. We originally had planned to use paint, but a test piece, cooled to 78 K, had its layer of paint crack off. The major problem with the operation was what to do about the stainless steel bellows welded onto the end of the bath. By applying water glass ($Na_2Si_4O_9$) to the bellows between the acid bath that removed the scale (pickling stage) and the immersion in the liquid zinc (galvanize stage), we prevented the zinc from bonding to the bellows convolutions. The steel flanges (now coated with zinc) were filed smooth, and the stainless steel flange welded to the bellows had the zinc etched off by a dilute sulphuric acid (H_2SO_4) solution.

Currently the Stratochamber is being readied for its first cooling trials. For these we will use chunks of dry ice surrounded by styrofoam peanuts. The chamber has already been used to collect some room temperature ozone spectra. With a Welch 1397 two-stage vacuum pump it takes about an hour to pump down to 20 μ through the 3.81 m (1.5") diameter connection. The leak rate is about 50 μ/hour. The mirror control system worked well at room temperature, and since it requires no lubrication, should function well at low temperatures too. A Stolab 921PL digital platinum resistance thermometer will be used to monitor the temperature.

5. STUDY OF SOME KEY REACTIONS OF PROBABLE IMPORTANCE IN PHOTOCHEMICAL SMOG FORMATION

INTRODUCTION

One important aspect of the current work involves the kinetic study of certain key reactions which appear to be of importance in photochemical smog systems. During the first year of this study we have investigated the kinetic behavior of nitrous acid through its formation reactions, $H_2O + NO + NO_2 \rightarrow 2HONO$, and its decomposition reaction, $2HONO \rightarrow H_2O + NO + NO_2$.[35,36] This study provided the necessary ground work to help establish for us the kinetic behavior of HONO and the potential problems associated with its use as a photochemical source of the important HO-radical. The photochemical reactor which was constructed during the first phase of this work, coupled with the FTIRS system provided to us by the Environmental Protection Agency, have been utilized in this research effort during the past year to obtain significant new information related to several chemical systems of seeming importance in the lower and upper atmosphere. The photolysis of dilute mixtures of HONO, NO_2, and NO, in synthetic air provided the HO-radical through the reaction, $HONO + h\nu(\lambda < 4300\text{Å}) \rightarrow HO + NO$. Through the addition of CO gas to the HONO, NO_2, NO_2 mixture in air, the controlled generation of HO_2 radicals could be effected through the reactions, $HO + CO \rightarrow H + CO_2$, $H + O_2 + M \rightarrow HO_2 + M$. The system which we have picked is ideal in some respects to follow the HO- and HO_2-radical reactions. The FTIRS system can establish the [HONO] at any time, and this is directly related to the rate of HO-radical generation by the photolysis of HONO. In addition, the $[CO_2]$ can be monitored directly with the FTIRS system and the rate of CO_2 formation derived from these data is equal to the rate of HO_2-radical formation. By a careful control of the proportions of the mixture of HONO, NO, NO_2, and CO in air, either a dominance of HO or HO_2- radicals can be easily obtained.

Two reaction systems have been studied in some detail during the past year. The first of these involves the important reaction of HO-radicals with CO: $HO + CO \rightarrow H + CO_2$. This reaction is not only of intrinsic interest in its own right as an important sink for atmospheric CO, but also has rather significant added importance since it is often used as a reference reaction in the study of HO-reactions with many species. In the following Section B of this report we describe the determination of the rate constant for this reaction and identify conclusively the pressure dependence of this constant. This work is of special value in the determination of the rate constants for such important reactions as, $HO + SO_2\ (+ M) \rightarrow HOSO_2\ (+ M)$, $HO + NO_2\ (+ M) \rightarrow HONO_2\ (+ M)$, etc.

In the following Section C we present the results of our studies of the $HO_2 + NO_2$ reactions. This work provides the first direct kinetic estimates of the rate constants for the formation of the highly reactive compound, HO_2NO_2. The results of these studies indicate that this species, peroxynitric acid, is a probable component of photochemical smog. Some of its kinetic properties have been determined, and further studies of this and other related species are being made in continuing work on this project.

In Sections D and E, experiments of photolysis work are discussed.

In Section F, infrared spectra of several compounds of special interest in the study of both stratospheric and tropospheric reactions are presented.

THE PRESSURE DEPENDENCE OF THE RATE CONSTANT FOR THE REACTION: $HO + CO \rightarrow H + CO_2$.

The gas phase reaction of the hydroxyl radical with carbon monoxide,

$$HO + CO \rightarrow H + CO_2 \qquad (17)$$

is one of the most thoroughly studied of its many important reactions. The high degree of interest in reaction (17) relates to its significance in combustion processes and in atmospheric reactions. The early work on this reaction has been reviewed by Baulch, Drysdale, and Lloyd (37) and more recently by Wilson (38). A variety of both direct and indirect methods of k_{17} determination has been employed, and several new measurements have appeared: the time dependence of the HO-radical concentration was monitored by ESR in a flow reactor (39), by resonance fluorescence (40,41) and by resonance absorption techniques following HO-radical generation by pulse photolysis (42,43) or radiolysis (44) of the appropriate gaseous mixtures. Our current interest in this reaction was stimulated by the results of other recent studies which employed steady state photolysis at total pressures up to one atmosphere; these involved the competitive rate measurement of the HO-radical with CO and H_2 in reactions (17) and (18). (45,46).

$$HO + H_2 \rightarrow H_2O + H \qquad (18)$$

Both groups of workers concluded that the rate constant for reaction (17) is pressure dependent and very much faster at 1 atm pressure than had been assumed from the earlier low pressure studies. A unique test of the pressure dependence of k_{17} was not possible from the work of Cox, et al. (45), since their experiments were carried out at a fixed pressure of 1 atm (largely air). However they found the ratio of k_{17}/k_{18} to be equal to about twice that observed by other experimentalists who used much lower pressures of reactants and added gas, and they suggested that the hypothesis of a pressure dependent k_{17} seemed most compatible with these results. In the work of Sie, et al. (46), the pressure of added gases (H_2, He, SF_6) was varied from 20 to 774 Torr with an observed increase in k_{17} with pressure by over a factor of two in this pressure range of added H_2 or SF_6.

The results of these findings seemed to us to be incompatible with those of other recent studies in which a much more direct measure of the [HO] was possible and no indication of a pressure dependence of k_{17} was seen; thus Davis, et al. (41), Greiner (47), and Stuhl and Niki (40) found no change in k_{17} in varying added helium pressure from low pressures up to 100 Torr. Smith and Zellner also reported an insensitivity of this rate constant to variation of CO over a 3-fold pressure range (42). Also the value of k_{17} derived by Gordon and Mulac (44) from pulse radiolysis experiments with 10 Torr CO, 10 Torr H_2O, and 710 Torr of added Ar was identical, within the experimental error, to that found at low pressures by previous workers (37,38). The earlier work of Ung and Back (48) and of Overend, Paraskevopoulos, and Cvetanovic (43) gave some indication of a pressure dependence to k_{17}, and both groups of workers have invoked the influence of third body M on the reaction of HO with CO as one alternative in the explanation of their results. However, both studies involved complications attendent with the photolysis of H_2O vapor containing systems, and both groups remained unconvinced of the uniqueness of this explanation.

It is most important to atmospheric scientists that further confirmation be obtained of the apparent pressure effect on reaction (17) for several reasons. First, a potential factor of two increase in k_{17} over the range of pressure 100-760 Torr results in a serious perturbation of the simulated rates of reaction (17) in the troposphere and the stratosphere. Second, many of the rate constants of other reactions of HO-radicals which are employed in the simulations of the atmospheric reactions are based upon relative rate measurements using the low pressure value of k_{17} as the reference value; obviously if k_{17} is a factor of two larger than formerly believed, then several recent estimates of the rate constants for the reactions of HO with NO, NO_2, and SO_2 are also a factor of two faster than originally suggested. Last, if we are to apply these kinetic considerations to the actual atmosphere, then it is necessary that we determine the effect on the value of k_{17} of varied pressures of the actual molecules present in air (N_2,O_2), since the effects noted to date appear to be strongly dependent on the nature of the added gas; helium shows little effect, while added SF_6 and H_2 cause a rather marked influence. (46)

With these considerations in mind, we have carried out a series of kinetic experiments designed to determine k_{17} for conditions comparable to those present in the troposphere and stratosphere. We have photolyzed dilute mixtures of HONO, CO, isobutane, and NO_x in synthetic air at 700 and 100 Torr pressure in a large photochemical reactor. The product rate data were determined unambiguously using a long path Fourier transform infrared system. These results provide a direct test of the sensitivity of k_{17} to the air pressure and provide a firm basis for the choice of a rate constant for reaction (17) which is appropriate for the simulation of chemical changes in the troposphere.

The photolysis cell, 6.3 m in length and 445 liters in volume, was constructed of 30.5 cm diameter Pyrex tubing. Its construction is illustrated in Figure 27. The cell was evacuable and enclosed the modified White optics of a multiple reflection system used for the in situ, infrared analysis of the reactants and products (49); a 170 m path was employed in this work normally. The cell was surrounded by black-light fluorescent

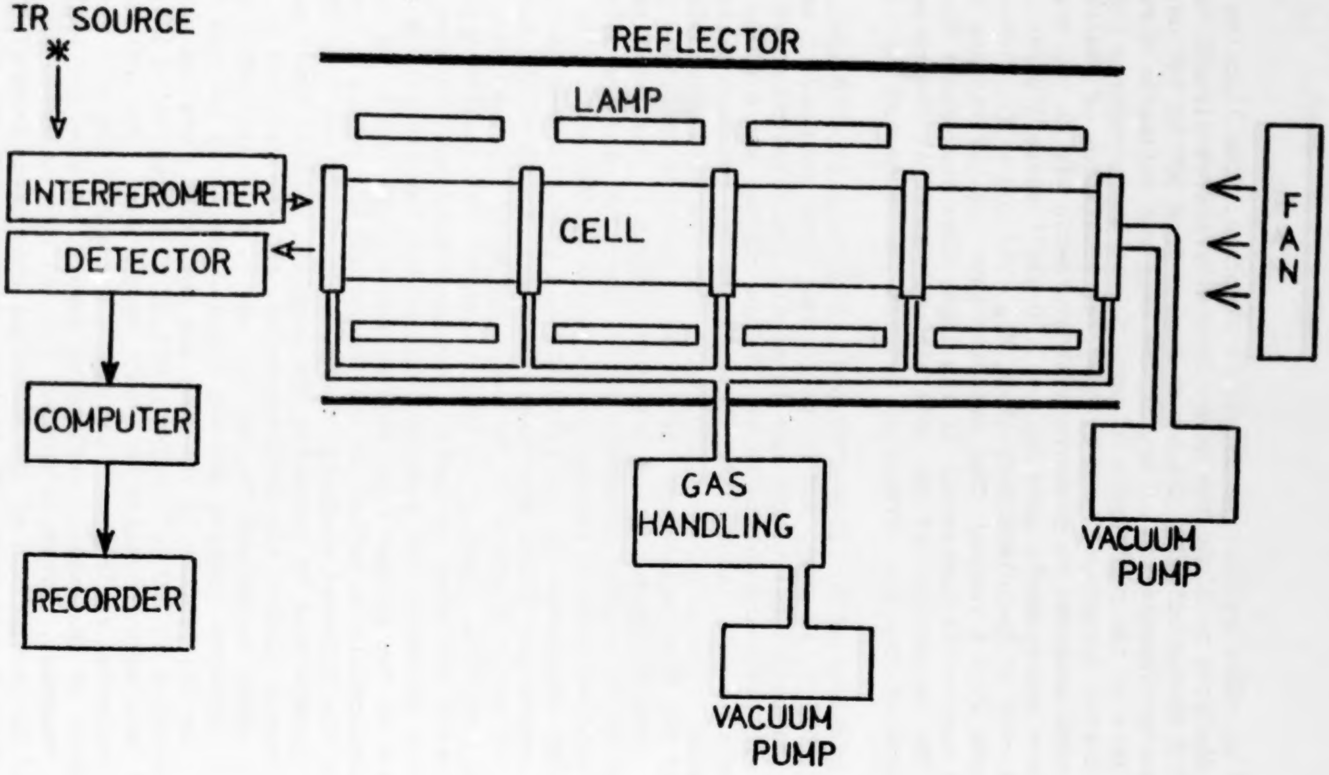
IR SOURCE
INTERFEROMETER
DETECTOR
COMPUTER
RECORDER
REFLECTOR
LAMP
CELL
FAN
GAS HANDLING
VACUUM PUMP
VACUUM PUMP

Figure 27. The experimental photolysis system employed in this work.

lamps and an outer reflective shield of aluminum. The lighting of the cell was designed to mimic the solar intensity and wavelength distribution in the photochemically important region from 300 to 430 nm. The rate of photo-dissociation of NO_2 in the cell was estimated directly from the rate of the photolysis of pure NO_2 at low pressures [$-R_{NO_2}$ = 2 (Rate of O-atom formation)] and by computer simulation of reactant and product rates measured in mixtures with synthetic air at 700 Torr pressure. These measurements gave $k_{NO_2} = 0.60\ min^{-1}$ where $d[O]/dt = [NO_2]k_{NO_2}$ gives the rate of the elementary step, $NO_2 + h\nu \rightarrow O + NO$. Integrated measurements with a radiant flux detector gave similar results and indicated a reasonable homogenity of the light flux throughout the cell volume. The temperature of the cell was maintained in the range 25 ± 2°C by means of room air circulated between the lamps and the cell.

Gas mixtures of CO (1039-2078 ppm), isobutane (30-220 ppm), HONO (< 4 ppm), NO_2 (< 10 ppm), and NO (< 10 ppm) were prepared by measurements of the individual components in an all glass introduction system equipped with standard volume bulbs, Teflon valves, and a glass spiral gauge used as a null instrument. The mixtures of reactant gases and O_2 and N_2 (added to either 700 or 100 Torr) were standard commercial products, and the HONO vapors were generated as we have described previously (36). Interferograms of the infrared spectra of the reacting mixture were recorded at regular intervals during the runs, and the data were resolved into wavelength-transmission spectra by computer. The concentration-time dependence of the reactants and products were derived by computer comparison of the absorbance data with those of the pure compounds. The major products of the reaction were: CO_2, NO, NO_2, $\underline{t}$-$C_4H_9ONO_2$, CH_3COCH_3, $HONO_2$, O_3, CH_2O together with smaller amounts of other nitrates and other products. For our considerations here only the CO_2, organic nitrates, and acetone analyses are important. In the determination of the product CO_2, special precautions had to be taken to avoid unpredictable variation in the background absorption of carbon dioxide in the infrared analysis beam outside of the reaction chamber. This was accomplished by enclosing the complete optical train associated with the Nernst glower, the interferometer, and the detector in a special housing in which background CO_2 and H_2O vapors were controlled through the use of nitrogen flushing gas and exposed dishes of KOH and NaOH pellets. The CO_2 product in the runs was estimated from its characteristic absorption at 720 cm^{-1} using $\epsilon = 1.70 \times 10^{-4}\ ppm^{-1}m^{-1}$; $\ln(I_o/I) = \epsilon c \ell$. All data were collected at 1 cm^{-1} resolution. The acetone absorption was estimated at 1218 cm^{-1} using $\epsilon = 6.4 \times 10^{-4}\ ppm^{-1}m^{-1}$ after computer removal of the small, overlapping absorption from the tail of the isobutane reactant. Previous workers (50,51) have observed that the position and the extinction of the structureless, broad band of the organic nitrates ($RONO_2$) near 1300 cm^{-1} is insensitive to the structure of R. We have taken $\epsilon = 4.5 \times 10^{-3} ppm^{-1}m^{-1}$ at 1310 cm^{-1} in our estimation of the organic nitrates. The extent of the reaction of the CO and $\underline{iso}$-C_4H_{10} reactants during these experiments amounted to only a few percent of the starting materials.

We have measured the rate constant of reaction (17) through the use of the competitive reactions of the HO-radical with CO and isobutane:

$$HO + CO \rightarrow H + CO_2 \qquad (17)$$

$$HO + \underline{iso}\text{-}C_4H_{10} \rightarrow H_2O + \underline{t}\text{-}C_4H_9 \qquad (19a)$$

$$\rightarrow H_2O + \underline{iso}\text{-}C_4H_9 \qquad (19b)$$

The rate constant $k_{19} = k_{19a} + k_{19b}$ as measured by Greiner (52) was accepted as the reference in the estimation of k_{17}. The primary source of HO-radicals in this work was the photolysis of HONO. Photochemical experiments with mixtures of HONO, $\underline{iso}$-C_4H_{10}, NO_2, NO in air in the absence of added CO gave negligible amounts of CO_2 product, and it is reasonable to assume that CO_2 is formed almost exclusively through reaction (17) in the CO-containing mixtures of HONO and $\underline{iso}$-C_4H_{10} in air, at least during the early minutes of the experiments. Also it can be shown by a detailed kinetic analysis of the system that the only significant agent which results in isobutane decomposition for our conditions is the HO-radical and the primary reactions (19a) and (19b). Also about 99% of the rate of the HO attack on isobutane molecules can be accounted for in the summation of the rates of formation of the organic nitrates (largely $\underline{t}$-$C_4H_9ONO_2$) and acetone for our conditions; $[\Delta C_4H_{10}]_t \simeq [C_4H_9ONO_2]_t + [CH_3COCH_3]_t$. Thus the rate of CO_2 formation can be used to monitor the rate of (17), and the sum of the rates of organic nitrates plus acetone formation is a good measure of the sum of the rates of reactions (19a) and (19b). The ratio of the product concentrations, $[CO_2]_t/[\Delta C_4H_{10}]_t$ at a given time t should be related to the ratio of the rate constants, k_{17}/k_{19}, by the simple relation (20):

$$[CO_2]_t/[\Delta C_4H_{10}]_t = (k_{17}/k_{19})\ ([CO]_t/[C_4H_{10}]_t \qquad (20)$$

The reactant concentrations and product ratios obtained in separate sets of experiments carried out in this work at total pressures of 700 and 100 Torr of air are summarized in Table VI. The appropriate product data have been plotted versus the $[CO]/[C_4H_{10}]$ ratio in Figure 28. It is seen that the theoretically expected linear form of relation (20) describes the two sets of data well, and the intercepts of the least squares lines through the points are equal to zero within the statistical standard deviation. The 700 Torr data define the line: $\underline{y} = -(0.040 \pm 0.23) + (0.127 \pm 0.007)\underline{x}$; the 100 Torr data are represented by: $\underline{y} = (0.10 \pm 0.38) + (0.0586 \pm 0.0084)\underline{x}$. From the slopes of these lines and the value of k_{19} reported by Greiner for 25°C (52), $k_{19} = 3.46 \times 10^3$ $ppm^{-1}min^{-1}$, we estimate $k_{17} = 439 \pm 24$ $ppm^{-1}min^{-1}$ in air at 700 Torr; $k_{17} = 203 \pm 29$ $ppm^{-1}min^{-1}$ in air at 100 Torr (25°C). These estimates for k_{17} are in reasonable accord with those derived by Cox, et al. (45), and Sie, et al. (46); Cox and co-workers estimated $k_{17} = 398 \pm 29$ ppm^{-1} min^{-1} in air at 760 Torr. Sie, et al., give $k_{17} = 468 \pm 42$, 507 ± 32, and 216 ± 14 $ppm^{-1}min^{-1}$ for added H_2 pressures of 774, 702, and 82 Torr, respectively. Preliminary recent data of Paraskevopoulos and colleagues (53) give $k_{17} = 480 \pm 48$ for added pressures of SF_6 of 350 and 200 Torr, and $k_{17} = 301 \pm 30$ $ppm^{-1}min^{-1}$ at 50 Torr of added He.

Summary of Rate Data fr
Mixtures with CO, _iso_-C.

Initial concentrations, ppm[b]	
[CO]	[_iso_-C_4H_{10}]
(a) Total pressure, 700 Torr	
2078	195
2078	103
2078	73.1
2078	42.9
2078	30.0
1039	220
1039	158
(b) Total pressure, 100 Torr	
2078	219
2078	73.1
2078	40.7
2078	30.2

[a] Temperature, 25 ± 2 C.

[b] The unit ppm used here is de
at 25°C.

[c] $[\Delta C_4H_{10}]_t = [C_4H_9ONO_2]_t +$ [C
$\overline{[CO_2]_t/[\Delta C_4H_{10}]_t}$ was calcula
intervals during the first 2

TABLE VI

rom the Photolysis of HONO in
-C_4H_{10}, NO_x, in Synthetic Air[a)]

$[CO]_o/[\underline{iso}\text{-}C_4H_{10}]_o$	$\overline{[CO_2]_t/[\Delta C_4H_{10}]_t}$ [c)]
10.7	1.33 ± 0.12
20.2	2.74 ± 0.12
28.4	2.88 ± 0.02
48.4	5.93 ± 0.04
69.3	9.10 ± 0.15
4.72	0.80 ± 0.05
6.58	0.90 ± 0.08
9.49	0.61 ± 0.03
28.4	1.64 ± 0.05
51.1	3.53 ± 0.09
68.8	3.87 ± 0.07

efined as [pressure(Torr)/760] x 10^6

$CH_3COCH_3]_t$; the average of the ratios,
ated from data taken at four 5-min
20 min of the experiment.

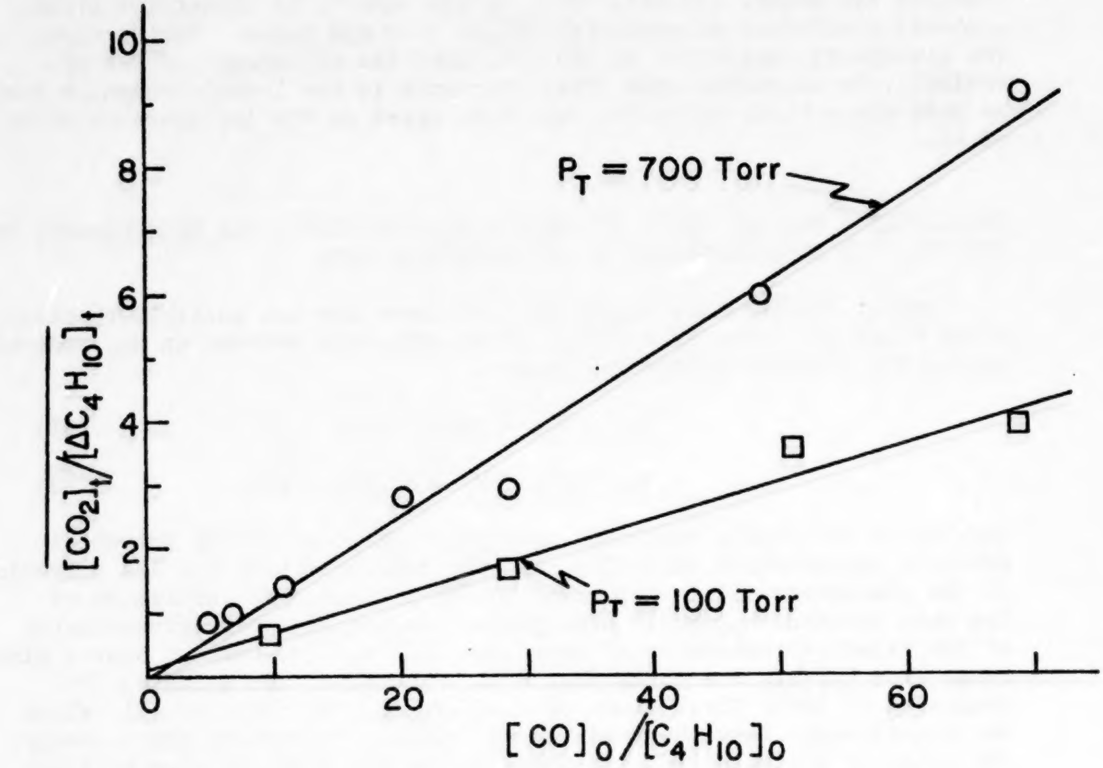

Fig. 28 Plot of the ratio $\overline{[CO_2]_t/[\Delta C_4H_{10}]_t}$ versus $[CO]_0/[\underline{\text{iso}}\text{-}C_4H_{10}]_0$ from the photolysis of HONO, CO, $\underline{\text{iso}}\text{-}C_4H_{10}$, NO_x mixtures in synthetic air; open circles refer to experiments at 700 Torr total pressure; squares are from experiments at 100 Torr total pressure.

In conclusion, we confirm that the rate constant for reaction (17) is pressure dependent in the range 100-700 Torr of air in accord with the original ideas of Ung and Back (48) and Overend, et al. (43) and in agreement with the recent more extensive studies of Cox, et al. (45), and Sie, et al. (46) We recommend that an average "best estimate" value in the range $k_{17} = 453 \pm 33$ $\text{ppm}^{-1}\text{min}^{-1}$, be used by modellers of chemical reactions in the lower troposphere, and an average of the present and previous estimates, (37-42), 216 ± 11 $\text{ppm}^{-1}\text{min}^{-1}$, be chosen for stratospheric conditions at pressures of 100 Torr and below. Furthermore, the atmospheric scientist should note that the adjustment of the HO-radical rate constants with other reactants in the lower atmosphere must be made where these estimates have been based on the low pressure value of k_{17}.

THE KINETICS AND MECHANISM OF THE HO_2-NO_2 REACTIONS; THE SIGNIFICANCE OF PEROXYNITRIC ACID FORMATION IN PHOTOCHEMICAL SMOG

Recent studies have suggested that there are two possible reaction modes which may occur as a result of an encounter between an HO_2 radical and an NO_2 molecule in the gas phase:

$$HO_2 + NO_2 \rightarrow HONO + O_2 \tag{21}$$

$$HO_2 + NO_2\ (+M) \rightarrow HO_2NO_2\ (+M) \tag{22}$$

In view of the highly reactive, oxidizing character of the potential product, peroxynitric acid (54), and the high potential for its formation in the atmosphere, it is important to obtain meaningful estimates of the rate constant k_{22} under atmospheric conditions. Current estimates of the relative importance of reactions (21) and (22) extend over a wide range from $k_{21}/k_{22} \simeq \infty$ to $k_{21}/k_{22} \simeq 0$. Simonaitis and Heicklen (55) suggested in their first study of this system that reaction (21) alone was significant; they observed through visible absorption spectroscopy, the rates of NO_2 formation and decay in the 213.9 nm photolysis of N_2O in O_2, H_2, NO, and NO_2 mixtures. For their conditions (temperature, 25°C, $P_{H_2} \simeq 700$ Torr), they estimated $k_{23}/k_{21} = 7 \pm 1$.

$$HO_2 + NO \rightarrow HO + NO_2 \tag{23}$$

Cox and Derwent (56) arrived at a very similar conclusion; they photolyzed dilute mixtures of HONO with CO, NO, and NO_2 in air at 1 atm and 23 ± 2°C. Using chemiluminescence measurements the rates of formation and decay of NO and NO_x ($NO + NO_2$) were determined, and the rate constant ratio, $k_{23}/k_{21} = 10 \pm 2$ was derived. Taking $k_{24} = 3.3 \times 10^{-12}$ cc $\text{molec}^{-1}\ \text{sec}^{-1}$, they estimated: $k_{23} = (1.2 \pm 0.3) \times 10^{-12}$; $k_{21} = (1.2 \pm 0.3) \times 10^{-13}$ cc $\text{molec}^{-1}\text{sec}^{-1}$.

$$2HO_2 \rightarrow H_2O_2 + O_2 \tag{24}$$

Reaction (22) was not considered to be significant.

Recently Simonaitis and Heicklen (57) have restudied the 213.9 nm photolysis of N_2O in mixtures of H_2, O_2, and NO. In this study they followed the concentration of NO as a function of time by chemiluminescence analysis methods. These rate data showed an interesting and unexpected result: the oxidation of NO continued to occur after termination of the initiating radiation. This observation and the kinetics of the [NO]-time data suggested to the authors that an intermediate species of finite lifetime, presumably HO_2NO_2, was formed and that reaction (22) as well as (21) occurred in this HO_2-NO_2 system. From their results they estimated that $k_{22}/(k_{21} + k_{22})$ was in the range, 0.3 to 1; assuming $k_{24} = 3.3 \times 10^{-12}$ cc $molec^{-1}sec^{-1}$, they obtained $k_{21} + k_{22} \simeq (2.0 \pm 0.7) \times 10^{-13}$ and $k_{22} = 9.3 \times 10^{-13}$ cc $molec^{-1}sec^{-1}$. However, in none of the previous work was any direct evidence for the presence of HONO or HO_2NO_2 products obtained; their involvement was inferred from the measurements of NO and/or NO_2.

Recently Niki, et al (58), have identified for the first time through FTIR spectroscopy, the formation of peroxynitric acid in irradiated dilute mixtures of Cl_2, H_2, and NO_2 in air. It was suggested that reaction (22) was the origin of this product. The spectrum now attributed to HO_2NO_2 is the same as that observed previously in irradiated dilute Cl_2, CH_2O, NO_2, air mixtures by Gay, et al. (59), and Niki, et al. (60); this was first attributed to peroxyformyl nitrate by both research groups. However, in view of the facts that there was no carbonyl absorption band in the unknown compound spectrum and that the formyl group need not be present in the reactants to form the observed product in Niki's work, it was reasoned that HO_2NO_2 and not $HCOO_2NO_2$ was the likely compound. Hanst and Gay (61) now accept the recent HO_2NO_2 assignment of Niki, et al. (58). Both groups concluded that reaction (22) may be the exclusive route of the HO_2-NO_2 interaction, since HONO could not be detected among the products in their systems.

We wish to report here significant new information related to reactions (21) and (22) and further confirmation of the nature of the proposed product, HO_2NO_2. We have conducted a series of experiments employing an FTSIR, long-path system in the study of HONO photolysis in mixtures of interest to atmospheric chemists. As part of these studies a series of experiments were carried out using HONO, CO, NO_x mixtures in air. Time dependent reactants and products (CO_2, O_3, $HONO_2$, N_2O_5, HO_2NO_2, HONO, NO, NO_2) of the reactions were followed as a function of time directly through their characteristic infrared absorption band. Computer simulation of these kinetic data provide new evidence of the HO_2NO_2 identification and kinetic parameters related to reactions (21) and (22).

The experimental data for the present study were obtained using a Digilab 496 interferometer in a manner described previously (36), but some minor differences should be noted. The multiple-pass, modified White optical system was housed in a borosilicate glass cell, 6 m in length with an internal diameter of 30 cm. The optical path between mirrors was 5.3 m; 32 traversals were used in this study, giving a total path length of 170 m. The HONO, NO, and NO_2 gases, all in the ppm range, were introduced into the cell with varied quantities of CO and pressurized to 700 Torr (24 ± 2°C) with synthetic air. The method of HONO addition inadvertently introduced small quantities of water vapor (< 100 ppm). HONO photolysis was induced using banks of black-light fluorescent tubes surrounding the cell such that the total intensity of light within the HONO and NO_2 chemically active absorption regions ($\lambda < 4300$ Å) was very near that in sunlight at sea level and solar zenith angle, 0°. All of the IR spectra were recorded at 1 cm^{-1} spectral resolution.

The kinetic model used for the present computer simulation of the HONO-NO-NO_2-CO-air system consisted of 30 reactions summarized in Table VII; the rate constants for the well studied reactions used in this model were obtained from the NBS tables (62) with the updating of those values which have been redetermined since the original compilation. Detailed kinetic analysis of product and reactant rates in simple NO_2 and HONO systems irradiated in our system gave the values of $k_{25} = 0.60$ and $k_{31} = 0.11$ min^{-1}. Our recent estimate of $k_{17} = 4.4 \times 10^2 ppm^{-1}min^{-1}$, in accord with other recent high values (45,46,63), was chosen. The latest evaluation (45) of k_{29} and k_{30} which utilized the "high" value of k_{24}, places these constants for 1 atm air at $\approx 2.0 \times 10^4$ ppm min^{-1}. For our system (700 Torr air), we have taken $k_{29} = 1.6 \times 10^4$ and $k_{30} = 1.9 \times 10^4$ $ppm^{-1}min^{-1}$, reflecting the somewhat lowered efficiency of reaction (29) compared to (30) which is expected to accompany the smaller number of degrees of freedom in the HO-NO system. We have chosen $k_{23} = 1.25 \times 10^3$ $ppm^{-1}min^{-1}$ in this work, an average of the earlier values reported by Hack, et al. (64), Davis, et al. (65), and the more recent estimates of Cox and Derwent (56), and Simonaitis and Heicklen (57). The rate constant for reaction (32) has been taken as 8.5×10^3 $ppm^{-1}min^{-1}$, in accord with the recent estimate of Cox, et al. (45)

The infrared spectral features tentatively assigned by Niki, et al. (58) to the molecule $HOONO_2$, consist of bands attributed to the nitrate group (1728.3, 1303.9, and 802.7 cm^{-1}), an OH-bending mode (1396.5 cm^{-1}), an OH-stretching mode (3540.1 cm^{-1}), and a broad combination band common to nitrate compounds (≈ 3000 cm^{-1}). These characteristic absorption peaks have been identified as resulting from a product formed in both the irradiated Cl_2, H_2, NO_2, air system and the Cl_2, CH_2O, NO_2, air systems. Attributing these features to the HO_2NO_2 molecule seems to be a most reasonable hypothesis to us, and reaction (22) is the probable source of the product. In the Cl_2, CH_2O, NO_2, air system the HO_2 reactant in reaction (22) is likely formed through the sequence:

$$Cl_2 + h\nu \rightarrow 2Cl$$

$$Cl + CH_2O \rightarrow HCl + HCO$$

$$HCO + O_2 \rightarrow HO_2 + CO$$

TABLE VII

Summary of the Reaction Mechanism and Rate Constants Employed in the Simulation of HONO, NO_x, CO, Air Mixture Photolyses[a)]

Reaction	Rate Constant[b)]
(21) $HO_2 + NO_2 \rightarrow HONO + O_2$	5.3×10^{1}
(22) $HO_2 + NO_2\ (+M) \rightarrow HO_2NO_2\ (+M)$	7.2×10^{1}
(23) $HO_2 + NO \rightarrow HO + NO_2$	1.25×10^{3}
(24) $2HO_2 \rightarrow H_2O_2 + O_2$	5.3×10^{3}
(25) $NO_2 + h\nu \rightarrow NO + O$	0.60
(26) $O + O_2\ (+M) \rightarrow O_3\ (+M)$	2.0×10^{1}
(27) $NO + O_3 \rightarrow NO_2 + O_2$	2.2×10^{1}
(17) $HO + CO \rightarrow H + CO_2$	4.4×10^{2}
(28) $H + O_2\ (+M) \rightarrow HO_2\ (+M)$	1.7×10^{3}
(29) $HO + NO\ (+M) \rightarrow HONO\ (+M)$	1.6×10^{4}
(30) $HO + NO_2\ (+M) \rightarrow HONO_2\ (+M)$	1.9×10^{4}
(31) $HONO + h\nu \rightarrow HO + NO$	0.11
(32) $HO + HONO \rightarrow H_2O + NO_2$	8.5×10^{3}
(33) $NO_2 + O_3 \rightarrow NO_3 + O_2$	4.6×10^{-2}
(34) $NO + NO_3 \rightarrow 2NO_2$	1.5×10^{4}
(35) $NO_2 + NO_3 \rightarrow N_2O_5$	5.6×10^{3}
(36) $NO_2 + NO_3 \rightarrow NO_2 + NO + O_2$	1.2×10^{1}
(37) $2NO_3 \rightarrow 2NO_2 + O_2$	3.2×10^{-1}
(38) $N_2O_5 + H_2O \rightarrow 2HONO_2$	2.5×10^{-3}
(39) $NO_2 + O \rightarrow NO + O_2$	1.3×10^{4}
(40) $NO_2 + O\ (+M) \rightarrow NO_3\ (+M)$	3.4×10^{3}
(41) $N_2O_5 \rightarrow NO_2 + NO_3$	1.5×10^{1}
(42) $2NO + O_2 \rightarrow 2NO_2$	7.5×10^{-10}
(43) $2HONO \rightarrow NO + NO_2 + H_2O$	1.4×10^{-3}
(44) $NO + NO_2 + H_2O \rightarrow 2HONO$	2.2×10^{-9}
(45) $H_2O_2 + h\nu \rightarrow 2HO$	1.5×10^{-3}
(46) $O + NO\ (+M) \rightarrow NO_2\ (+M)$	3.6×10^{3}
(47) $HO_2NO_2 \rightarrow HO_2NO_2$ (Wall)	9.1×10^{-2}
(48) HO_2NO_2 (Wall) $\rightarrow HONO$ (Wall) $+ O_2$	large
(49) $2HONO$ (Wall) $\rightarrow NO + NO_2 + H_2O$	large

---

a) Temperature, 24 ± 2°C: pressure of air, 700 Torr.

b) The units on rate constants are $ppm^{-1}min^{-1}$ for all but reactions (25), (31), (41), (45), and (47) which are min^{-1}, and (42) and (44) which are $ppm^{-2}min^{-1}$; the unit ppm used here is defined as [pressure(Torr)/760] x 10^{6} at 24°C. Data are from reference [62] except as noted in the text.

In the Cl_2, H_2, NO_2, air experiments the major source of the HO_2 is the reaction sequence:

$$Cl_2 + h\nu \rightarrow 2Cl$$

$$Cl + H_2 \rightarrow HCl + H$$

$$H + O_2\ (+M) \rightarrow HO_2\ (+M)$$

In this work a product with the identical infrared spectral properties was formed in irradiated dilute mixtures of HONO, NO, NO_2, CO, in air. Note in Figure 29a and 29b that in the absence of added CO, irradiation of the HONO, NO, NO_2 mixture in air gives no evidence after 5.9 min of the formation of the characteristic bands at 802.7 and 1303.9 cm^{-1} attributed to HO_2NO_2. This is quantitatively predictable from the known kinetic character of this system; little HO_2 radical development is expected in this system. However when an excess of CO was added to the HONO-NO_x-air mixture, the irradiation for 5.9 min created peaks attributable to HO_2NO_2; in Figure 29d the absorptions at 802.7 and 1303.9 cm^{-1} are seen readily after computer subtraction of the bands due to HONO, CH_4, and H_2O from the complete product spectrum shown in Figure 29c. Absorptions due to ozone and N_2O_5 have not been ratioed from the spectrum in that there is no significant contribution from these compounds to the HO_2NO_2 absorption regions, and further product ratioing increases the noise level of the remaining spectral features. There is an exact correspondence of the characteristic absorption bands with those of the product designated as HO_2NO_2 obtained in the Cl_2, H_2, NO_2, air system by Niki, et al. (58) and the irradiated Cl_2, CH_2O, NO_2, air system by Hanst and Gay (60). This can be seen in Figures 29e and 29f. The IR absorptions due to products of the Cl_2, H_2, NO_2, air mixture irradiated in our system for 6.0 min are shown in Figure 29e. In Figure 29f the absorptions due to $ClNO_2$ and $HONO_2$ have been computer subtracted using pure compound spectra, and the characteristic bands attributable to HO_2NO_2 at 802.7 and 1303.9 cm^{-1} are seen. These observations lend support to the assignment of these bands to HO_2NO_2 by Niki et al. (58), and Hanst and Gay (60). There is no other obvious product which would be common to these rather diverse systems and to which one might attribute these absorptions. It appears to us that the HONO, CO, NO_2, air system employed in our studies offers the simplest route to HO_2NO_2 yet observed. Here the source of the HO_2 radical is largely the reaction sequence:

$$HONO + h\nu \rightarrow HO + NO$$

$$HO + CO \rightarrow H + CO_2$$

$$H + O_2\ (+M) \rightarrow HO_2\ (+M)$$

There are some significant advantages of the HONO, CO, NO_2 system over the Cl_2-containing ones for the study of the HO_2NO_2 formation and decay kinetics. The complexity of products of the Cl_2-containing systems, including $ClNO_2$, ClNO, and HCl, is eliminated. The infrared observable

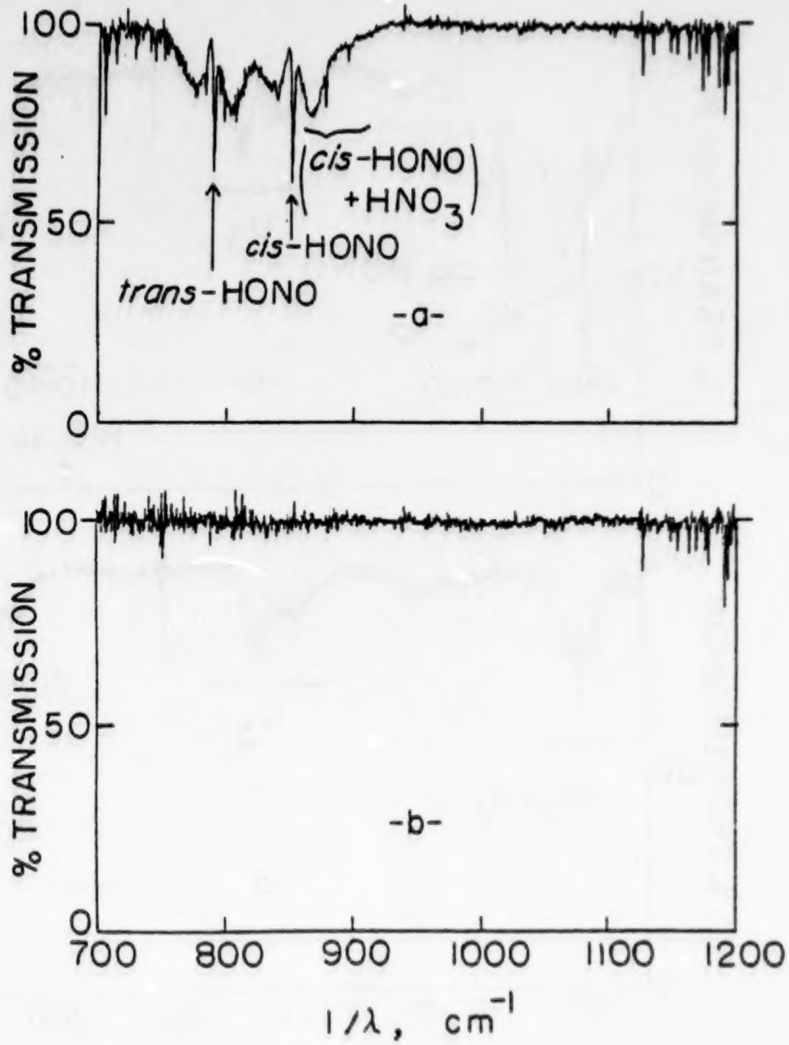

Fig. 29 Spectra of uv-irradiated HONO, NO$_x$, CO, air and Cl$_2$, NO$_2$, H$_2$, air mixtures; (a) spectrum of cell contents after 5.9 min irradiation of the initial mixture; total [HONO]$_0$ = 2.70, [NO]$_0$ = 2.77, [NO$_2$]$_0$ = 1.5, [CO]$_0$ = 0.0 ppm in synthetic air, 700 Torr; (b) residual spectrum resulting from that of (a) following computer subtraction of remaining *cis*, *trans*-HONO, HONO$_2$, and H$_2$O; note absence of HO$_2$NO$_2$.

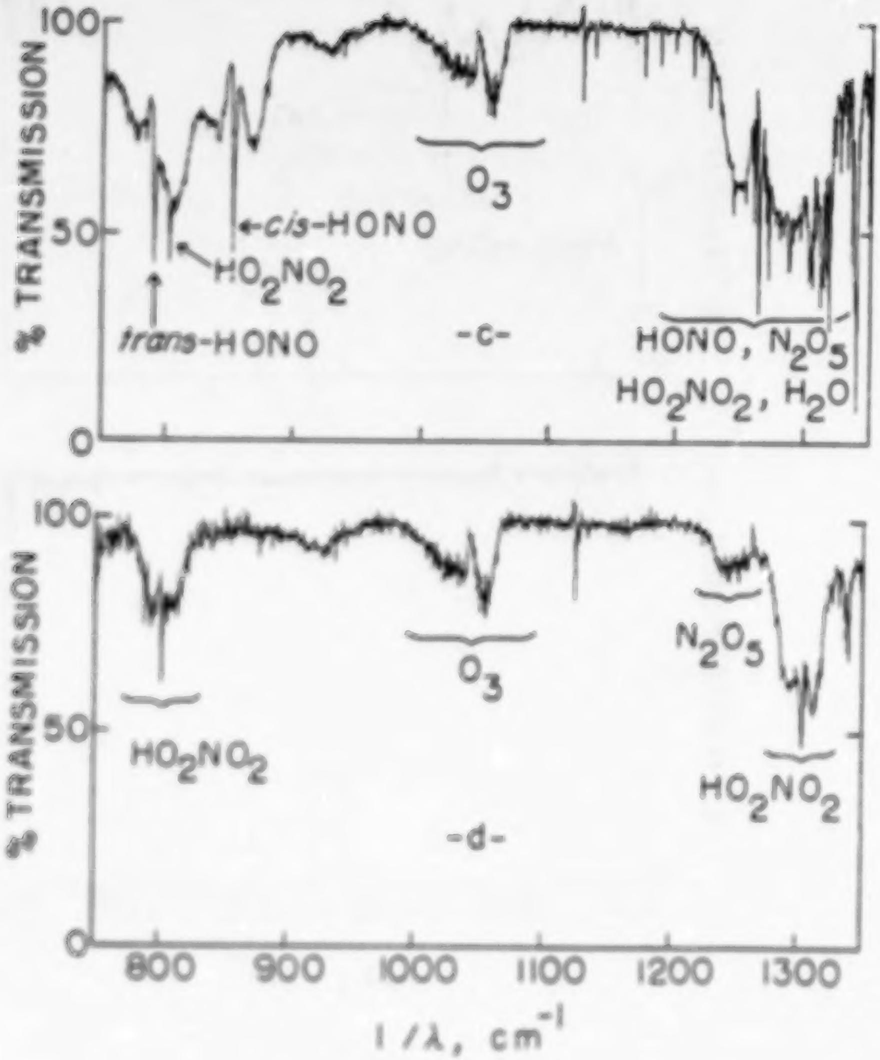

Fig. 29 (c) spectrum of cell contents following 5.9 min irradiation of the initial mixture: total $[HONO]_0 = 4.29$, $[NO]_0 = 2.8$, $[NO_2]_0 = 1.1$, $[CO]_0 = 3.8 \times 10^4$ ppm in synthetic air, 700 Torr; (d) residual spectrum resulting from that of (c) following computer subtraction of remaining cis, trans-HONO, CH_4, and H_2O.

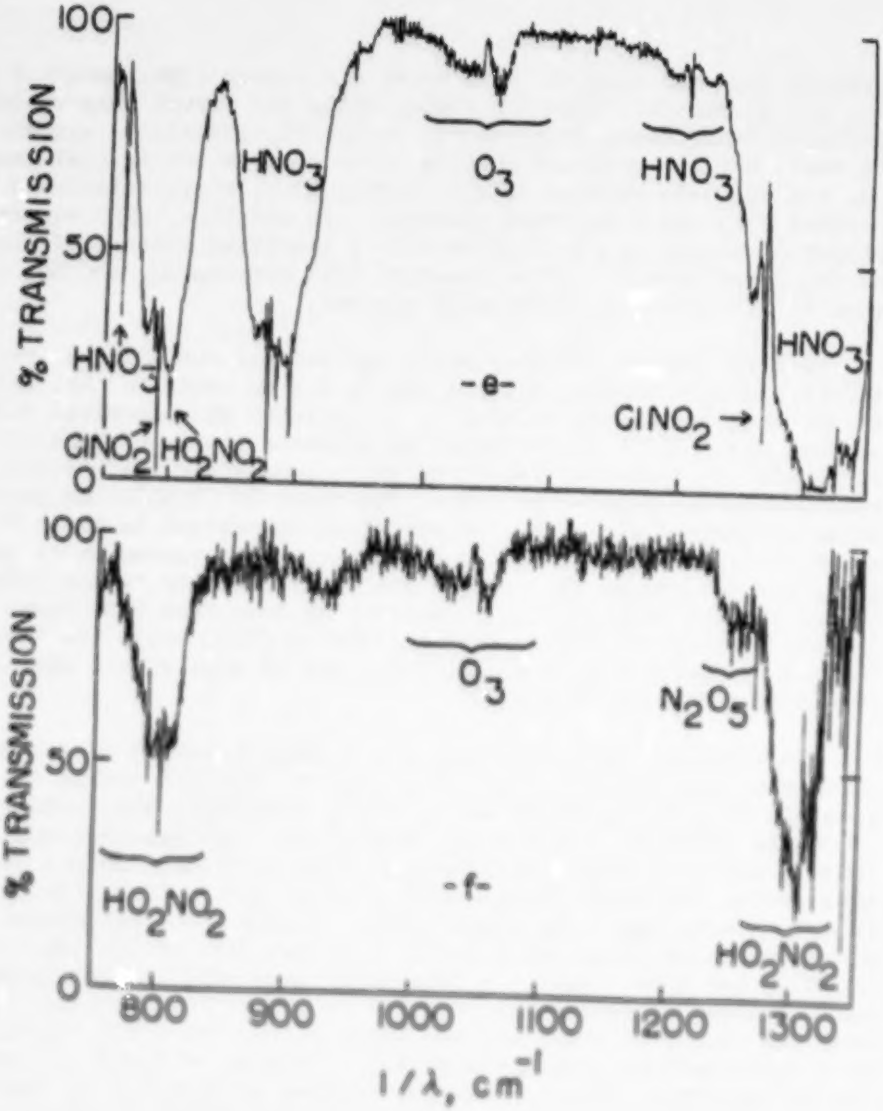

Fig. 29 (e) spectrum of cell contents following 6.0 min irradiation of the initial mixture: $[Cl_2]_0 = 30$, $[NO_2]_0 = 22$, $[H_2]_0 = 8026$ ppm in synthetic air at 700 Torr; (f) residual spectrum resulting from that of (e) following computer subtraction of the remaining $HONO_2$ and $ClNO_2$ products; compare the characteristic absorption peaks of HO_2NO_2 at 802.7 and 1303.9 cm^{-1} in (d) and (f).

product CO_2 and reactant HONO provide a rather direct monitor of the HO_2 and HO radical formation steps, while the direct observation of the infrared transparent reactant Cl_2 in the Cl_2-containing systems cannot be made, but its presence must be inferred from the initial charge of Cl_2 and the mass balance of HCl, $ClNO_2$, NOCl, etc., calculated to be present from the absorption spectrum. In addition, HONO vapors are attacked readily by Cl-atoms so that a sensitive measure of the extent of the possible alternative reaction (21) between HO_2 and NO_2 is not possible from the Cl_2-containing systems.

A first series of experiments was carried out using a very simple dilute mixture of HONO, NO, and NO_2 in air in order to test the accuracy of the rate parameters related to our primary photochemical radical source, HONO. With this mixture we minimize the generation of HO_2 and eliminate its series of reactions which complicate the resolution of the rate parameters related to HONO. The observed [HONO]-time profiles and those calculated employing the reactions summarized in Table VII are shown in Figure 30a for one of these runs. The agreement is reasonably good, and deviations from run to run are relatively random with the choice of rate data finally selected. In this case HONO formation occurs largely through the recombination reaction (29), while the loss reactions involve the photolysis reaction (31), and to some extent the HO-radical attack on HONO, reaction (32).

In a second series of runs, a moderate amount of CO gas was added so that a rather direct monitor of the [HO] profile during the run was possible from the measured rates of CO_2 formation; the dominant source of CO_2 is reaction (17) for our conditions. The measured and calculated [HONO]- and [CO_2]-time profiles are shown in Figure 30b for one run in this series for which $[CO]_0 = 2.23 \times 10^3$, $[NO]_0 = 20.4$, $[NO_2]_0 = 17.4$, $[HONO]_0 = 4.35$ ppm. For these initial reactant concentrations the rate of HO attack on CO is about twice the total rate of its reaction with NO, NO_2, and HONO. Again, a reasonably good match of the experimental and simulated concentration profiles is seen. The reactions which influence the [HONO] in this case are largely (29) and (31); reaction (32) is no longer important since almost all of the HO produced now reacts with CO, NO, and NO_2. Although the HO_2 radical is formed at a significant rate in this system, reactions (21) and (22) should be relatively unimportant here since the HO_2-NO reaction (23) is the dominant loss reaction for HO_2 under these conditions. The combined effect of the NO and NO_2 formation and decay reactions leads to an [NO] increase during the course of the run; after 1 hr irradiation, the simulation predicted an [NO] of 29 ppm compared to the observed concentration of 26 ppm. Thus, reactions (21) and (22) cannot be important here, and HO_2NO_2 was below the detection limits for these conditions, as expected from simulations of this system.

With the general accuracy of the model now proven for the simplest reaction mixtures, the influence of reactions (21) and (22) could be tested by selecting conditions which favor these reactions. This was accomplished in another series of experiments by increasing the $[CO]_0$

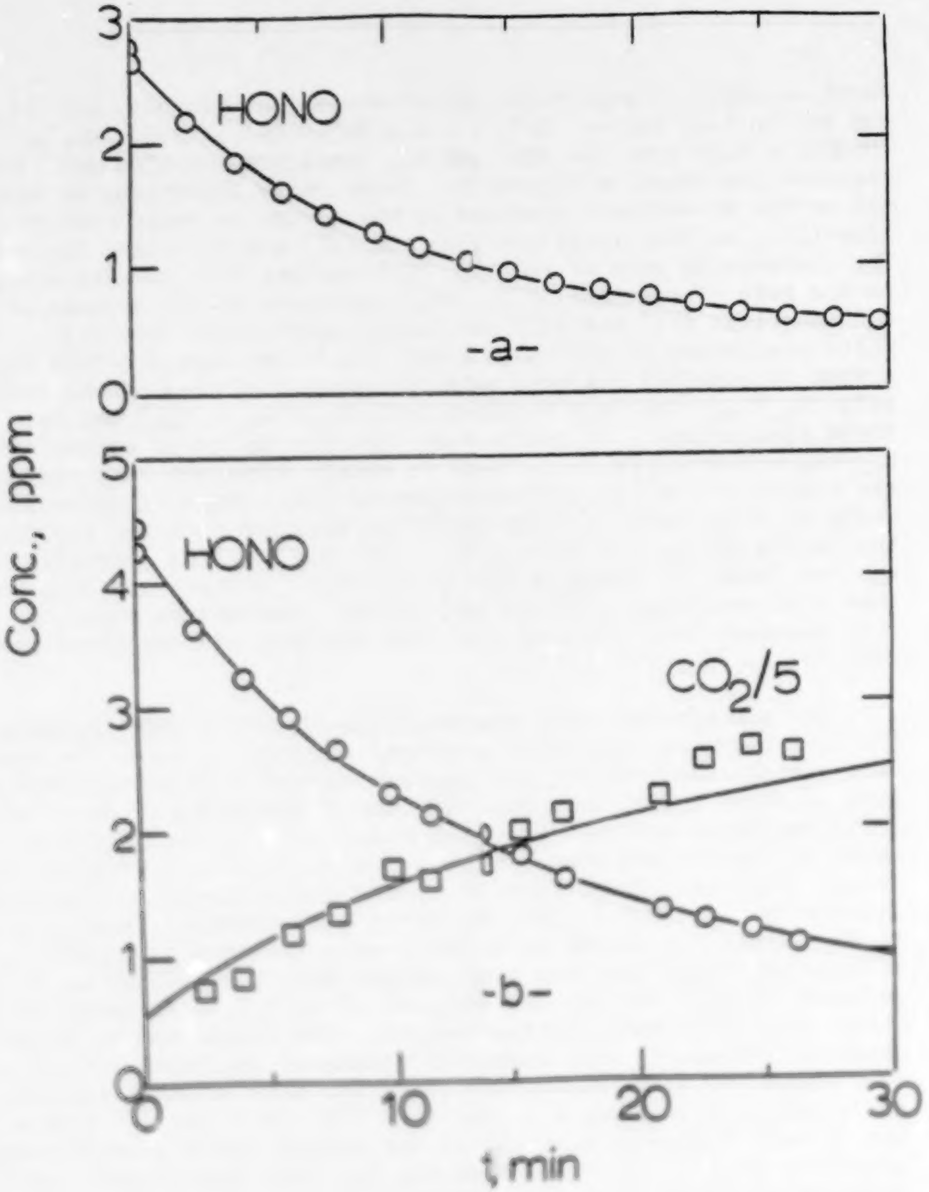

Fig. 30 Comparison of observed tota [HONO]- and [CO_2]-time data with those predicted by the simulation model for irradiated HONO, NO_x, CO mixtures in air; (a initial concentrations: total $[HONO]_0$ = 2.70, $[NO]_0$ = 2.7, $[NO_2]_0$ = 1.5 ppm in synthetic air, 700 Torr; (b) initial concetrations: total $[HONO]_0$ = 4.35, $[NO]_0$ = 20.4, $[NO_2]_0$ = 17.4 $[CO]_0$ = 2.23 x 10^3 ppm in synthetic air, 700 Torr.

about an order of magnitude, while decreasing the $[NO]_0$ and $[NO_2]_0$. In one run in this series $[CO]_0 = 3.8 \times 10^4$, $[NO]_0 = 2.8$, $[NO_2]_0 = 1.1$; $[HONO]_0 = 4.29$ ppm; the HONO and CO_2 concentration-time profiles for this run are shown in Figure 31. Under these conditions we expect nearly all of the HO-radicals produced in the system to react with CO in reaction (17), so that reactions (29) and (32) are no longer important. The increase in rate of reaction (17) results in a corresponding increase in the rate of reaction (23), $[NO_2]$ increases at the expense of the $[NO]$, and reactions (21) and (22) can become competitive with (23). The computer simulation of the [HONO]- and $[CO_2]$-time data for this high [CO] system (Figure 31) has been made for several choices of the rate constant ratio k_{21}/k_{22}; the rate constant ratio $k_{22}/(k_{21} + k_{22})$ was held at 10 in these simulations. It can be seen that the choice of either extreme, $k_{21}/k_{22} = 0$ or $k_{21}/k_{22} = \infty$ leads to widely divergent rate curves. With the former choice, no HONO formation in (21), $[CO_2]$ is underestimated badly at long times, and the [HONO] is depleted much too rapidly. With the choice of $k_{22} = 0$ and $k_{23}/k_{21} = 10$, the $[CO_2]$ is overestimated badly and the [HONO] is depleted much too slowly. Clearly the data suggest that both reactions (21) and (22) occur. Simulations employing several rate constant ratio choices show that the data are described reasonably well for $k_{21}/k_{22} \simeq 0.7 \pm 0.4$.

The peroxynitric acid concentration-time data from the same high [CO] run provides further information. In runs in which the uv-lights were extinguished, the HO_2NO_2 spectrum decayed with an apparent half-life of about 8 min, in accord with the observations of Niki, et al. (58), and Hanst and Gay (61). See Figure 32. In reactant-depleted mixtures no significant change in this rate was observed with the lights on or off. In view of the very low ultraviolet absorption of peroxyacetyl nitrate for $\lambda > 3000$ Å (66), the direct photochemical decomposition of HO_2NO_2 within our system or in the lower atmosphere is probably slow. It appears likely that the decay process for HO_2NO_2 which we observe, reflects largely the rate of transport of HO_2NO_2 to the wall of the cell where subsequent decomposition results. Simonaitis and Heicklen (55) observed indirectly much shorter lifetimes of the intermediate which they suggested to be HO_2NO_2 (~50 sec), but this is understandable since their reaction cell was a 1 liter bulb (12.4 cm diameter) with a lower gas to wall transport time than in the larger diameter glass tanks employed by Niki et al. (58), Hanst and Gay (59), and in our work (30 cm diameter cylinder of considerable length). We observed that NO_2 rises as HO_2NO_2 decays in the dark. A simple mechanistic route which may rationalize this course of events is the following:

$$HO_2NO_2 \rightarrow HO_2NO_2(\text{Wall}) \tag{47}$$

$$HO_2NO_2(\text{Wall}) \rightarrow HONO(\text{Wall}) + O_2 \tag{48}$$

$$2HONO(\text{Wall}) \rightarrow NO_2 + NO + H_2O \tag{49}$$

Thus we picture the wall as a catalytic surface which promotes the simple rearrangement of HO_2NO_2 to HONO and O_2 with the further decomposition of

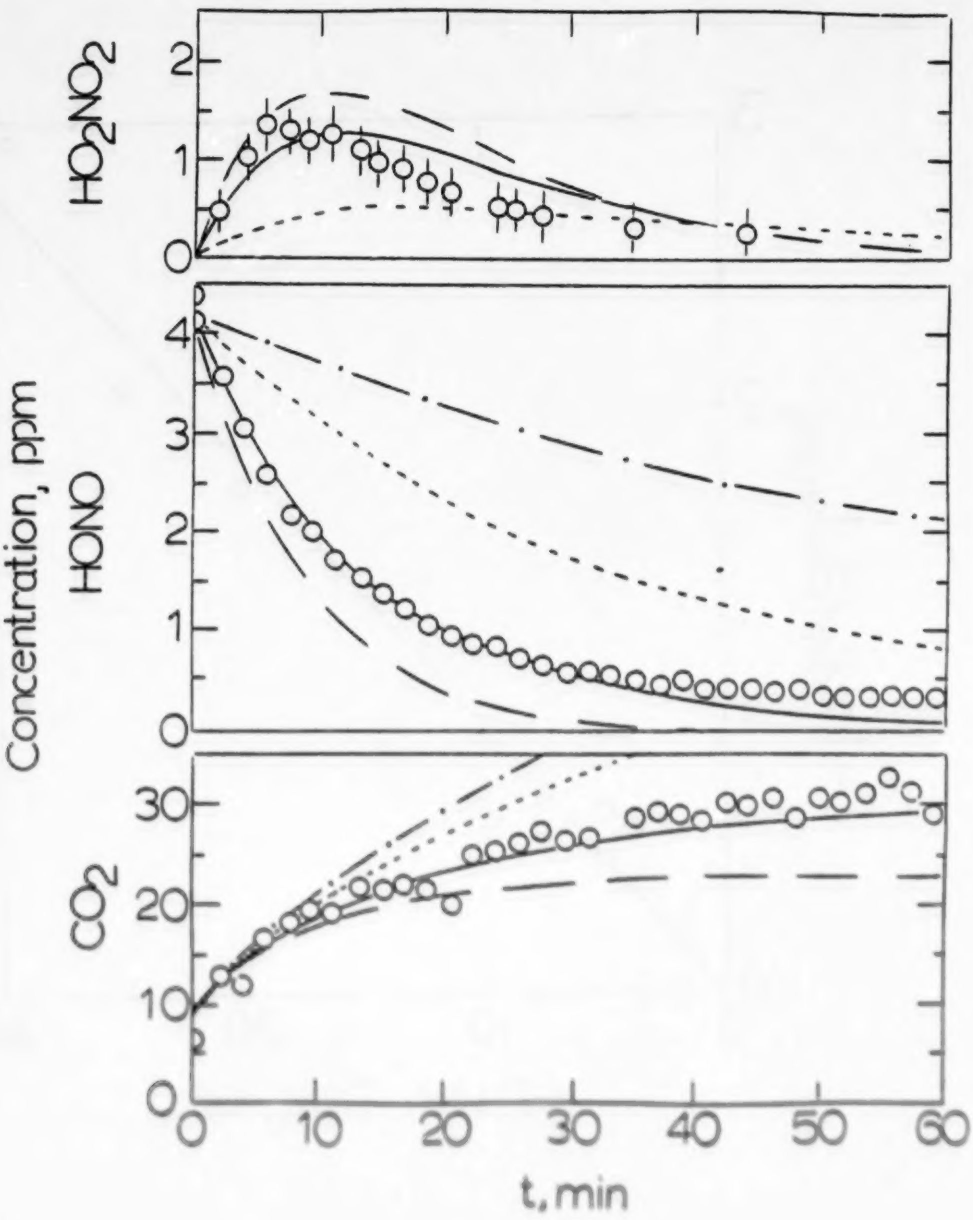

Fig. 31 Comparison of observed total [HONO]-, $[CO_2]$-, and $[HO_2NO_2]$-time data with those predicted by the simulation model involving reactions (21) through (49), Table VII, initial concentrations, total $[HONO]_0 = 4.29$, $[NO]_0 = 2.8$, $[NO_2]_0 = 1.1$, $[CO]_0 = 3.8 \times 10^4$ ppm, in synthetic air, 700 Torr; values of k_{21}/k_{22} chosen in simulations: ∞ (—o—); 5.0 (------); 0.74 (———); 0.00 (— — —); $k_{23}/(k_{21} + k_{22}) = 10$ in all runs shown.

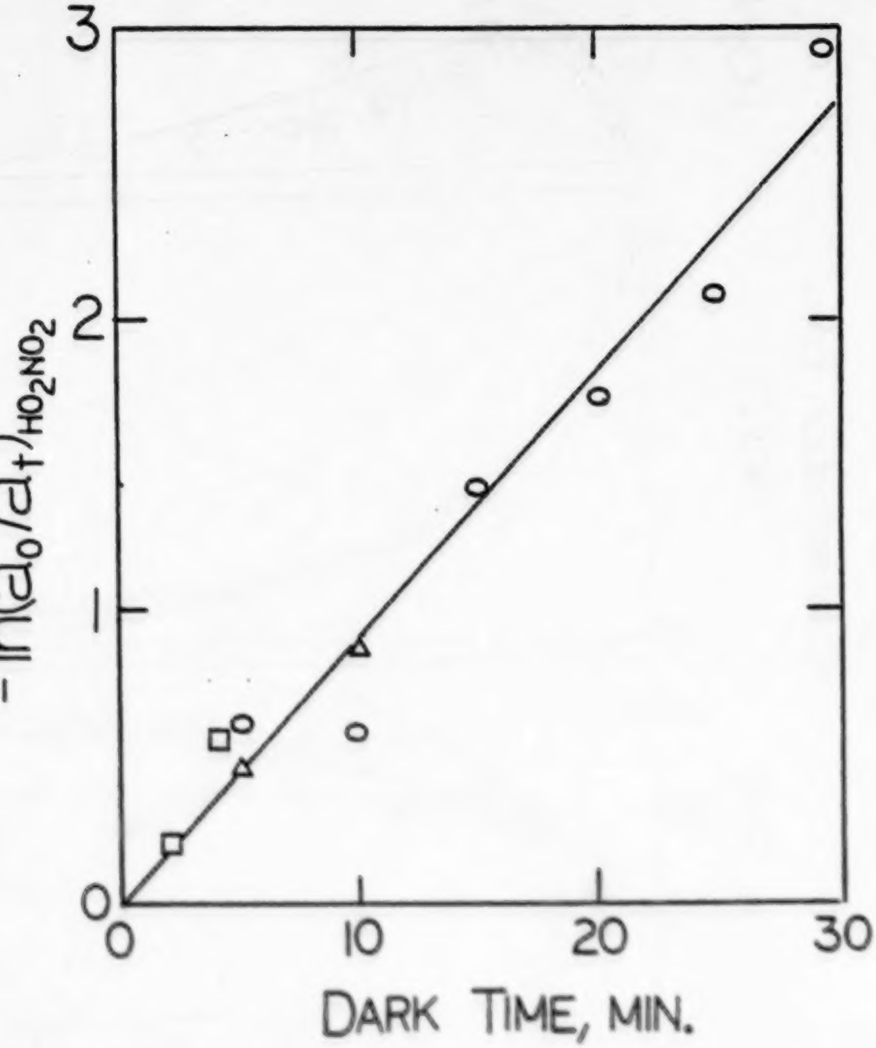

Fig. 32 The first order loss of HO_2NO_2 in three different dark runs; the squares are from data taken from a run with HONO-NO-NO_2-CO mixture; the remaining data points are from two different Cl_2-H_2-NO-NO_2 mixtures. The slope of this plot gives a first order loss constant of 9.1×10^{-2} min^{-1}.

HONO to its gaseous products. For our conditions of [NO], [NO_2], and [H_2O] present in the cell, the equilibrium level of HONO is very low (≈10^{-2}ppm), and the catalysis at the wall will result largely in HONO decomposition. Presumably the NO released in (49) will be oxidized quickly to NO_2 through its dark reactions with the products O_3 and NO_3 (N_2O_5), reactions (27) and (34), so that the only significant product which we see increase experimentally would be NO_2.

The simulations of [HO_2NO_2]-time profiles are given in Figure 31 for several choices of the rate constant ratio k_{21}/k_{22}. It is evident that the general form of the concentration-time profiles can be described adequately using k_{21}/k_{22} ratios which are most consistent with the [HONO] and [CO_2]-time curves as well. It appears to us that a ratio in the range $k_{21}/k_{22} = 0.7 \pm 0.4$ leads to the most consistent match of the kinetic data at hand. It is in qualitative agreement with the indirect estimate, $k_{21}/k_{22} = 1.1 \pm 1.1$, of Simonaitis and Heicklen from experiments without observation of either HONO or HO_2NO_2 (57). It is our feeling that the failure of previous workers to observe HONO in irradiated Cl_2, H_2, NO_2, air and Cl_2, CH_2O, NO_2, air systems, and thus consideration of reaction (21) as unimportant relative to (22), may be a consequence of the expected high reactivity of HONO toward Cl-atoms: $Cl + HONO \rightarrow HCl + NO_2$. In fact, we do observe very small amounts of HONO among the products (≈0.2 ppm) after only a short irradiation (1 min) of Cl_2, NO_2, H_2, air mixtures similar to those employed by Niki, et al. (58). This is the order of magnitude of HONO expected if reaction (21) occurs, as we suggest, but the HONO-Cl reaction rate constant is large. See Figure 33. The characteristic spikes of the HONO spectrum (Figure 33a) are seen clearly in the products of the Cl_2, H_2, NO, NO_2 photolysis after 1 min irradiation time (Figure 33b-2). This is more clearly demonstrated in the spectrum shown in 33b-3 where the CH_4 contribution (impurity in the O_2 used to prepare the synthetic air) has been removed. That the peaks in this spectrum are truly at exactly those positions due to HONO is evident in the removal of the three peaks by absorbance subtraction of the spectrum 33-a from that of 33b-3; this is shown in spectrum 33b-4.

The preliminary kinetic analysis of some of the dilute Cl_2, NO_2, NO, H_2 mixtures in synthetic air has been made. The mechanism is much more complex in the Cl_2-H_2-NO_2-air system. The additional reactions (50) through (65) (see Table VIII) are added to (21-49) in this case to simulate the chemical changes. The experimental product time data (curves a) and the computer simulations using reactions (21-65), curves b, may be compared in Figures 34 and 35. The initial reactant concentrations are shown in the captions of each figure.

In the simulations shown in Figures 34 and 35, the best fit of the data was had with the rate constants for reactions (21) and (22) chosen to be 3.5×10^1 and 9.0×10^1 $ppm^{-1}min^{-1}$, respectively. This checks well within the experimental error determined earlier in the HONO, NO_x, CO system.

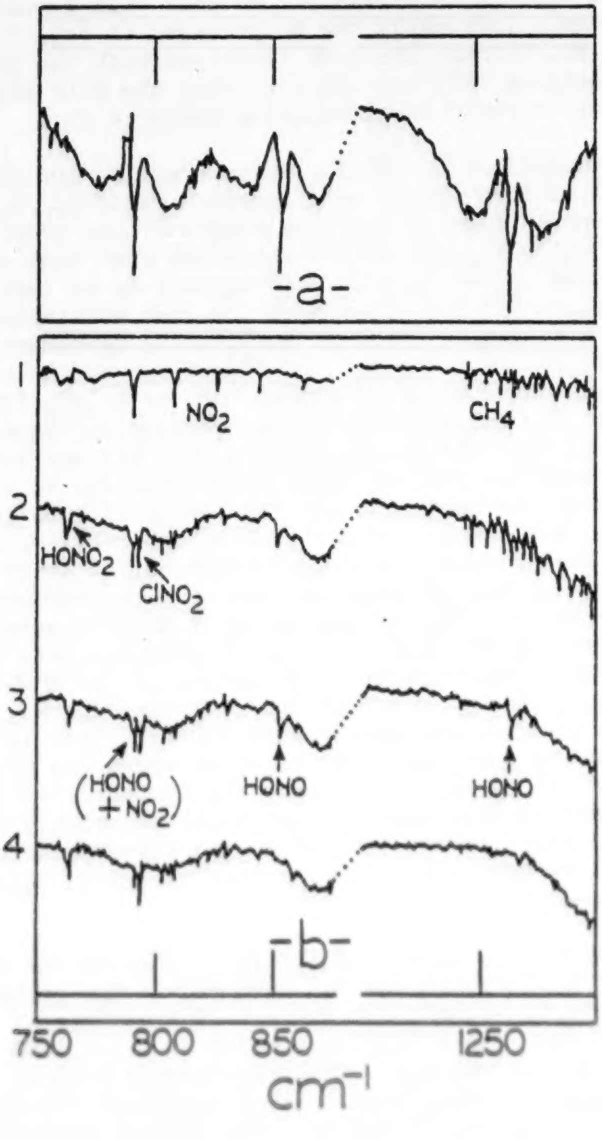

Fig. 33 (a) 3.2 ppm HONO; (b) initial conditions of Cl_2 = 7.5, H_2 = 8026, NO = 3.25 and NO_2 = 2.74 ppm. In (b) the spectrum 1 represents the filled cell at start before the lights are turned on, 2 is the spectrum after almost 1 min of irradiation time, 3 is the same mixture as spectrum 2 but with CH_4 subtracted out, 4 is the same mixture as spectrum 2 but with CH_4 and 6% of spectrum (a) subtracted out.

TABLE VIII

Additional Reactions and Rate Constants Required in the Simulation of the Dilute Cl_2, NO_2, NO, H_2 Mixtures in Air.[a]

Reaction	Rate Constant
(50) $Cl_2 + h\nu \rightarrow 2Cl$	0.10
(51) $Cl + O_2\ (+M) \rightarrow ClO_2\ (+M)$	2.0×10^{1}
(52) $ClO_2\ (+M) \rightarrow Cl + O_2\ (+M)$	1.8×10^{8}
(53) $Cl + H_2 \rightarrow H + HCl$	1.5×10^{1}
(54) $HO + H_2 \rightarrow H_2O + H$	1.03×10^{1}
(55) $HO + HCl \rightarrow H_2O + Cl$	1.0×10^{3}
(56) $Cl + HONO \rightarrow HCl + NO_2$	1.0×10^{5}
(57) $Cl + O_3 \rightarrow ClO + O_2$	2.7×10^{4}
(58) $Cl + H_2O_2 \rightarrow HCl + HO_2$	8.0×10^{2}
(59) $Cl + NO\ (+M) \rightarrow ClNO\ (+M)$	3.7×10^{3}
(60) $ClNO + h\nu \rightarrow Cl + NO$	0.34
(61) $Cl + NO_2\ (+M) \rightarrow ClNO_2\ (+M)$	1.0×10^{4}
(62) $ClNO_2 + h\nu \rightarrow Cl + NO_2$	0.03
(63) $Cl + ClNO_2 \rightarrow Cl_2 + NO_2$	5.0×10^{1}
(64) $ClO + NO \rightarrow NO_2 + Cl$	2.5×10^{4}
(65) $2ClO \rightarrow Cl_2 + O_2$	3.4×10^{3}

---

[a] These reactions and those in Table VII were used to simulate the Cl_2-NO_x-H_2-air system.

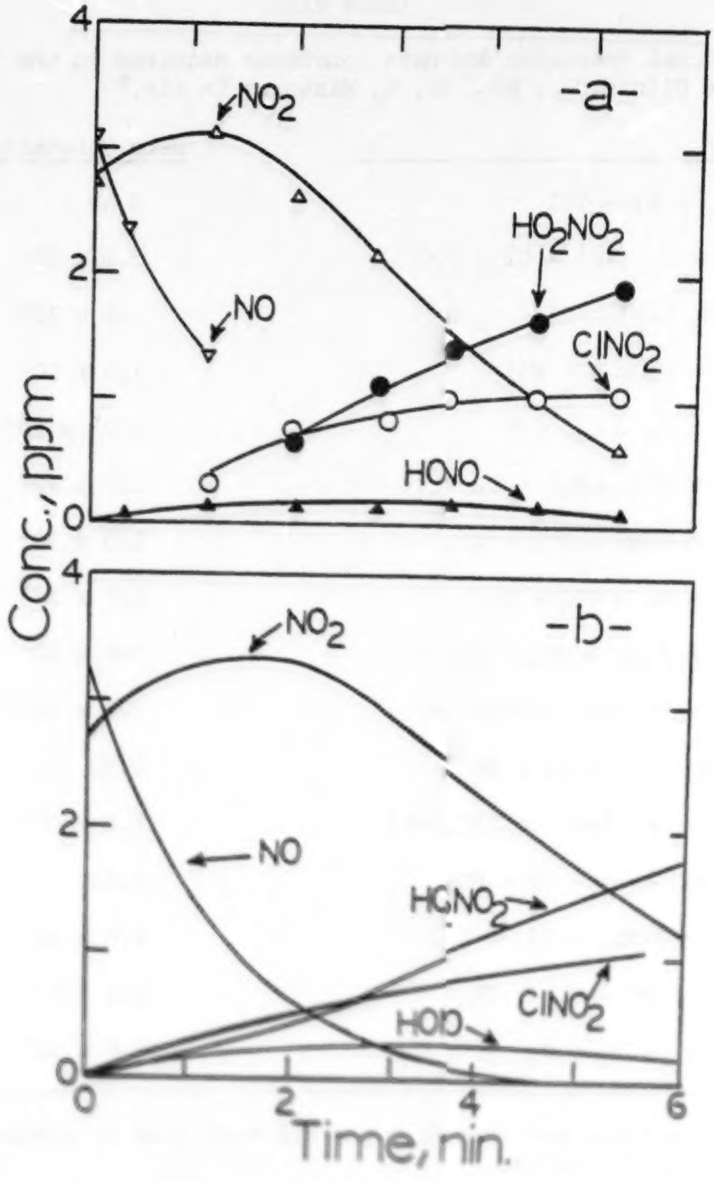

Fig. 34 Photolysis of Cl_2, H_2, NO_x, mixure in synthetic air; initial concentrations (ppm): $(Cl_2) = .5$; $(H_2) = 8026$; $(NO) = 3.25$; $(NO_2) = 2.74$; air added to a tol pressure of 700 Torr; (a) experimental data; (b) computersimulation.

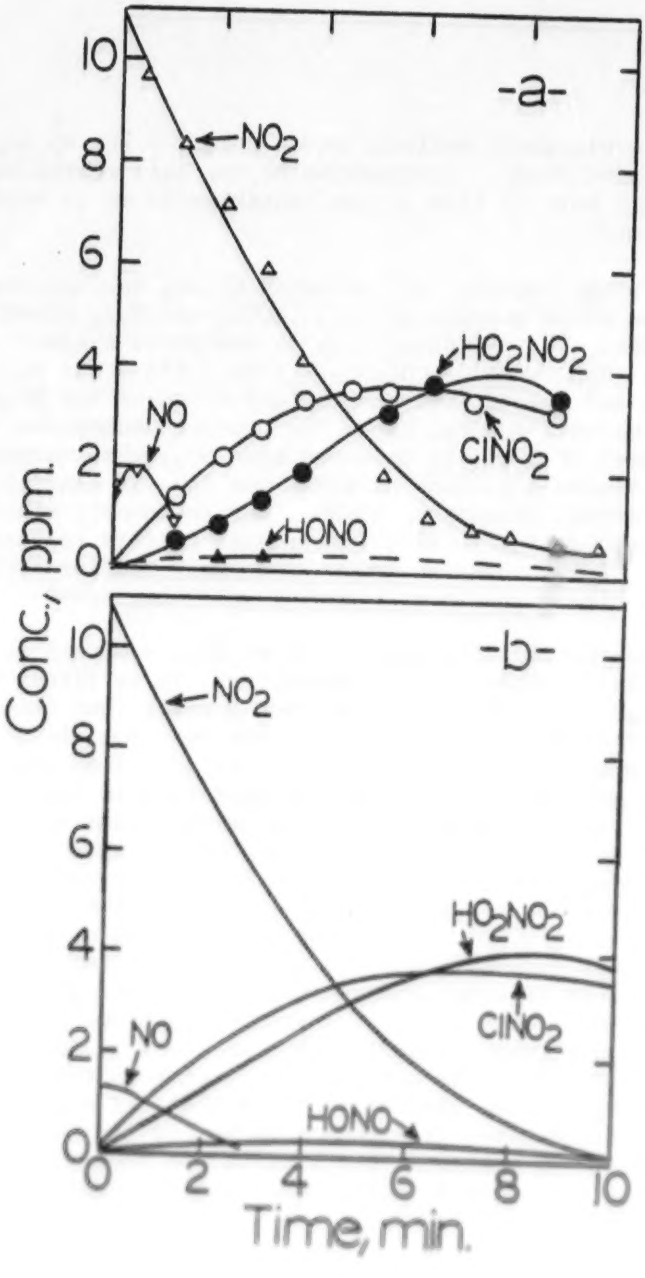

Fig. 35 Photolysis of Cl_2, H_2, NO_x, mixture in synthetic air; initial concentrations (ppm): $(Cl_2) = 15$; $(H_2) = 8026$; $(NO) = 1.28$; $(NO_2) = 11.1$; total pressure of 700 Torr; (a) experimental data; (b) computer simulation.

The preliminary analysis given here for the HO_2NO_2 reactions is under further study. Alternative HO_2NO_2 loss mechanisms are under test, and further work to firm up the mechanism is to be continued during the coming year.

Years ago Schwarz (54) prepared HO_2NO_2 through the reaction between pulverized solid samples of H_2O_2 (100%) and N_2O_5 mixed at -80°C in a vacuum line. The evidence which he presented suggests strongly that the reaction: $H_2O_2 + N_2O_5 \rightarrow HO_2NO_2 + HONO_2$, did occur on warming the mixture. Isolation and quantitative characterization of the HO_2NO_2 was not possible in Schwarz's work, since the product decomposed rapidly, liberating a great deal of heat, O_2 gas, and some NO_2, when warmed to -30°C. However, in dilute solutions of $HONO_2$ and H_2O_2 in glacial acetic acid, the product formed, presumably HO_2NO_2, was reasonably stable; under these conditions the highly oxidizing product readily released Br_2 from KBr solution. It is apparent from these early studies that HO_2NO_2 is an unstable, highly reactive, powerful oxidizing agent.

Since the wall destruction of HO_2NO_2, dominant in our systems, will be essentially absent in the atmosphere, it is likely that its lifetime in the lower atmosphere will be much greater than that which we observed here. Furthermore, simulations of the reactions in a typical NO_x-RH-RCHO-polluted atmosphere exposed to sunlight show that the theoretical rate of HO_2NO_2 generation is similar in magnitude to those expected (and observed in real atmospheres) for the peroxyacylnitrates. In view of these findings, we conclude that HO_2NO_2 may be an important product of photochemical smog. Because of its reported highly oxidizing character which was discovered years ago (54), we feel that it may contribute to eye irritation, plant damage, and other undesirable aspects of smog, as Hanst and Gay suggest. (61) It is important that specific analyses for HO_2NO_2 be made in urban atmospheres to evaluate directly the concentrations and the effects of this seemingly important compound. Niki, et al. (58), have proposed that HO_2NO_2 may be a potential sink for NO_x in the stratosphere; it is difficult to test this hypothesis on the basis of our present rate data, since the effect, if any, of the lower pressure of the stratosphere on the rate constant of the HO_2-NO_2 combination reaction (22) is unknown. Our studies are continuing to define better the kinetic behavior of this interesting compound both at tropospheric and stratospheric pressures.

EXPERIMENTAL DETAILS OF FTIRS AND PHOTOLYSIS CELL

The various chemical and photochemical experiments were carried out using a Digilab FTS-20 Fourier Transform Spectrometer (model 496 interferometer) coupled to a photolysis cell constructed of 30.5 cm diameter pyrex tubing 6.3 m long (445 ℓ) (see Figure 27). The cell housed modified White optics (49) giving traversal in increments of eight (instead of the usual four) with a base path of 5.3 m. All experiments were carried out at 170 m (32 traversals) which gave adequate absorption for compounds in the ppm concentration range having extinction coefficients of 10^{-4} - 10^{-2} $ppm^{-1}m^{-1}$ (at 1 cm^{-1} resolution and 700 Torr).

In order to study kinetics occuring on the minute time scale and have spectra of adequate signal-to-noise ratio, an appropriate choice of resolution and number of coadded interferograms must be chosen (both of these require time). For our experimental system, in conjunction with our apparatus, we chose 1 cm^{-1} resolution (1 cm optical retardation) and usually four scans (0.08 minutes per scan and 0.12 minutes delay for the first scan with out apparatus). Another convenient time-saving decision was to collect only 8K data points per interferogram by collecting data every other laser fringe (time saved in computation is more than a factor of two for 8K versus 16K). The resolution is not affected by such undersampling (the optical retardation is still 1 cm) and the useful spectral range is 0 to 4000 cm^{-1} (versus 0 to 8000 cm^{-1} for 16K data points) which is still greater than our useful system spectral window of 450 to 2400 cm^{-1}. This window is determined by our Nernst glower, Mullard liquid helium cooled Cu:Ge detector and KBr windows. The region from 1800 to > 4000 cm^{-1} can be covered by our Santa Barbara Research liquid nitrogen cooled In:Sb detector. The spectra were computed from interferograms in conjunction with box-car apodization in order not to sacrifice our 1 cm^{-1} nominal resolution.

The cell lighting was designed to mimic ground level solar radiation both in distribution and intensity which it does quite well. In Figure 18 from the previous final report (for Grant Number R803868-1) the distribution from 300 to 400 nm is similar. Our NO_2 photolysis rate of 0.6 min^{-1} is typical of atmospheric values for low zenith angles attesting to our intensity being in the range of ground level solar intensities.

In order to obtain a more uniform light distribution within the cell it is surrounded by an outer reflective shield of aluminum foil. Measurements with a Hewlett-Packard Radiant Flux Detector (model 8334A) at four different locations within the cell indicate uniformity to within ± 10%.

Temperature control during photolysis work is obtained by circulating room air between the cell and lights with a fan. A 2°C temperature rise within the cell is observed in 10 min with a 2°C differential between the two ends of the cell on the outside.

In order to overcome problems of varying water vapor and CO_2 absorption in the transfer optics between the Nernst glower source, interferometer, cell and detector the entire optical system was enclosed in a plastic (acrylic) box and purged with nitrogen with exposed dishes of NaOH and KOH. Absorptions due to degassing from the plastic were not a problem.

The gases were measured out in an all glass grease and mercury free system employing teflon stopcocks. The mechanical pump was isolated from the gas handling system by a liquid nitrogen trap. Pressures were measured using a glass spiral gauge which was set using Wallace-Tiernan absolute pressure gauges which insured that the gases only came in contact with glass or teflon. The gas handling rack was constructed with eight calibrated volumes (1 to 100 ml) with double valves for positive injection of samples. Larger calibrated bulbs were readily hooked up to the system with Cajon stainless steel quick-release vacuum pittings for injection of larger samples, or for use with gases having low working pressures.

The main surfaces inside the cell with which the gas mixtures come into contact (mainly through turbulent mixing of the gases due to temperature gradients) are pyrex and stainless steel (mirror supports, cell tubing spacers and end plates). Some corrosion of the stainless steel has been observed probably due to the action of HCl on the slightly moist surface. The teflon surface area due to the teflon sealing gaskets (8) between the pyrex cell tubing sections and end plates is small. The glass mirrors with aluminum reflective surfaces have a thin (1/8 wave) overcoat of silicon monoxide and show no signs of damage after fourteen months of use. The KBr windows (2 1/4 in. diameter) are transparent at a slightly longer wavelength than NaCl.

The treatment of time dependent transmission spectra from individual runs consisted of determining absorbances for individual species when no overlapping of spectral features occur. Concentrations were then obtained by using extinction coefficients for various gases determined at the same total pressure, resolution and transform method (8K data points, no zero filling of the interferogram and box-car apodization). See Table IX. In cases where spectral features of two species overlap, one species is removed by absorbance subtraction using calibrated reference files and the remaining species is then measured.

Various types of experiments have been carried out in the photochemical reactor. Numerous calibrations of gas used in the experiments were done either by direct pressure measurement of the gas, by chemical synthesis of the species in conjunction with mass balancing, or by simultaneously taking the spectrum and titrating another sample in the case of nitric acid. The cell was designed mainly to photolyse samples and study the kinetics of various system of interest from a stratospheric air pollution standpoint. A starting point for studying the kinetics of any photochemical system is to determine the primary photolysis rate for all species undergoing photodecomposition in our cell.

EXPERIMENTAL DETAIL OF PHOTOCHEMICAL AND SPECTRAL MEASUREMENTS

Peroxynitric acid (HO_2NO_2) formation by Cl_2 photolysis with NO_2 and H_2 present in air

Mixtures of Cl_2 (7.5 to 30 ppm), NO_2 (3 to 25 ppm), NO (0.7 ppm, due to inadvertant NO_2 photolysis during injection or from the slightly decomposed NO_2 sample), H_2 (4000 to 34000 ppm), N_2 (560 Torr) and O_2 (140 Torr) were photolysed to form peroxynitric acid (HO_2NO_2). The gases were standard commercial products used without further purification except for NO_2 which was degassed at 0°C. Methane (2 ppm) and CO (0.14 ppm) impurities were present.

TABLE IX

Extinction Coefficients
(base e, 1 cm^{-1} resolution, 700 Torr pressure,
25°C, 170 meter path, box-car apodization)

Molecule	Wavenumber (cm^{-1})	ϵ (ppm^{-1} m^{-1})
CO_2	720	1.70×10^{-4}
NO	1876	2.74×10^{-4}
NO_2	826	3.40×10^{-5}
	1575+	4.41×10^{-4}
	1585+	1.23×10^{-3}
	1600+ (10 cm^{-1} res)	1.99×10^{-3}
	1627+ (10 cm^{-1} res)	2.69×10^{-3}
O_3	1000+	1.29×10^{-4}
	1055+	9.74×10^{-4}
	1055+ (P_T = 100 Torr)	8.62×10^{-4}
cis-HONO	853	6.06×10^{-3}
trans-HONO	1264	3.84×10^{-3}
$HONO_2$	762	5.46×10^{-4}
	878	1.75×10^{-3}
	894	1.23×10^{-3}
N_2O_5	740+	4.0×10^{-3}
ClNO	1808+	5.51×10^{-3}
$ClNO_2$	780+	4.65×10^{-4}
	793	2.46×10^{-3}
	1267	1.19×10^{-3}
HO_2NO_2	802.7	2.35×10^{-3}
	810+	1.14×10^{-3}
CH_4	1305	1.67×10^{-3}
HCO_2H	1105	3.28×10^{-3}
H_2CO	1744	1.11×10^{-3}

+ broader structure - less resolution dependent

The lights were on for 6 to 15 minutes and the cell contents were monitored for another 40 minutes in the dark. Each spectra is computed from four coadded interferograms which requires 0.32 minutes to collect.

The measurement of most species in the spectra were from absorption measurements of selected spectral features. Nitryl chloride ($ClNO_2$) was removed and measured through absorbance subtraction using a calibrated reference file in order to measure the underlying HO_2NO_2 at around 800 cm^{-1}.

Mass balance of nitrogen and chlorine is not good in these runs, particularly at late times, due to chlorine and nitrogen active species on the walls forming stable compounds and coming off the walls. Spurious $ClNO_2$ and HNO_3 have been observed. Before chlorine gas and other chlorine containing species were introduced into the system, these problems were not observed. We concentrate our analysis on data from the first few minutes when wall effects should be less important.

Cl_2 photolysis in H_2 and air

30 ppm of Cl_2 was photolysed in 8066 and 34211 ppm of H_2 in a synthetic air mixture (700 Torr total pressure) in order to determine the primary photolysis rate of Cl_2 in our cell. Standard unpurified commercial gases were used. Methane (2 ppm) and CO (0.14 ppm) were present.

The photolyses were 15 min long with each spectrum corresponding to one interferogram (0.08 minutes collection time). A liquid nitrogen cooled In:Sb detector was used to follow the growth of HCl with time. Since HCl lines did not follow Beers Law, absorbance versus concentration curves (up to 60 ppm) were plotted for many of the HCl lines and used to measure HCl in the Cl_2 photolysis spectra.

Nitrosyl Chloride (ClNO) photolysis in H_2 and N_2

1 to 20 ppm of ClNO was photolysed in 34211 ppm of H_2 and 674 Torr of N_2 - 700 Torr total pressure. Standard commercial gases were used. The ClNO was degassed at liquid nitrogen temperature.

The mixtures were photolysed from 10 to 30 minutes with four scans (0.32 minutes) collected per spectrum. The Cu:Ge detector was used in all but one experiment (In:Sb detector used). Both ClNO decay and NO growth were followed by the absorption.

Nitryl Chloride ($ClNO_2$) synthesis and photolysis

Two methods were used to synthesize $ClNO_2$ in order to calibrate its absorption strength and to photolyse it.

The first method involved photolysis of Cl_2 (7 to 30 ppm) and NO_2 (7 tp 35 ppm) in either nitrogen or synthetic air at 700 Torr total pressure for ten to thirty minutes. Each spectra resulted from four coadded interferograms (0.32 minutes). $ClNO_2$ quantities were determined from nitrogen mass balances (NO_2, NO, N_2O_5, HNO_3, $ClNO_2$). Unfortunately, extinction coefficient consistency between runs and precision within a run was poor due to spurious wall effects.

The more successful quantitative method for measuring $ClNO_2$ involved the dark reaction between O_3 and ClNO.

Ozone was generated by applying a Tesla coil discharge externally on glass tubing through which oxygen was flowing into the cell. 2 to 7.5 ppm of O_3 was mixed with 1.5 ppm ClNO (degassed at liquid N_2 temperature). These mixtures contained from 6 to 50 Torr of O_2 and were pressurized to 700 Torr with N_2. The growth of $ClNO_2$ was monitored for a time period of 1 1/2 to 4 hours. Four interferograms were recorded for each spectra. The drop in ClNO was used as the measure for $ClNO_2$ with precision of the extinction coefficients better than 10% within a run.

One mixture which sat for four hours was photolysed in an attempt to measure the rate of $ClNO_2$ photolysis. It contained 1 ppm $ClNO_2$, 0.16 ppm O_3, 0.4 ppm ClNO, 0.38 ppm NO_2, 18 Torr O_2 and 682 Torr of N_2 when the lights were turned on. The $ClNO_2$ absorbance exhibited first order kinetics over the ten minute period that the lights were on.

Chlorine nitrate ($ClONO_2$) synthesis

$ClONO_2$ was synthesized by photolysing mixtures of Cl_2 (90 ppm), NO_2 (7 to 13 ppm) and O_3 (18 to 28 ppm) in synthetic air at 700 Torr for one to two minutes. It is very unstable at photolysis times longer than one minute due to reactions with other species and the walls. It was stable in the dark for 23 minutes.

Standard commercial gases were used. The NO_2 was degassed at ice temperature. O_3 was generated by discharging a Tesla coil externally on glass tubing through which oxygen was flowing into the cell. Methane (3.5 ppm) and CO (0.14 ppm) were present as impurities.

Spectra were derived from single scan interferograms (0.08 minutes). Mass balancing of nitrogen was not good as observed in other Cl_2 photolysis work due to wall problems ($ClNO_2$ always appears when O_3 and NO_2 are present). $ClONO_2$ was monitored using infrared extinction data from the literature (67) which was recorded at 125 Torr total pressure (the pressure correction for 700 Torr is not known).

HOCl synthesis

Mixtures of Cl_2 (60 ppm), O_3 ($\approx$ 20 ppm), and hydrocarbons (ethane, propane or isobutane at 5 ppm) in synthetic air at 700 Torr were photolysed for four minutes. The maximum amount of HOCl was observed at two minutes and was gone at four minutes probably due to photodecomposition.

Standard commercial gases were used without further purification. The small methane impurity (≈ 2 ppm) resulted in no detectable HOCl formation in a blank run, although spurious HNO_3 formation was seen. Ozone was formed by discharging a Tesla coil externally on glass tubing through which oxygen was flowing into the cell.

The spectra were derived from four coadded interferograms (0.32 minutes). In the runs with propane and isobutane, the acetone which is formed interferes with the HOCl absorption and was removed by computer subtraction of a calibrated reference acetone spectrum. Mass balancing of chlorine containing species would allow the quantitative determination of HOCl. Unfortunately, the frequency range of our system does not allow the simultaneous monitoring of HOCl and HCl which is necessary to carry out the chlorine mass balance.

N_2O_5 synthesis

Mixtures of NO_2 (2 to 15 ppm) and O_3 (2 to 8 ppm) in O_2 ($\approx$ 20 Torr) and N_2 ($\approx$ 680 Torr) react quickly in the dark to form N_2O_5 which slowly decays away.

Standard commercial gases were used. The NO_2 was degassed at ice temperature. Ozone was formed by discharging a Tesla coil externally on glass tubing through which oxygen was flowing into the cell.

Four or twenty interferograms were coadded for each spectrum. $ClNO_2$ is always observed when N_2O_5 is present, presumably due to some reactive chlorine species on the walls. The validity of nitrogen mass balancing in this work is valid only if no extra nitrogen comes off the wall or is lost to the wall.

Nitric Acid calibration

The vapor above a degassed sample of 70% nitric acid solution was allowed to enter two standard volumes and one calibrated trap simultaneously (the combined $HONO_2$ and H_2O vapor pressure was between 5 and 6 Torr at room temperature). The contents of the calibrated trap was frozen at liquid nitrogen temperature and titrated with a standard NaOH solution using the phenolphthalein end point. The contents of one of the calibrated volumes was then frozen into the trap at liquid nitrogen temperature and another titration performed. The two titrations were checked for consistency taking into account the different volume sizes. The contents of the third calibrated bulb was injected into the cell and pressurized to 700 Torr with nitrogen. Twenty interferograms were co-added per spectrum and usually two spectrum were taken for averaging of absorbance data.

From the titration data, the volume sizes, and the ideal gas law, the concentration of nitric acid in a given spectrum was readily calculated. A standard deviation of 20% was obtained for extinction coefficients determined from eight different nitric acid samples.

INFRARED SPECTRA OF COMPOUNDS

The following are infrared spectra of compounds used in the photolysis work and not included in the previous report of this project. All were recorded at 25 ± 2°C, 170 m path length, 1 cm^{-1} resolution (1 cm retardation), 8192 data points per interferogram with box-car apodization, usually 20 interferograms coadded per spectra, and 700 Torr total pressure.

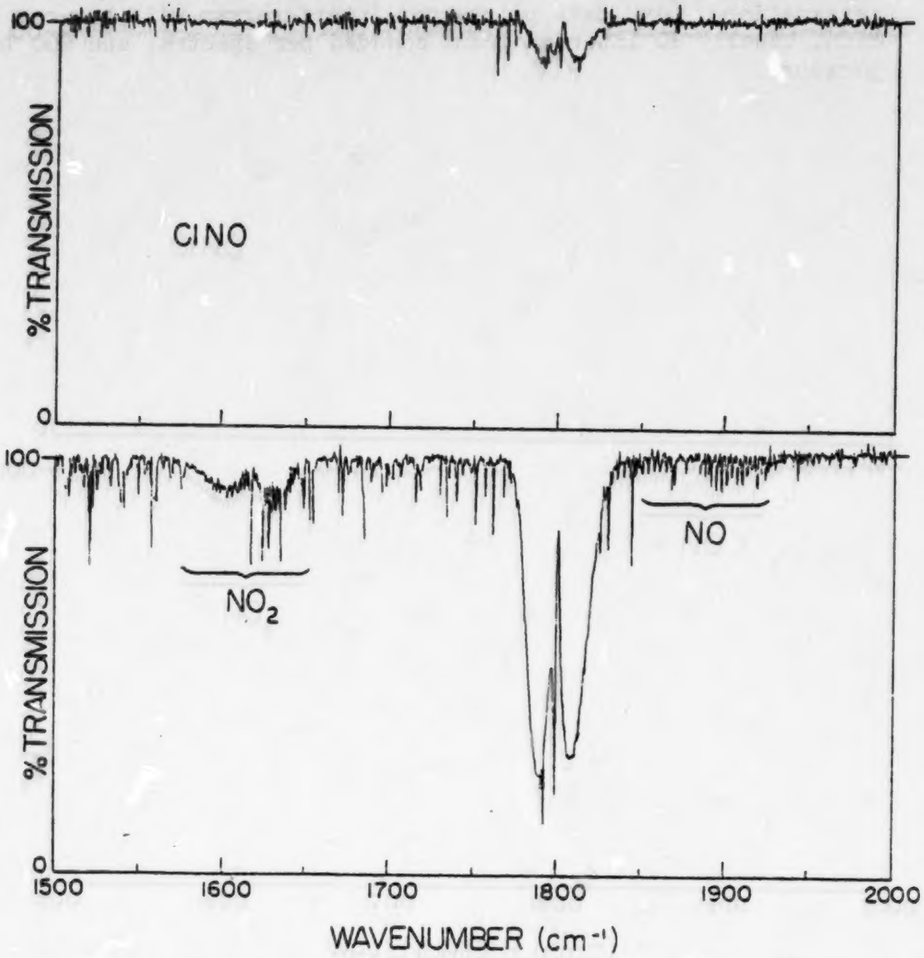

Fig. 36 Infrared spectrum of ClNO (nitrosyl chloride), top spectrum = 0.10 ppm, bottom spectrum = 1.36 ppm

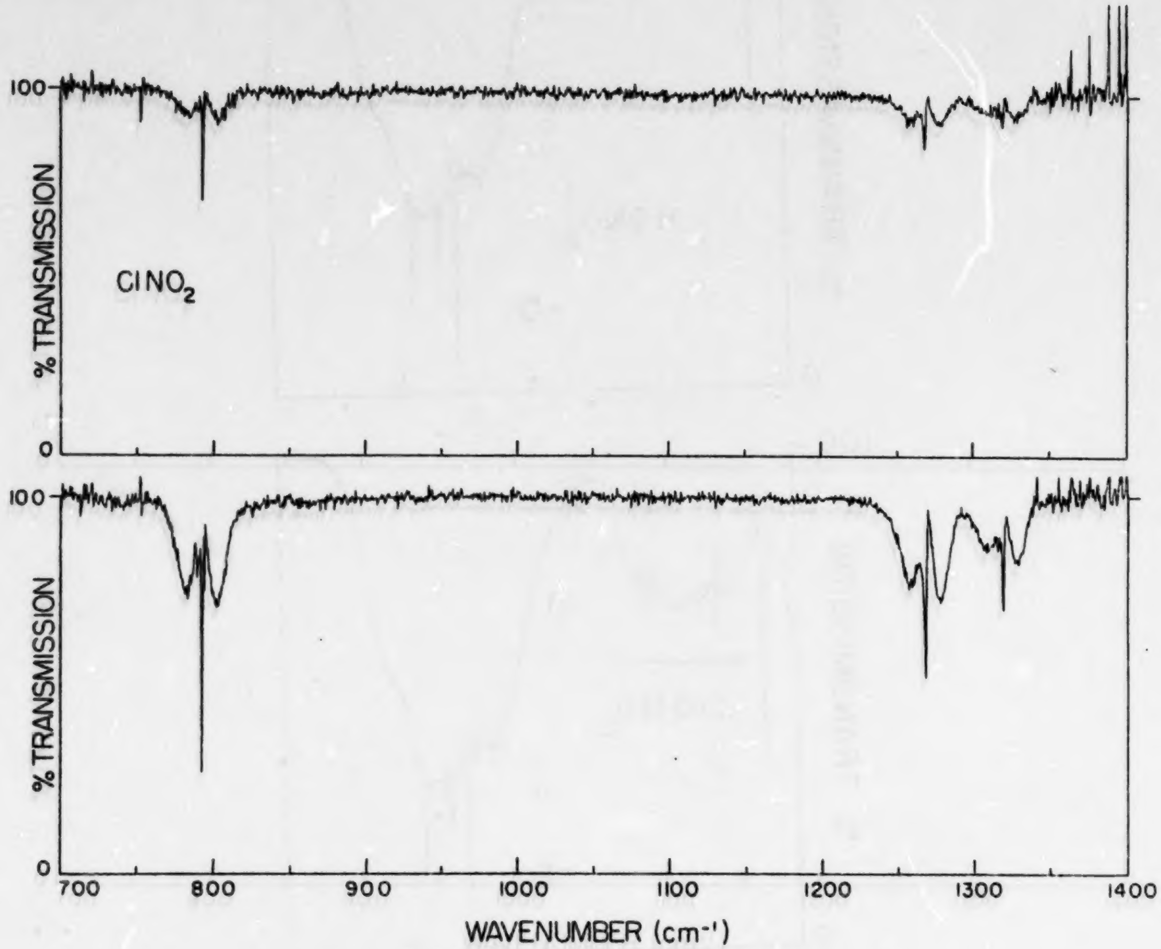

Fig. 37 Infrared spectrum of $ClNO_2$ (nitryl chloride), top spectrum = 0.88 ppm, bottom spectrum = 3.38 ppm

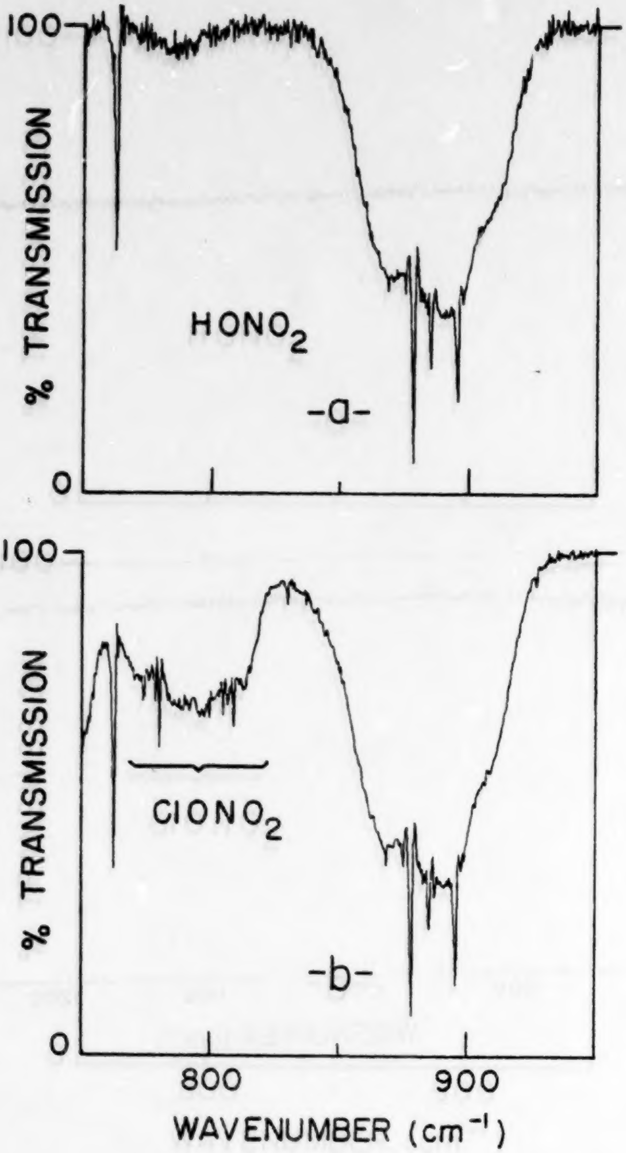

Fig. 38 a) 7.5 ppm $HONO_2$
b) ≈ 1.5 ppm $ClONO_2$ and 7.5 ppm $HONO_2$ formed during photolysis (0.7 min) of Cl_2 (90 ppm), NO_2 (13 ppm), O_3 (18 ppm) in a synthetic air mixture (P_T = 700 Torr)

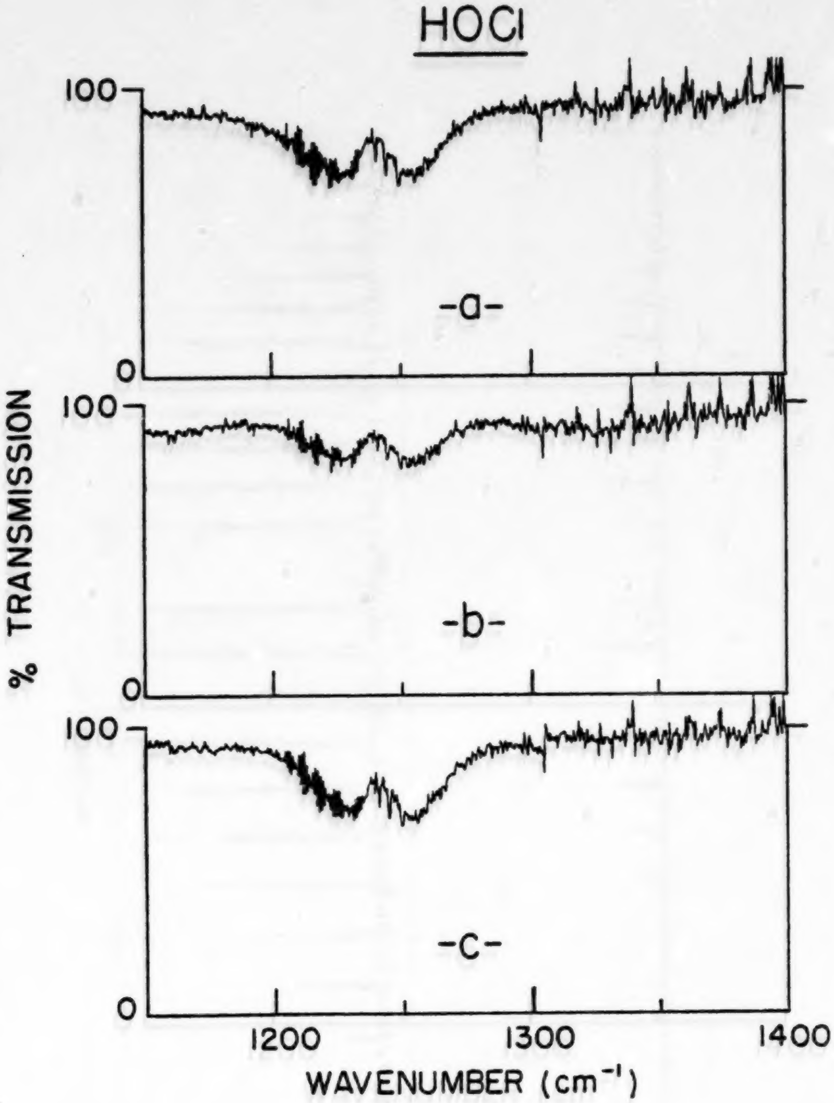

Fig. 39 HOCl formed during photolysis of Cl_2 (90 ppm), O_3 (20 ppm), hydrocarbon (5 ppm) mixtures in synthetic air (P_T = 700 Torr)

a) from iso-butane (2 min photolysis) with 4.3 ppm $(CH_3)_2CO$ removed

b) from propane (1 min photolysis) with 3.2 ppm $(CH_3)_2CO$ removed

c) from ethane (2 min photolysis)

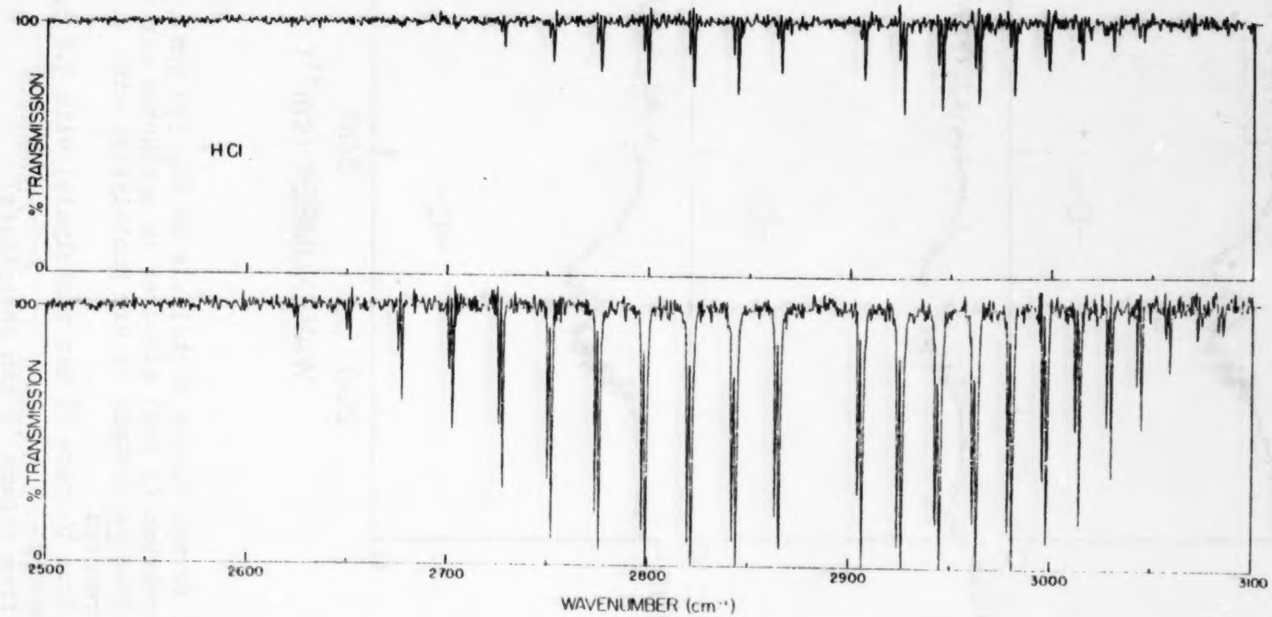

Fig. 40 Infrared spectrum of HCl, top spectrum = 1.83 ppm, bottom spectrum = 68.3 ppm

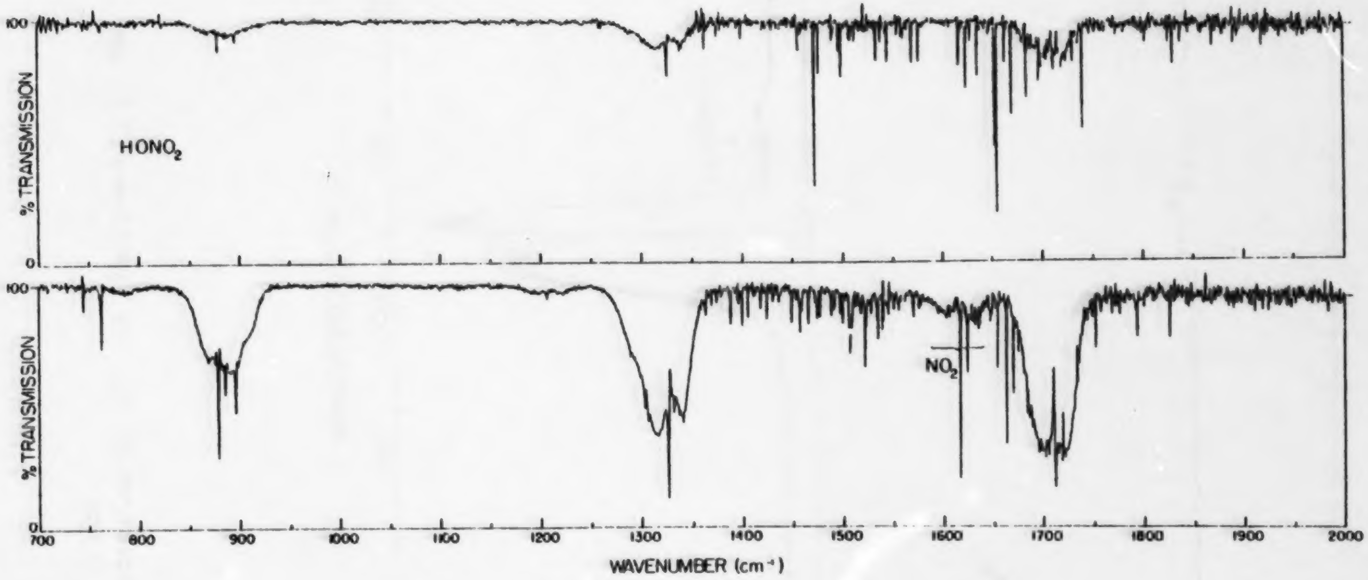

Fig. 41 Infrared spectrum of $HONO_2$, top spectrum = 0.39 ppm, bottom spectrum = 3.43 ppm

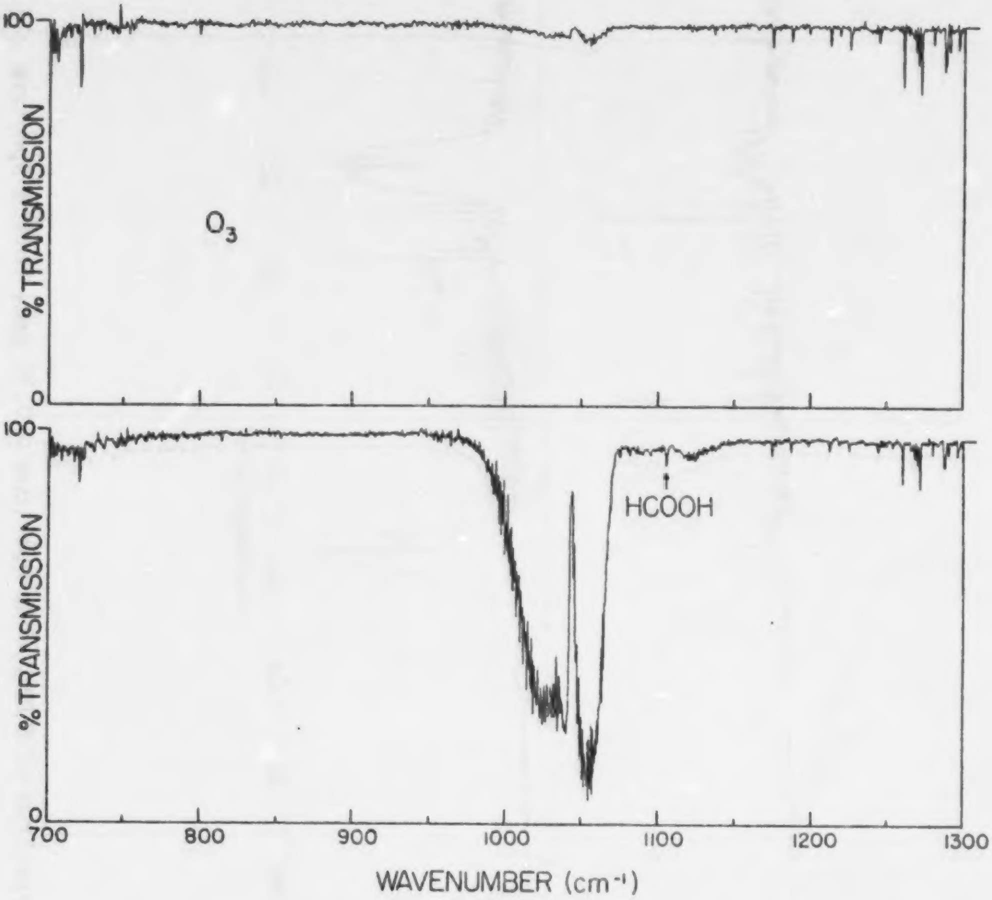

Fig. 42 Infrared spectrum of O_3, top spectrum = 0.26 ppm, bottom spectrum = 12.0 ppm

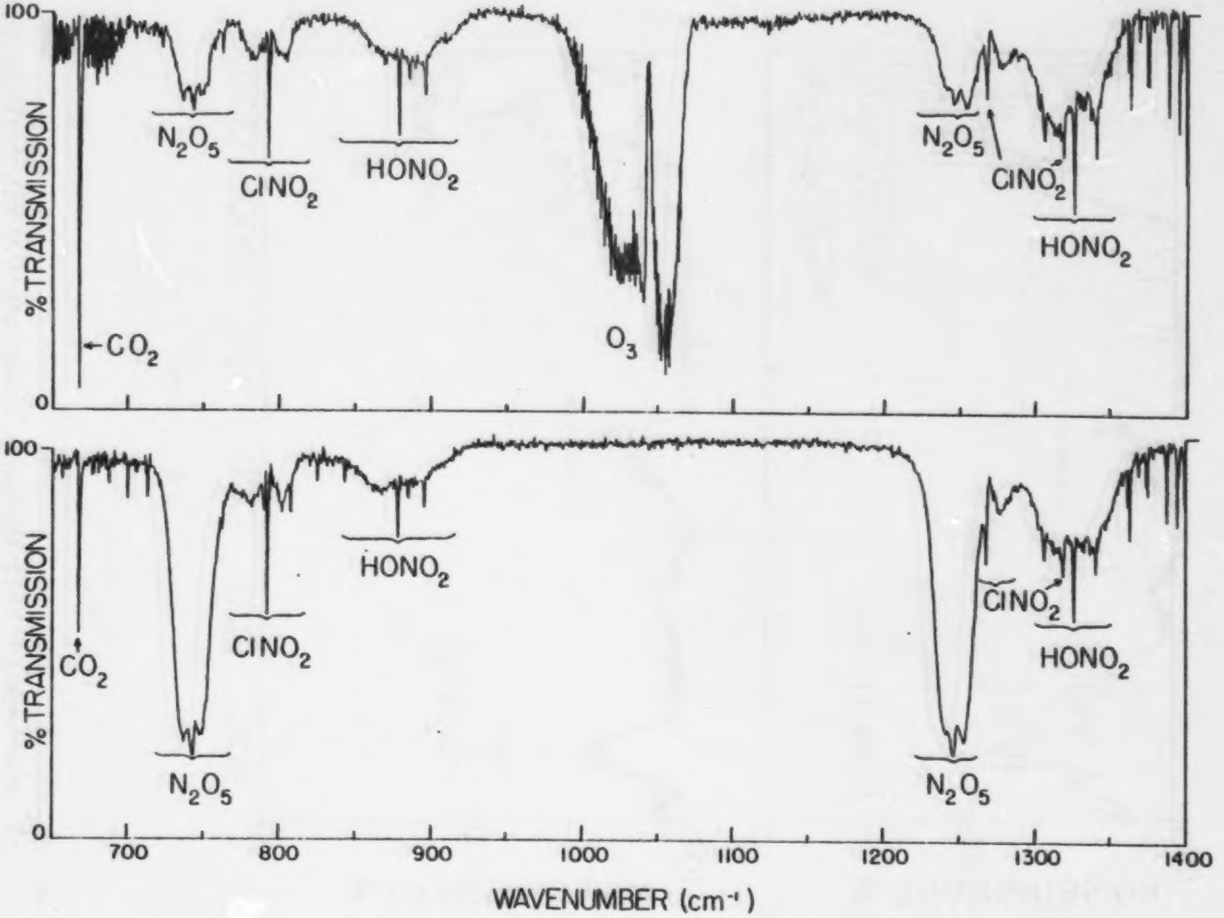

Fig. 43 Infrared spectrum of N_2O_5, top spectrum = 0.4 ppm, bottom spectrum = 2.2 ppm

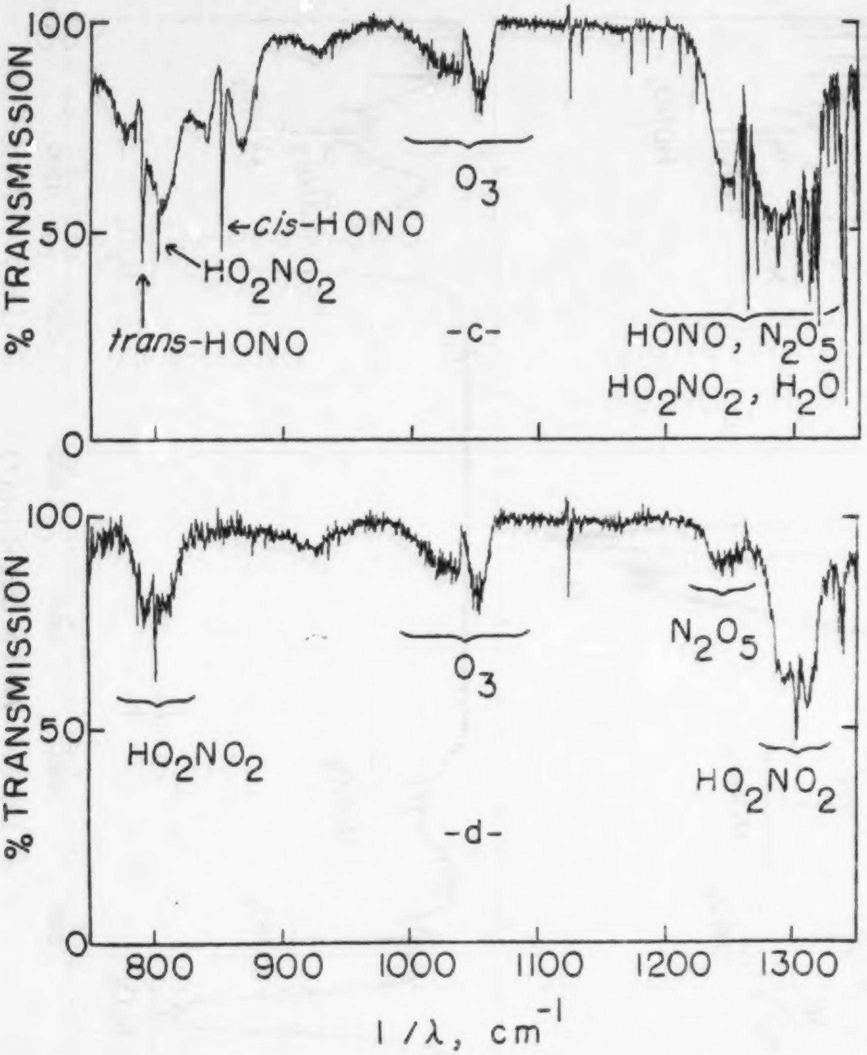

Fig. 44 HO_2NO_2 (1.1 ppm)

c) spectrum of cell contents following 5.9 min irradiation of the initial mixture: total $[HONO]_o$ = 4.3 ppm, $[NO]_o$ = 2.8, $[NO_2]_o$ = 1.1, $[CO]_o$ = 3.8 x 10^4 ppm in synthetic air

d) residual spectrum resulting from c) following computer subtraction of cis, trans-HONO, CH_4, and H_2O

FUTURE PLANS 1977-78

	Year III
A. Identification of Trace Atmospheric Constituents	
1. Solar spectra collection and analysis	major effort
2. Spectra of long paths of ground air	minor effort
3. Exploration of techniques for spectral data reduction and analysis	minor effort
B. The Study of Some Key Reactions of Possible Importance in Photochemical Smog Formation and the Natural Removal Mechanisms of Freons and Their Influence on O_3 Levels in the Stratosphere	
1. Reactions of alkylperoxy radicals with NO and NO_2	major effort
2. Role of aldehydes in photochemical smog formation	minor effort
3. A study of some potentially important atmospheric SO_2 removal mechanisms	minor effort
4. Natural removal mechanisms of freons	minor effort
C. Library of Spectra	minor effort
D. Research on Problems Identified from Previous Work	
1. Computer generated spectra	minor effort
2. Band intensity measurements and parameter ratios	minor effort
3. Installation of Nicolet interferometer	major effort

REFERENCES

1. M. Ackerman, D. Frimout, A. Girard, M. Gottignies, and C. Muller, Stratospheric HCl From Infrared Spectra, Geophys. Res. Lett., 3, 81-83 (1976).

2. C. B. Farmer, O. F. Raper, and R. H. Norton, Spectroscopic Detection and Vertical Distribution of HCl in the Troposphere and Stratosphere, Geophys. Res. Lett., 3, 13-16 (1976).

3. O. F. Raper, C. B. Farmer, and R. A. Toth, The Vertical Distribution of HCl in the 20-40 km Region of the Stratosphere. Paper presented at the International Conference on the Stratosphere and Related Problems, Logan, Utah, September 15-17, 1976.

4. W. J. Williams, J. J. Kosters, A. Goldman, and D. G. Murcray, Measurement of the Stratospheric Mixing Ratio of HCl using Infrared Absorption Technique, Geophys. Res. Lett., 3, 383-385 (1976).

5. D. H. Enhalt, L. E. Heidt, R. A. Lueb, and E. A. Martell, "Concentrations of CH_4, CO, CO_2, H_2, H_2O and N_2O in the Upper Atmosphere," J. Atm. Sci., 32, 163-169 (1975).

6. E. L. Heidt, R. Lueb, W. Pollock, and D. H. Enhalt, "Stratospheric Profiles of CCl_3F and CCl_2F_2," Geophys. Res. Lett., 2, 445-447 (1975).

7. N. E. Hester, E. R. Stephens, and O. C. Taylor, "Fluorocarbon Air Pollutants," III, Environ. Sci. and Technol., 9, 875-876 (1975).

8. P. W. Krey, R. J Lagomarsino, and J. J. Frey, "Stratospheric Concentrations of CCl_3F in 1974," J. Geophys. Res., 81, 1557-1560 (1976).

9. J. E. Lovelock, "Atmospheric Halocarbons and Stratospheric Ozone," Nature, 252, 292-294 (1974).

10. J. E. Lovelock, R. J. Maggs, and R. J. Wade, "Halogenated Hydrocarbons in and over the Atlantic," Nature, 241, 194ff (1973).

11. A. L. Schmeltekopf, P. D. Goldan, W. R. Henderson, W. J. Harrop, T. L. Thompson, F. C. Fehsenfeld, H. I. Schiff, P. J. Crutzen, I. S. A. Isaksen, and E. E. Ferguson, "Measurement of Stratospheric $CFCl_3$, CF_2Cl_2, and N_2O, "Geophys. Res. Lett., 2, 393-396 (1975).

12. B. T. Tyson, R. B. Brewer, J. A. Arveson, and J. F. Vedder, "Concentrations of Freon 12 and Nitrous Oxide in the Stratosphere." Paper presented at the International Conference on the Stratosphere and Related Problems, Logan, Utah, September 15-17, 1976.

13. W. J. Williams, J. J. Kosters, A. Goldman, and D. G. Murcray, "Simultaneous Stratospheric Measurements." Paper presented at the fall AGU Meeting, San Francisco, December 1975.

14. L. Zafonte, N. E. Hester, E. R. Stephens, and O. C. Taylor, "Background and Vertical Atmospheric Measurements of Fluorocarbon-11 and Fluorocarbon-12 over Southern California," Atm. Environ., 9, 1007-1009 (1975).

15. A. L. Schmeltekopf, P. D. Goldan, W. R. Henderson, W. J. Harrop, T. L. Thompson, F. C. Fehsenfeld, H. I. Schiff, P. J. Crutzen, I. S. S. Isaksen, and E. E. Ferguson, "Measurement of Stratospheric $CFCl_3$, CF_2Cl_2 and N_2O," Geophys. Res. Lett., 2, 393-396 (1975).

16. B. T. Tyson, R. B. Brewer, J. A. Arveson, and J. F. Vedder, "Concentrations of Freon 12 and Nitrous Oxide in the Stratosphere." Paper presented at the International Conference on the Stratosphere and Related Problems, Logan, Utah, September 15-17, 1976.

17. J. G. Anderson, Rocket Measurements of OH in the Mesosphere, J. Geophys. Res., 76, 7820-7824 (1971).

18. J. G. Anderson, The Absolute Concentration of OH $(X^2 \pi)$ in the Earth Earth's Stratosphere, Geophys. Res. Lett., 3, 165-168 (1976).

19. J. G. Anderson, A Simultaneous Measurement of Cl and ClO in the Earth's Stratosphere, paper presented at the International Conference on the Stratosphere and Related Problems, Logan, Utah, September 15-17, 1976.

20. R. A. McClatchey, W. S. Benedict, S. A. Clough, D. E. Burch, R. F. Calfee, K. Fox, L. S. Rothman, and J. S. Garing, "AFCRL Atmospheric Absorption Line Parameters Compilation." AFCRL-TR-73-0096, Environmental Research Paper No. 434 (1973).

21. R. J. Nordstrom, J. H. Shaw, W. R. Skinner, J. G. Calvert, W. H. Chan, and W. M. Uselman, A Comparison of High Resolution Observed and Computed Air Spectra Between 700 and 2300 cm^{-1}," Interim Report prepared under EPA Grant No. R803868-02 (August 1976).

22. J. Calvert, W. H. Chan, E. Niple, R. J. Nordstrom, J. H. Shaw, W. R. Skinner, and W. M. Uselman, Application of Fourier Transform Spectroscopy to Air Pollution Problems; report issued by The Ohio State University Research Foundation under EPA Grant No. R803868-1 (1976).

23. J. E. Harries and J. Chamberlain, Filter Radiometer: the Selective Interferometer, Appl. Optics 15, 2667-72 (1976).

24. A. R. Barringer and J. H. Davies, Investigations in Correlation Spectroscopy and Interferometry, Proceedings of the Joint Conference on Environmental Pollutants, Paper 71-1105 (Amer. Inst. Aeronautics and Astronautics, New York (1971).

25. P. G. Abell, P. Ellis, J. T. Houghton, G. Peckham, C. D. Rodgers, S. D. Smith, and E J. Williamson, Proc. R. Soc. A320, 35 (1970).

26. F. W. Taylor, J. T. Houghton, G. Peskett, C. D. Rogers, and E. J. Williamson, Appl. Opt. 11, 135 (1972).

27. S. D. Smith and L. R. Pigeon, Mem. Soc. R. Sci. Liège, 9336 (1964).

28. R. M. Goody, J. Opt. Soc. Amer. 58, 900 (1968).

29. V. E. Derr, M. H. Ackley, M. J. Post, and R. F. Calfee, Remote Sensing of Pollutants Computerized Reduction of Long-Path Absorption Data, NOAA Technical Report ERL 302-WPL 33, Boulder, Colorado (1974).

30. P. R. Bevington, Data Reduction and Error Analysis for the Physical Sciences, McGraw Hill Inc., New York (1969).

31. Y. S. Chang and J. H. Shaw, A Non Linear Least Squares Method of Determining Line Intensities and Half Widths, Applied Spectroscopy (In Press).

32. L. S. Rothman and R. A. McClatchey, Updating the AFCRL Atmosphere Absorption Line Parameters Compilations, Appl. Opt. 15, 2616-7 (1976).

33. W. R. Skinner and R. J. Nordstrom, Accuracy of the AFCRL Atmosphere Absorption Line Parameters Compilation, in the 10-µm Atmosphere Window, Appl. Opt. 15, 2616 (1976).

34. R. Blickensderfer, G. Ewing, and R. Leonard, Appl. Opt. 7, 2114 (1968).

35. W. H. Chan, R. J. Nordstrom, J. G. Calvert, and J. H. Shaw, An IRFTS Spectroscopic Study of the Kinetics and the Mechanism of the Reactions in the Gaseous System, HONO, NO, NO_2, H_2O, Chem. Phys. Letters, 37(3):441-446 (1976).

36. W. H. Chan, R. J. Nordstrom, J. G. Calvert, and J. H. Shaw, Kinetic Study of HONO Formation and Decay Reactions in Gaseous Mixtures of HONO, NO, NO_2, H_2O, and N_2, Environ. Sci. Technol., 10:674-682 (1976).

37. D. L. Baulch, D. D. Drysdale, and A. C. Lloyd, "High Temperature Reaction Rate Data," Department Physical Chemistry, University of Leeds, England, Vol. 1 (1968).

38. W. E. Wilson, Jr., A Critical Review of the Gas Phase Reaction Kinetics of the Hydroxyl Radical, J. Phys. Chem., Ref. Data, 1:535-573 (1972).

39. A. A. Westenberg and N. deHass, Rates of CO + OH and H_2 + OH over an Extended Temperature Range, J. Chem. Phys.:58, 4061-4065 (1973).

40. F. Stuhl and H. Niki, Pulsed Vacuum-UV Photochemical Study of Reactions of OH with H_2, D_2, and CO using a Resonance-Fluorescent Detection Method, J. Chem. Phys.:57, 3671-3677 (1972).

41. D. D. Davis, S. Fischer, and R. Schiff, Temperature Dependence of the Reactions $HO + CO \rightarrow CO_2 + H$ and $HO + CH_4 \rightarrow H_2O + CH_3$, J. Chem. Phys.:61, 2213-2219 (1974).

42. I. W. M. Smith and R. Zellner, Rate Measurements of Reactions of OH by Resonance Absorption, J. Chem. Soc., Faraday Trans. II:69, 1617-1627 (1973).

43. R. Overend, G. Paraskevopoulos, and R. J. Cuetanovic, Paper 6-4, HO-Radical Rate Measurements for Simple Species by Flash Photolysis Kinetic Spectroscopy, Abstracts 11th Informal Conference on Photochemistry, Vanderbilt University, Nashville, Tennessee, pp. 248-252 (1974).

44. S. Gordon and W. A. Mulac, Reaction of the $OH(X^2\pi)$ Radical Produced by Pulse Radiolysis of Water Vapor, Int. of Chem. Kinet.; Symp. No. 1:289-299 (1975).

45. R. A. Cox, R. G. Derwent, and P. M. Holt, Relative Rate Constants for the Reactions of OH Radicals with H_2, CH_4, CO, NO, and HONO at Atmospheric Pressure and 296° K, J. Chem. Soc., Faraday Trans. I:72, 2031-2043 (1976).

46. B. K. T. Sie, R. Simonaitis, and J. Heicklen, The Reaction of HO with CO, Int. J. Chem. Kinet.:8, 85-98 (1976).

47. R. Greiner, Hydroxyl-Radical Kinetics by Kinetic Spectroscopy, I, Reactions with H_2, CO, and CH_4 at 300° K, J. Chem. Phys.:46, 2795-2799 (1967).

48. A. Y. M. Ung and R. A. Back, The Photolysis of Water Vapor and Reactions of the HO-Radicals, Can. J. Chem.:42, 753-763 (1964).

49. P. L. Hanst, Spectroscopic Methods for Air Pollution Measurements, Adv. Environ. Sci. Technol.:2, 91-213 (1971).

50. R. A. G. Carrington, The Infra-Red Spectra of Some Organic Nitrates, Spectrochem. Acta:16, 1279-1293 (1960).

51. T. Urbanski and M. Witanowski, Infra-Red Spectra of Nitric Esters, Trans. Faraday Soc.:59, 1039-1045 (1963).

52. R. Greiner, Hydroxyl Radical Kinetic Spectroscopy, VI, Reactions with Alkanes in the Range 300-500° K, J. Chem. Phys.:53, 1070-1076 (1970).

53. G. Paraskevopoulos, Private Communication to One of the Investigators (J.S.C.)

54. R. Schwarz, Über die Peroxysalpetersäure, Feit. Anorg. Chem.:256, 3-9 (1948).

55. R. Simonaites and J. Heicklen, Reaction of HO_2 with NO and NO_2, J. Phys. Chem.:78, 653-657 (1974).

56. R. A. Cox and R. G. Derwent, Kinetics of the Reaction of HO_2 with NO and NO_2, J. Photochem.:4, 139-153 (1975).

57. R. Simonaitis and J. Heicklen, Reactions of HO_2 with NO and NO_2 and of OH with NO, J. Phys. Chem.:80, 1-7 (1976).

58. H. Niki, P. D. Maker, C. M. Savage, and L. P. Breitenbach, Fourier Transform IR Spectroscopic Observations of Pernitric Acid Formed Via $HO_2 + NO_2 \rightarrow HO_2NO_2$, Submitted for publication, Chem. Phys. Letters, September 1976.

59. B. W. Gay, Jr., R. C. Noonan, J. J. Bufalini, and P. L. Hanst, Photochemical Synthesis of Peroxyacyl Nitrates in Gas Phase Via Chlorine-Aldehyde Reaction, Environ. Sci. Technol.:10, 82-85 (1976).

60. H. Niki, P. Maker, C. Savage, and L. Breitenbach, Paper N2, IR Fourier-Transform Spectroscopic Studies of Atmospheric Reaction, Extended Abstracts of 12th Informal Conference on Photochemistry: June 28, 1976, N.B.S., Gaithersburg, Maryland, p. N2-1 to N2-4.

61. P. L. Hanst and B. W. Gay, Jr., Photochemical Reactions among Formaldehyde, Chlorine, and Nitrogen Dioxide in Air, Environ. Sci. Technol.: submitted for publication, September 1976.

62. R. F. Hampson, Jr. and D. Garvin, Chemical Kinetic and Photochemical Data for Modelling Atmospheric Chemistry, N.B.S. Technical Note 866 (1975).

63. W. H. Chan, W. M. Uselman, J. S. Calvert, and J. H. Shaw, The Pressure Dependence of the Rate Constant for the Reaction: $HO + CO \rightarrow H + CO_2$, Chem. Phys. Letters:45, 240-244 (1977).

64. W. Hack, K. Hoyerman, and H. G. Wagner, The Reaction $NO + HO_2 \rightarrow NO_2 + OH$ with $OH + H_2O_2 \rightarrow HO_2 + H_2O$ as the HO_2-Source, Inst. of Chem. Kinet.: Symp. No. 1, 329-339 (1975).

65. W. A. Payne, L. J. Stief, and D. D. Davis, A Kinetic Study of the Reaction of HO_2 with SO_2 and NO, J. Amer. Chem. Soc.:95, 7614-7619 (1973).

66. E. R. Stephens, The Formation, Reactions, and Properties of Peroxyacyl Nitrates (PANs) in Photochemical Air Pollution, Adv. Environ. Sci.:1, 119-146 (1969).

67. R. A. Graham, E. C. Tuazon, A. M. Winer, J. N. Pitts, Jr., L. T. Molina, L. Beaman, and M. J. Molina, High Resolution Infrared Absorptivities for Gaseous Chlorine Nitrate, Geophys. Res. Letters: 4, 3-5 (1977).

APPENDIX A

SUMMARY OF OBJECTIVES FROM 1975 PROPOSAL

I. SUMMARY OF OBJECTIVES

The primary objective of the research outlined in this proposal is to develop infrared fourier transform spectroscopic (FTS) techniques to characterize certain key air pollutants, their precursors and reaction products, and to establish quantitative kinetic and mechanistic details of the interrelationships between these pollutants both in simulated and real atmospheres. We have chosen for study during the three year period of this research effort the following important, yet unresolved, problems related to the transformations of contaminants in both the troposphere and stratosphere. These systems are particularly well suited for study with the FTS system and associated equipment now in use at the Ohio State University laboratories.

A. Study of the natural removal mechanisms of the Freons and their influence on the ozone concentration in the stratosphere:

1. The chlorine atom sensitized decomposition of ozone. The chemical kinetics and mechanism of interactions in the irradiated O_3, NO, NO_2, Cl_2 system.

2. The fate of the organic free radicals formed by photodissociation of the Freons in the stratosphere. The chemical kinetics and mechanisms of the reactions of the CF_2Cl and CCl_2F free radicals in air at stratospheric pressures.

3. The alteration of the stratospheric ozone concentration through Freon addition. The laboratory simulation of the photochemistry of the stratosphere perturbed by Freon addition.

B. Study of certain key reactions, seemingly important in photochemical smog systems:

1. The role of nitrous acid in the development of the important free radical chain carrier, HO, and its relation to smog formation in the urban atmosphere. A kinetic study of the NO, NO_2, HONO, CO system. The quantum efficiency of HO radical formation in the sunlight photolysis of HONO in air. The determination of important rate constants for the HO reactions with NO and NO_2, and HO_2 with NO will be made.

2. The role of the aldehydes in smog development in the urban atmosphere. The nature and mechanism of the formation of

the products formed in the photooxidation of formaldehyde. A kinetic study of the CH_2O, NO, NO_2, air, and the CH_2O, NO, NO_2, Cl_2, air systems. A search for the illusive peroxyformyl nitrate.

3. A study of some potentially important SO_2 removal mechanisms in the lower atmosphere. The rates of the primary reactions of HO and HO_2 with SO_2 from the FTS study of the CH_2O, SO_2, CO, air and HONO, SO_2, CO, air systems. The nature of the SO_2-oxidizing species formed in the O_3-olefin dark reaction.

4. The determination of high resolution infrared spectra of the common atmospheric contaminants and their products. Cataloging of the absorption coefficient-wavelength data for use in this work and by other investigators in the field.

5. Direct observation of the infrared absorption spectra of air samples in Columbus, Ohio. We will employ both in situ samples, observed using solar infrared transmission spectra in long atmospheric paths near sunset and sunrise, and confined samples in the laboratory long-path system (up to 1.5 km); spectra will be taken at regular intervals throughout the period.

APPENDIX B

PAPERS PRESENTED AT MEETINGS

1. "An IRFTS Spectroscopic Study of the Kinetics and the Mechanism of the Reactions in the Gaseous System, HONO, NO, NO_2, H_2O." Walter H. Chan, Robert J. Nordstrom, Jack G. Calvert and John H. Shaw, presented at the Centennial ACS meeting, New York City, April, 1976.

2. "A Partial Analysis of HONO Bands Between 750 and 1300 cm^{-1}." Walter H. Chan, C. Weldon Mathews and Robert J. Nordstrom, presented at the 31st Symposium of Molecular Structure and Spectroscopy, Columbus, Ohio, June, 1976.

3. "Infrared Spectroscopic Detection of Fluorocarbon-12 in the Atmosphere." Robert J. Nordstrom, W. R. Skinner, J. H. Shaw, W. H. Chan, W. M. Uselman, and J. G. Calvert, presented at the 31st Symposium of Molecular Structure and Spectroscopy, Columbus, Ohio, June, 1976.

4. "Comparison of Measured and Computer Spectra of Air Samples." R. J. Nordstrom, W. R. Skinner, J. H. Shaw, W. H. Chan, W. M. Uselman, and J. G. Calvert, presented at the 31st Symposium of Molecular Structure and Spectroscopy, Columbus, Ohio, June, 1976.

5. "Detection and Photochemistry of Selected Air Pollutants Using FT-IR Techniques." J. Shaw, Invited Paper, Coblentz Award Symposium, Pittsburgh Conference, March, 1977.

6. "Computer Assisted Technique of Analyzing Spectra." Y. S. Chang, J. H. Shaw, J. G. Calvert, and W. M. Uselman, presented at the 32nd Symposium of Molecular Spectroscopy Symposium, Columbus, Ohio, June, 1977.

7. "Investigations of Atmospheric Spectra." J. H. Shaw, Y. S. Chang, J. G. Calvert, and W. M. Uselman, presented at the International Conference on Fourier Transform Infrared Spectroscopy, Columbia, South Carolina, June, 1977.

APPENDIX C

PAPERS PUBLISHED OR ACCEPTED FOR PUBLICATION

1. "An IRFTS Spectroscopic Study of the Kinetics and the Mechanism of the Reactions in the Gaseous System, HONO, NO, NO_2, H_2O." Walter H. Chan, Robert J. Nordstrom, Jack G. Calvert, and John H. Shaw, Chemical Phys. Letters, 37, 441-446 (1976).

2. "A Kinetics Study of HONO Formation and Decay Reactions in Gaseous Mixtures of HONO, NO_2, H_2O and N_2." Walter H. Chan, Robert J. Nordstrom, Jack G. Calvert and John H. Shaw, Environmental Science and Technology, 10, 674-682 (1976).

3. "A Spectroscopic Study of the NO_2-N_2O_4 System by the Infrared Absorption Technique," Robert J. Nordstrom and Walter H. Chan, J. Phys. Chem., 80, 847-850 (1976).

4. "Accuracy of the AFCRL Atmospheric Absorption Line Parameters Compilation in the 10-μm Atmospheric Window." W. R. Skinner and R. J. Nordstrom, Appl. Opt. 15, 2616 (1976).

5. "Use of the AFCRL Line Parameters Compilation to Test the Performance of an Infrared Spectrometer System." Y. S. Chang, J. H. Shaw, W. M. Uselman, and J. A. Calvert, to appear in Applied Optics, 1977.

6. "Long Path Air Spectra." R. J. Nordstrom, W. R. Skinner, J. H. Shaw, W. H. Chan, J. G. Calvert, and W. M. Uselman, to appear in Applied Optics, June 1977.

7. "Application of Computer Simulated Infrared Solar Spectra to the Detection of Atmospheric Fluorocarbon-12." R. J. Nordstrom, J. H. Shaw, W. R. Skinner, W. H. Chan, J. G. Calvert, and W. M. Uselman, to appear in Applied Spectroscopy, 1977.

8. "The Pressure Dependence of the Rate Constant for the Reaction $HO + CO \rightarrow H + CO_2$." W. H. Chan, W. M. Uselman, J. G. Calvert and J. H. Shaw, Chem. Phys. Letters 45, 240-44, (1977)

9. "The Kinetics and Mechanism of the HO_2-NO_2 Reactions. The Significance of Peroxynitric Acid Formation in Photochemical Smog." S. Z. Levine, W. M. Uselman, W. H. Chan, J. G. Calvert and J. H. Shaw, to appear in Chem. Phys. Letter, 1977.